

CHAOS AND THERMALIZATION IN THE ONE-DIMENSIONAL
BOSE-HUBBARD MODEL IN THE CLASSICAL-FIELD APPROXIMATION

by

Amy C. Cassidy

A Dissertation Presented to the
FACULTY OF THE GRADUATE SCHOOL
UNIVERSITY OF SOUTHERN CALIFORNIA
In Partial Fulfillment of the
Requirements for the Degree
DOCTOR OF PHILOSOPHY
(PHYSICS)

May 2009

Copyright 2009

Amy C. Cassidy

Acknowledgements

There are a many people without whose support over the last six years I would not have completed this project. First of all, I would like to thank my advisor, Maxim for all that he has taught me, for his commitment to my development and for space to grow. Others whom I would like to acknowledge are: Vanja, for asking questions; Tameem, Richard and Yi-Chun, my classmates who got me through the first year; Ilya, for guidance at a critical time; Noah and Marcos, for physics conversations and tennis matches; Katie, for countless hours working together to encourage more women to pursue physics; Sam, for perspective; Courtney, for a lifelong friendship; Karla, for reminding me to stay balanced; Stephan, for getting me started and continued support; Werner and the department at USC, for flexibility; Bala and the department at UMass Boston, for welcoming me these last two years. Finally I would like to thank my family: my father who encouraged my intellectual curiosity; my mother, who taught me to be organized and persevere; Sara and Andrew for many words of wisdom; and Linda for encouragement and support.

Note: This document contains minor corrections and revisions from the original.

Table of Contents

Acknowledgements	ii
List of Tables	vi
List of Figures	vii
Abstract	x
1 Introduction	1
1.1 Introduction to Dynamical Systems	1
1.2 Dynamical Systems	2
1.2.1 Integrable Systems	4
1.2.2 Chaos	5
1.3 Statistical Mechanics	6
1.3.1 Statistical Ensembles	7
1.4 FPU Model and Results	10
1.4.1 KAM Theorem	12
1.4.2 Solitons and the Korteweg-de-Vries Equation	13
1.4.3 Chirikov Criterion	15
1.5 Relationship between Chaos and Thermalization	18
1.5.1 Thermalization in Classical Field Models	20
1.6 Quantum Degenerate Gases - Ultracold Atoms	22
1.6.1 Bose-Einstein Condensation	23
1.6.2 Bosons in Optical Lattices	25
1.6.3 Atom Chips	27
1.6.4 Classical Field Model of Bose Gas	27
1.6.5 Chaos and Integrability in Quantum Systems	29
1.6.6 Constrained equilibrium	31
1.7 Outline of Thesis	32
2 Thermalization and Chaos in the 1D Bose-Hubbard Model	34
2.1 Introduction	34

2.2	BHM: Hamiltonian and Equations of Motion	34
2.2.1	Real-Space Hamiltonian	35
2.2.2	Momentum-Space Representation	35
2.2.3	Action-Angle Representation	37
2.2.4	Validity of the Classical-Field Theory	38
2.2.5	Nearby Integrable Models	39
2.3	Time Dynamics	40
2.4	Chaos: Calculating Lyapunov Exponents	42
2.5	Thermalization: Calculating Spectral Entropy	43
2.5.1	Conserved Quantities	43
2.5.2	Hartree-Fock	44
2.5.3	Minimization of the Grand Potential	45
2.5.4	Spectral Entropy	47
2.6	Results: N=21 Sites, Three-Mode Initial Conditions	49
2.6.1	Fluctuations	51
2.7	Chaos Threshold for Different Lattice Sizes	54
2.8	Two Parametric Theory of the Chaos Threshold	56
2.8.1	Thermalization Times and Slow Relaxation	61
3	Resonance Model and Failure of Chirikov's Criterion	66
3.1	Perturbation Theory Study of BHM	66
3.1.1	Dynamics of an Initially Unpopulated Mode	67
3.1.2	Nonlinear Frequencies in the Real-Space Dynamics	71
3.2	Chirikov's Criterion	72
3.2.1	Classification of Resonances	74
3.2.2	First-Order Resonances in BOA	76
3.2.3	1-R Resonances in BOA. $\Omega_p = \Omega_q$	84
3.2.4	Second Order Resonances in BOA	85
3.3	Failure of Chirikov's Criterion	92
3.3.1	Thermodynamic Limit	96
3.3.2	Continuous Limit	96
4	Conserved Quantities of the Ablowitz-Ladik Lattice	98
4.1	Integrable Discrete Nonlinear Schrödinger (IDNLS) Equation	99
4.2	Conserved Quantities of the AL equation	101
4.2.1	AL equation	106
4.2.2	Direct Scattering Problem	107
4.2.3	Conservation Laws	111
4.2.4	Conserved Quantities	115
4.3	AL and BHM	115

5 Outlook and Conclusion	119
5.1 Summary of Results	119
5.2 Open Questions	121
Bibliography	122
A Thermodynamic Distribution within Hartree-Fock	127
A.1 Hartree Fock	127
A.2 Minimization of the Grand Potential	130

List of Tables

2.1	List of Parameters and Variables	37
2.2	Relationship between Parameters	39
2.3	Thermodynamic Limit and Scaling	53
3.1	Resonance Parameters	75
3.2	Bare Detuning: Generic Values	76

List of Figures

1.1	Time dependence of normal modes for cubic forces with $\beta = 8$. (Fermi <i>et al.</i> , 1974)	12
1.2	Space-time diagram of soliton trajectories. $u_0 = \cos(\pi x)$. $\delta = 0.022$. T_R is the recurrence time (Zabusky and Kuskal, 1965).	14
1.3	Schematic of Chirikov's criterion of the onset of chaos for the kicked rotor. J, ψ and J', ψ' are coordinates generated by two different canonical transformations. ΔJ and $\Delta J'$ are width of the separatrices. $J - J'$ represents the distance between the resonances	17
1.4	Velocity distribution of rubidium atoms. Left: prior to condensation. Center: just after condensation. Right: after further cooling (Anderson <i>et al.</i> , 1995)	24
1.5	$f(p_{ex})$, momentum distribution for (a) $\gamma_0=4$, $\tau=34$ ms. $t_{blue} = 15\tau$, $t_{red} = 30\tau$ (b) $\gamma_0=1$, $\tau=13$ ms. $t_{blue} = 15\tau$, $t_{red} = 40\tau$ (c) $\gamma_0=0.62$, $\tau=13$ ms. $t_{blue} = 15\tau$, $t_{red} = 40\tau$. Green is the initial momentum distribution averaged over the first period. (Kinoshita <i>et al.</i> , 2006)	31
2.1	Time evolution of the wavefunction at the center of the box for a typical run for $\kappa = 0.009, 0.09, 0.36, 0.9$ with identical initial conditions. (a) Time dynamics of the real part of the wavefunction, $\text{Re } \psi_{x=0}(t)$. (b) Frequencies of the real-space wavefunction, $ \text{FT}[\psi_{x=0}(t)] ^2$. For $\kappa = 0.009, 0.09$ the descendants of the unperturbed frequencies generated by the first, "integrable" term of the Hamiltonian (2.5) are labeled.	41
2.2	Initial, final and Hartree-Fock thermal momentum distributions for $\kappa = 0.09, 0.45, 1.8$, starting from the same initial state. $N_s = 21$. The initial state is a representative state and the final state is time-averaged. ϵ_T is the total energy per particle.	48
2.3	Ensemble-averaged finite-time maximal Lyapunov exponent, λ , and normalized spectral entropy, η , as a function of the nonlinearity, κ . $N_s = 21$	50

2.4	Normalized spectral entropy of the final time-averaged state versus finite-time maximal Lyapunov exponent for each of the 100 initial condition used to compute the averaged value for $\kappa = 0.36, 0.54, 0.72, 0.9$. $N_s = 21$.	51
2.5	Relative fluctuations in kinetic energy. Normalized standard deviation/mean for $N_s=21, 42, 63, 84$ lattice sites and $N_0 = 21$. Data points are for five sample runs with equivalent initial conditions for different lattice sizes and $\kappa = 2.69$.	54
2.6	Averaged Finite Time Lyapunov exponent, $\lambda[J]$, for three different system sizes, $N_s = 11, 21, 41$. For each κ , the same energy-per-particle was used for each lattice size. The error bars represent one standard deviation.	55
2.7	(a) Contour lines of the averaged FTMLE versus the nonlinearity, κ , and energy-per-particle, $\epsilon_T = (H - H_0)/N_a$, where H is the Hamiltonian (2.5), and $H_0 = -2J + (1/2)\mu_0$ is the ground state value of H . The solid contour line corresponds to $\lambda_c = 0.01$. The diagonal solid line represents the set of energies and nonlinearities used in Fig. 2.6. (b) Contour lines of the averaged normalized spectral entropy versus the nonlinearity, κ and energy-per-particle. Solid contour lines correspond to $\eta = 0.68$ and $\eta = 0.36$. For reference, the threshold line from the FTMLE in (a) is plotted (dashed line). $N_s = 11$.	57
2.8	Data points used for interpolation for contour plots in Fig. 2.7 superimposed on data for Lyapunov exponent.	58
2.9	Contour lines of the standard deviation of the NSE versus the nonlinearity, κ and energy-per-particle. Solid contour line corresponds to $\eta = 0.36$ and $\eta = 0.68$ from Fig. 2.7(b). $N_s = 11$.	60
2.10	Averaged normalized spectral entropy, η , for three different system sizes, $N_s = 11, 21, 41$. For each κ , the same energy-per-particle was used for each lattice size.	61
2.11	Sample time dependence of normalized spectral entropy, η . $\kappa = 0.09$, $\epsilon_T = 0.081J$, $N_s = 21$. Inset: Initial (dashed red), final (solid blue) and thermal (dotted black) momentum distributions.	62
2.12	Sample time dependence of normalized spectral entropy, η , for two different initial states. $\kappa = 0.54$, $\epsilon_T = 0.19J$ for both. $N_s = 21$. Inset: Initial (dashed red), final (solid blue) and thermal (dotted black) momentum distributions.	63

3.1	Frequencies of the real-space wavefunction at the center of the box, $ FT[\psi_{x=0}(t)]^2 $ for $\xi = 0.1, 1, 2, 3$	72
3.2	Real and imaginary parts of the fixed points of first-order Hamiltonian (3.28). $\Delta_{01} = -4$, $\bar{I}_1 = 1/3$	80
3.3	Action-angle phase-space plots for variables $\tilde{I}_n, \tilde{\theta}_n$ for the first-order resonant Hamiltonian (3.28). $(n+2, n+1) \rightarrow (n, n+3)$ ($\Delta_{01} = -4$). $\bar{I}_1 = 1/3$. (a) $\xi = 1$ (b) $\xi = 3.5$ (c) $\xi = \xi_{c1} = 4.3$ (d) $\xi = 7 > \xi_{c2}$. The black contour line corresponds to $\tilde{h}_n = 0$ and the white contour line to $\tilde{h}_n(\tilde{I}_n, \tilde{\theta}_n) = \tilde{h}_n(\tilde{I}_{n3}^*, -\pi)$	81
3.4	Real and imaginary parts of the solutions of $\tilde{h}_n = 0$ for the first-order Hamiltonian (3.28). $\Delta_{01} = -4$ $(n+1, n+2) \rightarrow (n, n+3)$, $\bar{I}_1 = 1/3$. For $\xi \leq \xi_{c1}$, \tilde{I}_{sep2} gives the separatrix for the the resonance at $(\tilde{I}_{n2}^*, \tilde{\theta}_n = \pm\pi)$. For $\xi \geq \xi_{c1}$, \tilde{I}_{sep1} gives the separatrix for the the resonance at $(\tilde{I}_{n1}^*, \tilde{\theta}_n = 0)$	83
3.5	Phase-space plots for the second order Hamiltonian. (a) $\xi = 0.5$ ($\kappa = 0.16$ for $N_s = 11$). There is no resonance in the range $0 \leq \tilde{I}_n \leq 1$ for $\xi < \xi_c = 1$. (b) $\xi = 1.5$ ($\kappa = 0.49$ for $N_s = 11$). $\bar{I}_2 = 1/3$, $\Delta_{02} = 2$. For $\xi > \xi_c$ the resonant value is given by (3.72) and the separatrix with is given by (3.73).	91
3.6	Resonant values and separatrix width for second-order resonance for $\Delta_{02} = 2 [(n+1, n-1) \rightarrow (n, n)]$ and for $\Delta_{02} = 8 [(n+2, n-2) \rightarrow (n, n)]$. $\bar{I} = 0.33$. Vertical lines: $\Delta_{20} = 2$: $\xi_{c1} = 1/3\bar{I}_2 = 1$, $\Delta_{02} = 8$: $\xi_{c2} = 4/3\bar{I}_2 = 4$. The upper x-axis gives the corresponding values of κ for $N_s = 11$	92

Abstract

One of the fundamental assertions of statistical mechanics is that the time average of a physical observable is equivalent to the average over phase space, with microcanonical measure. A system for which this is true is said to be ergodic and dynamical properties can be calculated from static phase-space averages. Dynamics of a system which is fully integrable, that is has as many conserved quantities as degrees of freedom, is constrained to a reduced phase space and thus not ergodic, although it may relax to a modified equilibrium.

In this thesis, we present a comprehensive study of chaos and thermalization of the one-dimensional Bose-Hubbard Model (BHM) within the classical field approximation. This model describes the dynamics of quantum degenerate gases in a lattice for sufficient occupation of every momentum mode and weak two-body scattering, and is of interest because of experimental advances of cooling and trapping alkali atoms in the quantum degenerate regime.

We study chaos and its relation to thermalization. Two quantitative measures are compared: the ensemble-averaged Finite-time Maximal Lyapunov exponent, a measure of chaos and the normalized spectral entropy, a measure of the distance between the numerical time-averaged momentum distribution and the one predicted by thermodynamics. A threshold for chaos is found, which depends on two parameters, the nonlinearity and the total energy-per-particle. Below the threshold, the dynamics are regular,

while far above the threshold, complete thermalization is observed, as measured by the normalized spectral entropy.

We study individual resonances in the Bose-Hubbard model to determine the criterion for chaos. The criterion based on Chirikov's method of overlapping resonances diverges in the thermodynamic limit, in contrast to the criterion parameters inferred from numerical calculations, signifying the failure of the standard Chirikov's approach.

The Ablowitz-Ladik lattice is one of several integrable models that are close to the BHM. We outline the method of Inverse Scattering Transform and generate the integrals of motion of the Ablowitz-Ladik lattice. Furthermore, we discuss the possible role of these quantities in the relaxation dynamics of the BHM.

Chapter 1

Introduction

1.1 Introduction to Dynamical Systems

The study of thermalization in nonlinear systems dates back to the early numerical studies of coupled anharmonic oscillators by Fermi, Pasta, and Ulam (FPU). At the time it was expected that any amount of nonlinearity, no matter how small, in a system with many degrees of freedom would lead to thermal behavior. Quite unexpectedly, thermalization was not observed. Later work found a threshold in the nonlinear coupling strength, with energy equipartition occurring above the threshold. The absence of thermalization for small nonlinearities has been explained in terms of the presence of a threshold for the onset of widespread chaos determined by Chirikov's criterion of overlapping resonances and also in terms of the closeness to a fully integrable model, the Korteweg-de-Vries equation. Additional studies on thermalization and approach to equilibrium have been carried out in many classical field theories.

Fermi, Pasta, Ulam (FPU) and Tsingou performed one of the first numerical experiments in the 1950's (Fermi *et al.*, 1974). Their discovery led to significant work and important discoveries in the field of nonlinear dynamics. The motivation for the experiment was to study the approach to equilibrium of a nonlinear system. The contemporary expectation was that a system with a large number of degrees of freedom would exhibit thermal behavior in the presence of any non-linearity, no matter how small. In particular

they were looking to observe the Fourier heat law for conduction. They numerically integrated a system of one-dimensional anharmonically coupled oscillators with quadratic and cubic forces.

The results found by FPU were completely surprising. In order to understand the prevalent view at the time and the significance of their results, let us take some time to review important concepts in Hamiltonian systems and statistical mechanics.

1.2 Dynamical Systems

Given a system whose state is completely known at some time t_0 , what can be said about the state at some future time $t > t_0$? What about its state at some time in the past, $t < t_0$? Classical mechanics addresses these questions. We begin with a short review of Hamiltonian dynamics, referring to Tabor (1989).

Hamiltonian Systems Consider a generic Hamiltonian of an N-particle system, $H(\{q_i, p_i\})$ where $\{q_i\}$ are the coordinates of the N-particles and $\{p_i\}$ are the corresponding momentum. The equations of motion are given by

$$\dot{q}_i = -\frac{\partial H}{\partial p_i}, \quad \dot{p}_i = \frac{\partial H}{\partial q_i}. \quad (1.1)$$

These equations, called the Hamilton's equations of motion, uniquely determine the time evolution of the state, from the initial state, which is specified by a complete set of values $\{q_i, p_i\}$. Note that canonical coordinates and momentum satisfy Liouville's theorem, so that a volume element in phase space moves like an incompressible fluid under the Hamiltonian flow.

Poisson Brackets For any dynamical quantities f, g in a system with canonical coordinates $\{q_i, p_i\}$, the Poisson brackets are defined as

$$\{f, g\} \equiv \sum_i \frac{\partial f}{\partial p_i} \frac{\partial g}{\partial q_i} - \frac{\partial f}{\partial q_i} \frac{\partial g}{\partial p_i}.$$

From this one can write the time dependence of a function $f(p, q, t)$ as

$$\begin{aligned} \frac{df}{dt} &= \sum_i \left(\frac{\partial f}{\partial q_i} \frac{\partial q_i}{\partial t} + \frac{\partial f}{\partial p_i} \frac{\partial p_i}{\partial t} \right) + \frac{\partial f}{\partial t} \\ &= \sum_i \left(\frac{\partial f}{\partial q_i} \frac{\partial H}{\partial p_i} - \frac{\partial f}{\partial p_i} \frac{\partial H}{\partial q_i} \right) + \frac{\partial f}{\partial t} \\ &= \{H, f\} + \frac{\partial f}{\partial t}. \end{aligned}$$

Thus any quantity that does not explicitly depend on time is a constant of motion if the Poisson bracket of that quantity vanishes. The Poisson brackets are antisymmetric and satisfy the identity

$$\{f, gh\} = g\{f, h\} + \{f, g\}h.$$

Canonical Transformations Oftentimes it is more convenient to work in one coordinate system than another. A canonical transformation is one in which the canonical form of Hamilton's equations is preserved. The phase volume is preserved under a canonical transformation. Thus the Jacobian, must be unity. Consider a transformation from one set of phase-space variables (p_i, q_i) to a new set of variables (P_i, Q_i) the preservation of phase volume is expressed as

$$\int dp_1 dq_1 \int dp_2 dq_2 \dots \int dp_N dq_N = \int dP_1 dQ_1 \int dP_2 dQ_2 \dots \int dP_N dQ_N$$

and the Jacobian must satisfy the condition

$$\frac{\partial(p_1, \dots, p_N, q_1, \dots, q_N)}{\partial(P_1, \dots, P_N, Q_1, \dots, Q_N)} = \frac{\partial(P_1, \dots, P_N, Q_1, \dots, Q_N)}{\partial(p_1, \dots, p_N, q_1, \dots, q_N)} = 1$$

(Tabor, 1989).

One of the representations of the canonical transformation, is through the type 2 generating function $\Phi(\theta, \tilde{I})$, which transforms $I, \theta \rightarrow \tilde{I}, \tilde{\theta}$. The Hamiltonian is transformed according to

$$\begin{aligned} \tilde{H}(\tilde{I}, \tilde{\theta}) &= H(I, \theta) + \frac{\partial \Phi}{\partial t} \\ I &= \frac{\partial \Phi}{\partial \theta} \\ \tilde{\theta} &= \frac{\partial \Phi}{\partial \tilde{I}}. \end{aligned} \tag{1.2}$$

1.2.1 Integrable Systems

An integrable system has as many independent constants of the motion as degrees of freedom. Stated another way, a systems with n degrees of freedom is completely integrable is there exist n integrals of motion which are in involution.

$$\begin{aligned} \{F_i, H\} &= 0, & i &= 1 \cdots n, & \{F_i\} &\text{ are constants of the motion} \\ \{F_i, F_j\} &= 0, & i &= 1 \cdots n, j = 1 \cdots n & \{F_i\} &\text{ are in involution} \end{aligned}$$

Ford makes the distinction that these must be in fact well-behaved integrals of motion (Ford, 1992). All one dimensional systems are integrable (Tabor, 1989). Examples of integrable systems with many degrees of freedom include the Toda lattice (infinite-dimensional countable), the Korteweg-de-Vries equation, sine-Gordon model and continuous nonlinear Schrödinger equation (infinite-dimensional continuous).

1.2.2 Chaos

The term chaos is commonly used to describe systems where the motion appears random, erratic or unpredictable. It is sometimes called “deterministic chaos” to emphasize that it refers to dynamical systems in which the motion is governed by deterministic equations of motion. A key feature of chaotic systems is extreme sensitivity to initial conditions. Imagine two identical systems that are governed by the same equations of motion and with initial conditions that are only slightly different. In a chaotic system, the initial different will grow rapidly and after some time the states of the two systems will be entirely different from one another. In contrast, in a regular system, the difference will grow slowly, so that two remain highly correlated. The difference between chaotic and regular motion is not only quantitative, but qualitative. The very functional form of the divergence is different: chaotic trajectories diverge exponentially while regular trajectories diverge linearly.

Lyapunov Exponents A chaotic system is characterized by local instability, specifically by exponential divergence of trajectories neighboring in phase space. This rate of divergence of is measured by the Lyapunov exponent. The maximal Lyapunov Exponent (MLE) of a system is defined as

$$\lambda(\mathbf{x}_0) = \lim_{t \rightarrow \infty} \lim_{\tilde{\mathbf{x}}_0 \rightarrow \mathbf{x}_0} \frac{1}{t} \ln \frac{\|\tilde{\mathbf{x}}(t) - \mathbf{x}(t)\|}{\|\tilde{\mathbf{x}}_0 - \mathbf{x}_0\|}$$

where $\mathbf{x}(t)$ and $\tilde{\mathbf{x}}(t)$ are two phase space trajectories (Tabor, 1989). Chaotic motion is characterized by positive MLE, $\lambda > 0$, in which case trajectories that are initially close in phase space will diverge exponentially. On the other hand, a zero MLE, $\lambda = 0$, indicates regular motion and linear divergence. The Lyapunov exponent is a function of an initial state and is thus a measure of local chaos. A system may have a mixed

phase space, consisting of both chaotic and regular regions (Zaslavsky, 1999). Thus initial states in the regular regions will have zero Lyapunov exponent while initial states in chaotic regions have a positive Lyapunov exponent. As a system transitions from regular to globally chaotic behavior, the volume of phase space corresponding to chaotic regions grows while the regular regions shrink. When the chaotic regions dominate the phase space, there can still exist regular regions, called islands of stability, which are surrounded by the chaotic sea.

1.3 Statistical Mechanics

Thermodynamics is a phenomenological theory that has very successfully described the equilibrium properties of isolated systems with many degrees of freedom. In this section we give an overview of basic concepts of statistical mechanics. The field arose in the study of macroscopic systems of atoms with $N \sim 10^{23}$ particles and correspondingly large volumes. One of the great success of thermodynamics is the Maxwell-Boltzmann distribution for ideal gases. It can be derived in two ways: (1) through the Boltzmann transport equation and (2) through the most probable distribution. Systems are described not by position and momentum of every particle in the system, but by probability distribution functions from which macroscopic properties such as pressure and temperature and volume can be determined. The aim of statistical mechanics is to derive the laws of thermodynamics from molecular dynamics.

For a system with N particles with canonical coordinates q_1, q_2, \dots, q_{3N} and conjugate momenta p_1, p_2, \dots, p_{3N} , the $6N$ dimensional space spanned by these coordinates is the *phase space* or Γ space. A *representative point* is a point in this Γ space that specifies the position and momentum of each of the N particles. The representative point will also be called a *microstate*. For each microstate, there is a corresponding macrostate

that specifies properties of the system such as density, temperature, and pressure. Many microstates and in fact, an infinite number, correspond to the same macrostate.

The dynamics of the individual N particles is governed by the Hamiltonian, $H(p, q)$ where $(p, q) = (p_1, p_2, \dots, p_{3N}, q_1, q_2, \dots, q_{3N})$. The equations of motion are given by the Hamilton's equations of motion,

$$\begin{aligned}\dot{q}_i &= \frac{\partial H}{\partial p_i} \\ \dot{p}_i &= -\frac{\partial H}{\partial q_i}.\end{aligned}$$

These equations become quickly intractable for systems with large numbers of degrees of freedom. Instead systems will be studied by various ensembles which give the distribution of representative points in phase space.

1.3.1 Statistical Ensembles

A statistical ensemble is a collection of microstates which correspond to the same macrostate. Geometrically the ensemble can be described by the distribution of representative points in the Γ space with the density distribution function $\rho(p, q, t)$ which is defined so that

$$\rho(p, q, t) d^{3N}p d^{3N}q$$

is the number of representative points in phase space volume $d^{3N}p d^{3N}q$ at time t .

Liouville Theorem

$$\frac{d\rho}{dt} + \sum_{i=1}^{3N} \left(\frac{d\rho}{dp_i} \dot{p}_i + \frac{d\rho}{dq_i} \dot{q}_i \right) = 0$$

The interpretation of the Liouville theorem is that the distribution of representative points in phase space move like an incompressible fluid.

Ensemble averages The ensemble average of an observable O is given by

$$\langle O \rangle = \frac{\int d^{3N}p d^{3N}q O(p, q) \rho(p, q, t)}{\int d^{3N}p d^{3N}q \rho(p, q, t)}$$

The time dependence of O comes from the time-dependence of ρ .

Postulate of Equal a Priori probability For a system in thermodynamic equilibrium, it is equally likely to be in any microstate (of the same phase volume) that satisfies the macroscopic conditions of the system.

For an isolated system, the distribution is described by the *microcanonical ensemble*, which corresponds to all microstates with the same energy, volume and number of particles. The density of representative points in phase space is given by

$$\rho(p, q) = \begin{cases} \text{const.} & E < H(p, q) < E + \Delta \\ 0 & \text{otherwise} \end{cases}$$

The question arises, what ensemble describes a system that is not in isolation, but instead is in equilibrium with another, larger system? A system in contact with a heat reservoir such that the temperature, volume and number of particles are constant is described by the *canonical ensemble*. It is also possible to have a system where particles can be exchanged with a larger system. Such a system, that is in contact with a heat reservoir and a particle reservoir is described by the *grand canonical ensemble*, in which temperature, volume and chemical potential are kept constant.

The most probable value of an observable is given by the value of O that the most members of the ensemble have. The most probable value and ensemble average are close if the mean square fluctuation

$$\frac{\langle O^2 \rangle - \langle O \rangle^2}{\langle O \rangle^2} \ll 1$$

is small.

Ergodic theorem Under certain conditions, a representative point in phase space will pass arbitrarily close to any other point in the accessible phase space, if one waits a sufficiently long time. Following from the postulate of equal a priori probability, the time average of some physical observable is equal to the ensemble average over phase-space, that is

$$\lim_{T \rightarrow \infty} \frac{1}{T} \int_0^T O(x, t) dt = \langle O(x, t) \rangle$$

Statistical mechanics does not specify whether a system is ergodic or not and there is no generic test for ergodicity. For an ergodic system, a single trajectory will uniformly cover the phase space. An integrable system will not be ergodic in the full phase space due to the additional conserved quantities that act as constraints. Ergodicity says nothing about the time-scale involved in covering the entire phase space. For typical thermodynamic systems, the size of the phase space is immense. A stronger condition than ergodicity is *mixing* (Tabor, 1989). In the long time limit, the values of a macroscopic observable in a system that is mixing will equal the ensemble average, without a need to time average over the trajectory as in an ergodic system.

1.4 FPU Model and Results

Let us now return to the numerical experiments of FPU. Recall that the expectation was that a nonlinear system with many degrees of freedom would exhibit thermal behavior for any non-linearity, no matter how small. The system studied was a chain of one-dimensional anharmonically coupled oscillators with quadratic and cubic forces. The Hamiltonians of these two models can be written as a sum of

$$H = H_0 + H_1, \quad (1.3)$$

where the integrable Hamiltonian

$$H_0 = \sum_{n=1}^{N-1} p_n^2 + \sum_{n=1}^{N-1} (x_{n+1} - x_n)^2, \quad (1.4)$$

is weakly perturbed by the non-integrable Hamiltonian H_1 , which for the α -model is

$$H_1 = \frac{\alpha}{3} \sum_{n=1}^{N-1} (x_{n+1} - x_n)^3 \quad (1.5)$$

and for the β -model is

$$H_1 = \frac{\beta}{4} \sum_{n=1}^{N-1} (x_{n+1} - x_n)^4. \quad (1.6)$$

The displacement of particle n from equilibrium is x_n and α and β are nonlinear interaction parameters. The resulting equations of motions for the α -model are

$$\ddot{x}_n = (x_{n+1} - 2x_n + x_{n-1}) + \alpha[(x_{n+1} - x_n)^2 - (x_n - x_{n-1})^2] \quad (1.7)$$

and for the β -model

$$\ddot{x}_n = (x_{n+1} - 2x_n + x_{n-1}) + \beta[(x_{n+1} - x_n)^3 - (x_n - x_{n-1})^3]. \quad (1.8)$$

The problem can be analyzed in terms of normal modes, $A_k(t)$, which are the Fourier modes of the displacement, $x_n(t)$,

$$A_k(t) = \sqrt{\frac{2}{N}} \sum_{n=1}^N x_n(t) \sin\left(\frac{\pi kn}{N}\right) \quad (1.9)$$

In terms of the normal modes, H_0 is a sum of harmonic oscillators and H_1 is a perturbing term that couples the oscillators.

$$H_0 = \frac{1}{2} \sum_k (\dot{A}_k^2 + \omega_k^2 A_k^2)$$

$$\omega_k = 2 \left| \sin\left(\frac{\pi k}{N}\right) \right|$$

For the linear system, that is when $\alpha = \beta = 0$, there is no interaction between normal modes, so that modes that are initially populated remain populated and modes that are initially unpopulated will remain unpopulated. What happens when nonlinearity is added? Would the coupling between the modes cause the energy to spread from a single mode to all of the other modes in the system? For the systems studied, thermalization would be marked by equipartition of energy among all of the modes, $A_k E_k = A_{k'} E_{k'}$ for all k, k' . The expectation was that thermal behavior would be observed. In Fig. 1.1 the time dependence of the normal modes is plotted for $N = 32$ oscillators with cubic forces and $\beta = 8$. The initial condition is given by a sine wave and the velocity is zero. The ends are fixed. The model preserves symmetry so that the effective number of particles is 16 and even modes have zero energy. As can be seen from the plot only a few modes are active in the dynamics and there are recurrences. Additionally the period of recurrence was found to decrease with increasing nonlinearity. Later work found a super period, where almost all of energy (99%) returns to the initial modes after about 80 000 T_1 . (Tuck and Menzel, 1972).

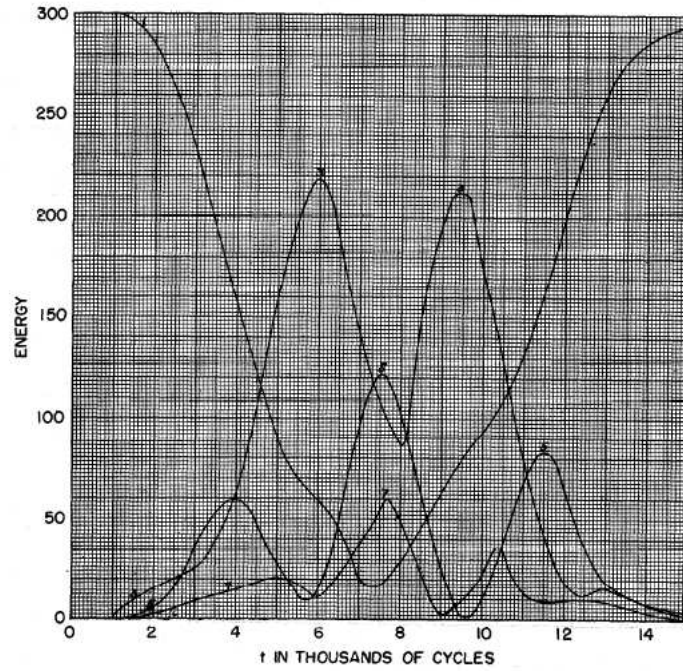


Figure 1.1: Time dependence of normal modes for cubic forces with $\beta = 8$. (Fermi *et al.*, 1974)

The failure of FPU to thermalize was very puzzling when first discovered and it was some time before explanations came out to explain the observed phenomena. The first explanation has to do with closeness to integrable systems and the second has to do with a stochasticity threshold with respect to the linear system.

1.4.1 KAM Theorem

A theorem outlined by Komologorov and subsequently proved by Arnold and Moser provided one resolution to the apparent paradox of FPU (Kolmogorov, 1954; Moser, 1962; Arnold, 1963). Consider an integrable Hamiltonian that is weakly perturbed: $H = H_0(\mathbf{I}) + \varepsilon H_1(\mathbf{I}, \theta)$ where H_0 is integrable with constants of motion \mathbf{I} and frequencies $\omega_i = \frac{\partial H_0}{\partial I_i}$ and H_1 is periodic in the original angle variables, $H_1(\mathbf{I}, \theta + 2\pi) = H_1(\mathbf{I}, \theta)$. The

motion of the unperturbed Hamiltonian corresponds to motion on an n -dimensional torus. It is assumed that the Hamiltonian is analytic on the complex domain and that the unperturbed Hamiltonian is non-degenerate,

$$\det \left| \frac{\partial^2 H_0}{\partial I_i \partial I_j} \right| \neq 0.$$

Consider a frequency vector of the unperturbed Hamiltonian, ω^* that is incommensurate ($\omega^* \cdot \mathbf{k} \neq 0$ for all integer k_i). The corresponding motion of the unperturbed system is on the torus $T_0(\omega^*)$.

One statement of the KAM theorem is

Theorem 1.4.1 *KAM Theorem* If H_1 is small enough, then for almost all ω^* , there exists an invariant torus $T(\omega^*)$ of the perturbed system such that $T(\omega^*)$ is close to $T_0(\omega^*)$. (Arnold and Avez, 1968).

Stated informally, KAM showed that if the perturbation is sufficiently small, then almost all of the tori of the unperturbed motion are preserved and the resulting motion is quasi-periodic.

1.4.2 Solitons and the Korteweg-de-Vries Equation

Soon after the proof of the KAM theorem, Zabusky and Kruskal discovered solitary wave solutions to the Korteweg-de-Vries (KdV) equation, which they termed “solitons” (Zabusky and Kuskal, 1965). Solitons are solitary wave that preserve their shape both under free propagation and after collisions. Zabusky and Kruskal also show that that the continuum limit of the β -FPU model is close to the KdV equation. In KdV the speed of the solitons depends only on their amplitude. The KdV equation is given by

$$u_t + uu_x + \delta^2 u_{xxx} = 0 \tag{1.10}$$

and was first found as a description of the motion of shallow water waves. Starting with

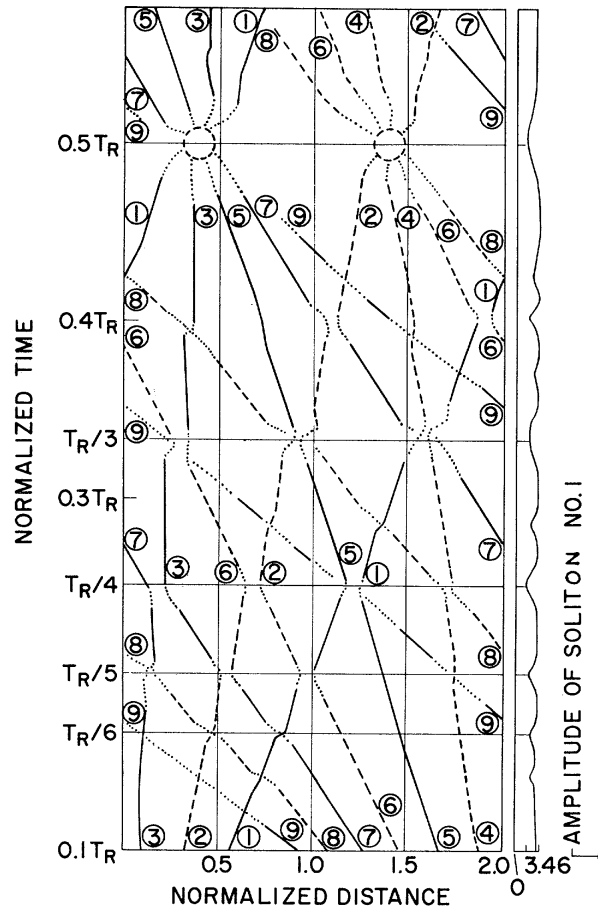


Figure 1.2: Space-time diagram of soliton trajectories. $u_0 = \cos(\pi x)$. $\delta = 0.022$. T_R is the recurrence time (Zabusky and Kuskal, 1965).

a cosine pulse, the negative slope regions of u steepen, and then oscillations develop on the steep front and grow in amplitude, and finally each solitary wave or “soliton” moves at a constant speed, which is proportional to the amplitude. The trajectories of interacting solitons are shown in Fig. 1.2. The solid (dashed) lines represent the odd-(even-)numbered solitons. From the trajectories, it is clear that when solitons interact, they emerge with the same speed and thus shape. The dotted lines represent interactions, during which the joint amplitude is less than the sum of the individual amplitudes due

to the non-linear interaction. At the recurrence time T_R , all of the solitons arrive at one point in space and almost reconstruct the initial state.

KdV was later shown to be fully integrable by the method of Inverse Scattering Transform (Gardner *et al.*, 1967). The discovery of the solitons of KdV provides one route for explaining the absence of thermal behavior in FPU. The KAM theorem provides another explanation. The nonlinearities of the FPU studies were insufficient to break the KAM tori and thus the motion remained quasi-periodic. Indeed later work showed that for larger nonlinearities, FPU did exhibit thermal behavior

1.4.3 Chirikov Criterion

A method for predicting the criterion for the onset of chaos in the FPU experiments was the theory of overlapping resonances developed by Chirikov in the context of plasma dynamics, and later applied to FPU (Izrailev and Chirikov, 1966).

Consider a one-dimensional non-linear oscillator perturbed by an external periodic force. Write the unperturbed system in action-angle variables (I, θ) and the external field as a Fourier series.

$$H = H_0(I) + \varepsilon \sum_{m,n} V_{mn}(I) e^{i(m\theta + n\phi)}$$

where H_0 is the unperturbed Hamiltonian with frequencies $\omega(I) = \frac{\partial H_0}{\partial I}$, $\phi = \Omega t + \phi_0$ is the phase of the external force and $\theta = \omega t + \phi'$. Resonances occur for the set of I_r such that $\omega(I_r)l = \Omega k$. The main ingredients are then to:

1. Assume that when the system is near a resonance, the resonance dominates the motion. Thus resonance are studied in isolation.

2. Make a canonical transformation from $(I, \theta) \rightarrow (J, \psi)$ into the rotating reference frame of the resonance. (ψ measures deviations from resonance). The old and new coordinates are related by

$$J = \frac{1}{l}(I - I_r), \quad \psi = l\theta - k\phi.$$

3. Integrate out the fast phase ϕ motion.
4. Expand the Hamiltonian about $I = I_r$ and keep terms up to second order in $H_0(I)$ and zeroth order in $V_{nm}(I)$.

The resulting Hamiltonian of this process is,

$$H_r = \frac{J^2}{2M} + \varepsilon V_{l,-k} \cos(\psi)$$

which is the Hamiltonian of a simple pendulum, with “mass” $M \equiv l^2 \left(\frac{\partial^2 H_0}{\partial I^2} \right)_{I=I_r}$. In Fig. 1.3 a schematic is plotted for J, ψ and J', ψ' coordinates generated by two different canonical transformations corresponding to two different resonances. The separatrices, which separate bounded and unbounded motion, are given by the black contour lines. An initial state inside the separatrix is captured by the resonance and both the action variable and the angle are bounded in phase-space. Outside of the separatrix, the angle is unbounded. When the resonances are well-separated in phase-space, that is $J' - J \gg \Delta J$, the motion near an individual resonance is dominated by that resonance. As the strength of the external drive increases, the width of the separatrix, ΔJ , grows. Eventually the width of the two separatrices becomes comparable to the distance between the resonances.

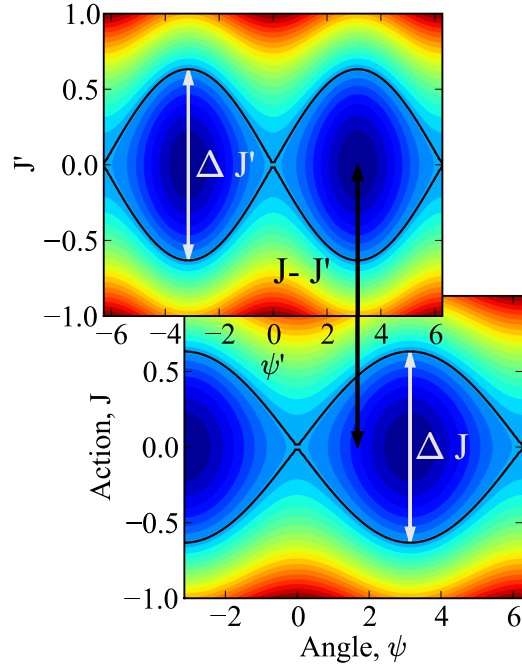


Figure 1.3: Schematic of Chirikov's criterion of the onset of chaos for the kicked rotor. J, ψ and J', ψ' are coordinates generated by two different canonical transformations. ΔJ and $\Delta J'$ are width of the separatrices. $J - J'$ represents the distance between the resonances

For two neighboring resonances, with resonant values I_A and I_B , the “distance” between the resonances is given by $I_B - I_A$. For separatrix width ΔI , the ratio of these two quantities,

$$\mathcal{K} \equiv \frac{\text{separatrix width}}{\text{distance between resonances}} = \frac{\Delta I}{I_B - I_A},$$

gives the condition for onset of chaos in the system

$$\mathcal{K} \gtrsim 1.$$

Crossing the threshold corresponds to the overlap of the separatrices of the two resonances in phase space, so that the action variable is free to travel between resonances and thus explore all of phase space. Complete chaos emerges when all of the neighboring resonances become coupled.

Chirikov applied this criterion to the FPU system. For a chain of N oscillators, and an excitation of momentum mode k , the conditions for chaos are given by:

Low modes

$$k \ll N : \quad 3\beta \left(\frac{\partial x}{\partial z} \right)_m^2 \sim \frac{3}{k} \quad (1.11)$$

High modes ($k \approx N$)

$$N - k \ll N : \quad 3\beta \left(\frac{\partial x}{\partial z} \right)_m^2 \sim \frac{3\pi^2}{N^2} \left(\frac{k}{N} \right)^2 \quad (1.12)$$

This criterion predicts that for initial excitation of low modes, there is only have stochasticity for large perturbations, while for the high mode have stochasticity even for small non-linearities when N is large. Data from FPU experiments show a threshold for thermalization that is close to the prediction of Chirikov.

1.5 Relationship between Chaos and Thermalization

Statistical mechanics dictates the of equilibrium state of a system, but it does not tell us whether a system will thermalize or not. How is it that statistical behavior can arise from dynamics?

Consider a system in equilibrium, with some constraint. Lift the constraint and let it evolve. What will the equilibrium state be, if in fact it reaches equilibrium? According to the second law of thermodynamics, when a constraint is lifted, the system moves to a state of greater entropy. To explain this further, consider a simple example a box of volume V with N particles, initially confined to 1/2 of the box. When Boltzmann first derived statistical mechanics for an ideal gas through kinetic equations, there were several objections that were raised (Zaslavsky, 1999):

Objection 1: Zermelo's Paradox (Recurrence) Poincaré's recurrence theorem states that after sufficiently long times, any trajectory will pass arbitrarily close to any phase space point, including the initial state. This would contradict the expected increase in entropy.

Objection 2: Loschmidt's Paradox (Reversibility) The equations of motion are invariant under time-reversal. If one simply reverses the velocities of particles, one goes back to the original state, a process that decreases entropy.

Microscopic Origins of Macroscopic Irreversibility The second objection to the can be restated, how is it that the microscopic equations of motion are reversible, but the macroscopic behavior is irreversible? Lebowitz argues that this question was satisfactorily settled years ago by Thomson, Maxwell and Boltzmann (Lebowitz, 1999). The essential ingredients of understanding this, according to Lebowitz are

1. the vast difference in scales between microstates and macrostates
2. initial conditions are special
3. significance of probabilities

Consider an isolated classical system of N particles. Let X be the microstate that completely specifies the system, $X = (\mathbf{r}_1, \mathbf{p}_1, \mathbf{r}_2, \mathbf{p}_2, \dots, \mathbf{r}_N, \mathbf{p}_N)$ in phase space Γ . Let M represent the macrostate of a system and let Γ_M be the the region of the phase space Γ that correspond to macrostate M . Note that there are many microstates X that correspond to the same macrostate M . The number of microstates that correspond to is so large as to make certain macrostates extremely unlikely. Consider the example of the gas of particles initially confined to half of a box. The initial state is indeed a special state. Once the constraint is lifted, the volume in phase space corresponding to all of the

particles in one-half of the box is vastly smaller than the volume of phase space that corresponds to a roughly equal distribution of the particles between the two halves of the box. Thus, the probability that it will return to the initial state is effectively zero. Boltzmann made a rough estimate of the Poincaré recurrence times and found them to be much larger than the lifetime of the universe and thus irrelevant. This interpretation of the second law of thermodynamics explains why FPU expected to see thermal behavior in their system. However, it fails to account for the thermalization threshold found in FPU. Additionally, thermal behavior has been observed in systems with at few degrees of freedom, where this reasoning does not apply.

Zaslavsky argues that chaotic dynamics introduce mixing properties in a system (Zaslavsky, 1999) that well resolves these paradoxes. Furthermore, he calculates the distribution of Poincaré recurrence times and concludes that they are irrelevant. While there is not a current consensus on the origins of statistical laws, this discussion highlights some relevant questions, namely,

- Is chaos necessary for thermalization?
- What is the role of chaos in thermalization in systems with many degrees of freedom?

1.5.1 Thermalization in Classical Field Models

Since the FPU studies on anharmonic oscillators, further studies on thermalization and approach to equilibrium have been carried out in several classical field theories, including recent studies on the classical ϕ^4 model (Boyanovsky *et al.*, 2004), nonlinear Klein-Gordon equation (NLKG) (Gerhardt *et al.*, 2002), nonlinear Schrödinger equation (NLSE) (Villain and Lewenstein, 2000; Herbst and Ablowitz, 1989), discrete nonlinear Schrödinger equation (DNLS) (Herbst and Ablowitz, 1989; Ablowitz *et al.*, 1993)

equivalent to the Bose-Hubbard model, and Integrable Discrete Non-Linear Schrödinger equation (IDNLS)(Herbst and Ablowitz, 1989).

No conventional thermalization is expected in the NLSE and IDNLS, which are both integrable. In NLKG, like in FPU, the ability of the system to reach thermal equilibrium in the course of time evolution emerges only when the degree of nonlinearity exceeds a certain critical value (see (Izrailev and Chirikov, 1966; Livi *et al.*, 1985) for the thermalization threshold in FPU). On the contrary, the ϕ^4 model eventually reaches equilibrium regardless of how small the nonlinearity is.

There are several other studies on thermalization and chaos in system with a large number of degrees of freedom that are highly relevant to the work presented here. Livi *et al.* (1985) investigated the equipartition threshold in the FPU β model in the thermodynamic limit. For N oscillators, $64 \leq N \leq 512$, the thermodynamic limit is simulated by initially exciting a block of modes, Δn , such that $\frac{\Delta n}{N}$ remains constant. The threshold for equipartition of energy is found to be independent of the number of degrees of freedom with respect to the relevant control parameter, the energy density, with a critical value of $\epsilon_c \simeq 0.35$. They also calculate the Asymptotic Reynolds number, R , given by

$$\left\langle \frac{O(NL)}{O(L)} \right\rangle_{space} = \frac{\beta}{N} \sum_{i=1}^{N-1} (\phi_{i+1} - \phi_i)^2 \rightarrow R \quad t \rightarrow \infty$$

which is a measure of ratio of strength of nonlinear to linear terms. Again, there is universal behavior with $R_c \simeq 0.03$, consistent with findings for energy density. There is evidence that the threshold energy is independent of the mode excited, when a narrow range of energies is initially excited. Note that very long equipartition times ($t \rightarrow \infty$) are not ruled out and they conclude that the results are relevant for long, but finite times. It is significant to note that the result that the threshold for FPU remains in the thermodynamics limit contradict the predictions of Chirikov's criterion of overlapping resonances.

Another study by the same group focuses on the relationship between chaotic dynamics and statistical mechanics in two nonlinear Hamiltonian systems, the FPU model of nonlinearly coupled oscillators and coupled rotators (Livi *et al.*, 1987). For both systems thermodynamic quantities are computed analytically using ensemble theory and compared with dynamical results from numerical simulations. For the FPU model, there is qualitative agreement between ensemble-averages and time-averages, independent of the stochasticity. That is the system is ergodic in both the chaotic and regular region. For the rotator model, there is good agreement between the ensemble-averages and time-averages at low temperatures but not at high temperatures where the system is strongly chaotic. This result is explained in terms of localized chaos. In conclusion it is possible that a system (a) is not chaotic, but is ergodic for some physically “relevant” quantities and also (b) is chaotic, but some observable are not ergodic. This study highlights the open questions in the relationship between stochasticity and thermalization, particularly in systems with many degrees of freedom.

1.6 Quantum Degenerate Gases - Ultracold Atoms

Advances in the cooling and trapping of alkali atoms into the quantum degenerate regime has led to an explosion of experimental and theoretical studies of ultracold atoms. In recent years Nobel prizes have been awarded for advances in laser cooling techniques (Phillips and Metcalf, 1982; Chu *et al.*, 1985; Aspect *et al.*, 1988) and the subsequent observation of Bose-Einstein condensation (BEC) (Davis *et al.*, 1995; Anderson *et al.*, 1995). The manipulation of atoms by electric and magnetic fields offers unprecedented control over parameters in the system and the ability to address fundamental questions in physics. Numerous proposals have been put forth for quantum simulators and applications have arisen in precision measurements. Studies in ultracold atoms have led to

fruitful collaborations across fields, such as condensed matter and quantum information. One application of these advances is using matter-wave interferometers based on ultracold atomic systems for high precision sensing of accelerations and gravitational fields (Gustavson *et al.*, 2000; Durfee *et al.*, 2006; Weiss *et al.*, 1994; Wicht *et al.*, 2002). Fundamental questions in physics related to out-of-equilibrium dynamics and thermalization in classical and quantum integrable systems have also been studied in one-dimensional ultracold atoms. Quasi-one-dimensional systems have been realized in optical lattices (Paredes *et al.*, 2004; Kinoshita *et al.*, 2006) and on atom chips, where BEC's have been created and manipulated (Esteve *et al.*, 2006; Schumm *et al.*, 2005; Wang *et al.*, 2005).

1.6.1 Bose-Einstein Condensation

Advances in laser cooling and trapping led to the realization of Bose-Einstein condensation (BEC) in alkali atoms (Davis *et al.*, 1995; Anderson *et al.*, 1995; Bradley *et al.*, 1995). BEC is a phase of matter, first proposed by Bose (1924) and Einstein (1925), in which there is macroscopic occupation of a single quantum state. Seventy year later BEC was created in Rb⁸⁷ gas (Anderson *et al.*, 1995), sodium (Davis *et al.*, 1995) and Li⁷ (Bradley *et al.*, 1995). Since the initial experiments, BEC has been observed in twelve species of alkali atoms as well as in Bose molecules (Yukalov, 2009). BEC was created by confining and cooling atoms to microkelvin temperatures with a magneto-optical trap (MOT), followed by evaporative cooling to nanokelvin temperatures. In Fig. 1.4 the velocity distribution of rubidium atoms is shown prior to and after condensation. The velocity distribution of rubidium atoms is measured by turning off the confining trap, allowing the atoms to expand and performing a time-of-flight measurement. The leftmost plot shows the velocity distribution just before condensation. The center

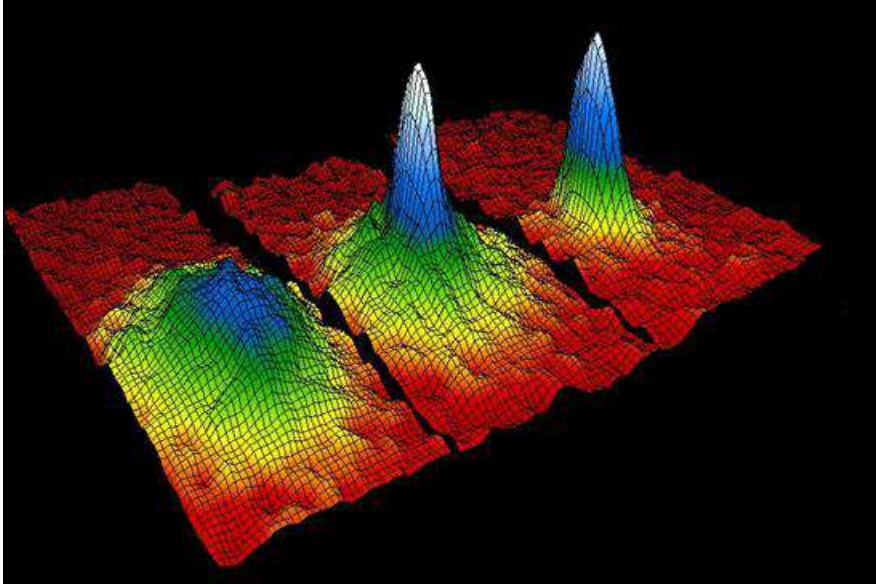


Figure 1.4: Velocity distribution of rubidium atoms. Left: prior to condensation. Center: just after condensation. Right: after further cooling (Anderson *et al.*, 1995)

plot is the velocity distribution just after condensation, where the sharp peak in velocity distribution clearly indicates the presence of the condensate. In rightmost plot, the system has been cooled further such that most of the atoms are in the condensate. The presence of the condensate was confirmed by the anisotropic velocity distribution due to the magnetic trap in contrast with the isotropic, thermal velocity distribution. BEC's demonstrate long-range phase coherence, confirmed experimentally by the observation of interference between two independent condensates (Andrews *et al.*, 1997).

Historically BEC was defined for a uniform, ideal gas as the macroscopic occupation of a single quantum state in the thermodynamic limit,

$$\lim_{\substack{N \rightarrow \infty, \\ V \rightarrow \infty, \\ N/V \rightarrow \text{const}}} \frac{N_0}{V} > 0$$

where N is the total number of particles, V is the volume and N_0 is the occupation number of a single quantum state (Yukalov, 2009). The question arises as to to define BEC

in a non-uniform system such as in presence of trap. Penrose and Onsager propose that a condensate is present when the largest eigenvalue of the single-particle density matrix is extensive (Penrose and Onsager, 1956). The Penrose-Onsager scheme is more general than idea of off-diagonal long-range order and applicable to both uniform systems and trapped systems. There is no true condensate in finite or 1D systems, which will be the focus of this work, however there can be a quasi-condensate in 1D, when the coherence length is much larger than the de Broglie wavelength (Castin, 2004).

1.6.2 Bosons in Optical Lattices

The versatility offered by optical lattices allows one to control parameters such as the interaction strength, lattice spacing and the dimensionality of the system. In particular, one-dimensional systems in cold atoms have been realized in optical lattices by tight confinement in two dimensions.

The dynamics of ultracold bosons in optical lattices can be described the Bose-Hubbard model (BHM). The Bose-Hubbard Hamiltonian (Jaksch *et al.*, 1998) is

$$H = -J \sum_{\langle i,j \rangle} \hat{b}_i^\dagger \hat{b}_j + \sum_i \varepsilon_i \hat{n}_i + \frac{1}{2} U \sum_i \hat{n}_i (\hat{n}_i - 1).$$

To derive this Hamiltonian, one begins with the Hamiltonian for bosonic atoms in an external potential

$$H = \int d^3x \psi^\dagger(\mathbf{x}) \left(-\frac{\hbar^2}{2m} \nabla^2 + V_0(\mathbf{x}) + V_T(\mathbf{x}) \right) \psi(\mathbf{x}) + \frac{1}{2} \frac{4\pi a_s \hbar^2}{m} \int d^3x \psi^\dagger(\mathbf{x}) \psi^\dagger(\mathbf{x}) \psi(\mathbf{x}) \psi(\mathbf{x})$$

where $\psi(\mathbf{x})$ is a boson field operator, $V_0(\mathbf{x})$ is the potential of the optical lattice, $V_T(\mathbf{x})$ is the trapping potential and a_s is the s-wave scattering length. For single atoms, energy

eigenfunctions are Bloch wave functions. If the energies involved are much less than the excitation energy to the second band then a single band model is justified. Wave functions localized at an individual lattice site, $w(\mathbf{x})$, which are called Wannier wave function are introduced and the energy eigenfunctions are expanded in the Wannier basis

$$\Psi(\mathbf{x}) = \sum_i b_i w(\mathbf{x} - \mathbf{x}_i).$$

The Bose-Hubbard Hamiltonian follows from this expansion, where the hopping energy between matrix elements is given by

$$J = \int d^3x w^*(\mathbf{x} - \mathbf{x}_i) \left[-\frac{\hbar^2}{2m} \nabla^2 + V_0(\mathbf{x}) \right] w(\mathbf{x} - \mathbf{x}_j),$$

the on-site repulsion is

$$U = \frac{4\pi a_s \hbar^2}{m} \int d^3x |w(\mathbf{x})|^4,$$

and the energy offset due to the lattice is

$$\varepsilon_i = \int d^3x V_T(\mathbf{x}) |w(\mathbf{x} - \mathbf{x}_i)|^2 \approx V_T(\mathbf{x}_i).$$

In the last step the trapping potential is assumed to be approximately constant over the spatial variation of a single Wannier function.

One expects a zero-temperature quantum phase transition from the superfluid (SF) state to the Mott insulator (MI) state and as the depth of the lattice is increased for integer fillings. The SF state supports long-range phase coherence while in the MI state, the atoms are localized and there is no phase coherence. This transition was observed in ultracold atoms by Greiner *et al.* (2002).

1.6.3 Atom Chips

Quasi-one-dimensional systems have also been realized on atom chips. The miniaturization and integration of matter-wave optics has led to the development of atom chips (Folman *et al.*, 2002; Fortagh and Zimmermann, 2007). It is now possible to confine, manipulate and measure atoms on a single device using electric, magnetic and optical fields. Bose-Einstein condensation has been created in magnetic microtraps (Ott *et al.*, 2001; Hansel *et al.*, 2001). The traps are highly elongated and the one-dimensional regime is realized when the transverse confining potential, $\hbar\omega_{\perp}$ is much greater than the relevant energy scales of the system, the thermal energy, $k_B T$ and chemical potential, μ . Esteve *et al.* (2006) realized both the ideal Bose Gas as well as the quasicondensate in a quasi-one-dimensional trap on an atom chip. Theoretical work has investigated the transition from the 1D Bose gas to the quasicondensate (Bouchoule *et al.*, 2007) as well as the growth of the quasicondensate (Proukakis *et al.*, 2006). Other experiments in one-dimensional traps include the demonstration of the first phase-preserving matter-wave beam-splitter on an atom chip (Schumm *et al.*, 2005) and of an atom Michelson interferometer on an atom chip (Wang *et al.*, 2005).

1.6.4 Classical Field Model of Bose Gas

In this thesis we numerically study the Bose-Hubbard model, presented earlier, within the classical-field approximation. The classical field approximation is equivalent to the first-order mean-field approximation. In this section we outline the validity of the classical field approach for studying the dynamics of interacting Bose gases.

The dynamics of a BEC can be well-described by the Gross-Pitaevskii equation (GPE) (Gross, 1961; Pitaevskii, 1961)

$$i\hbar \frac{\partial \Psi(\mathbf{r}, t)}{\partial t} = \left(-\frac{\hbar^2}{2m} \nabla^2 + V(\mathbf{r}) + g|\Psi(\mathbf{r}, t)|^2 \right) \Psi(\mathbf{r}, t),$$

where the coupling constant is given by $g = 4\pi\hbar^2 a/m$ (a = scattering length, m = mass). The Gross-Pitaevskii equation is a mean-field approximation and is equivalent to the continuous nonlinear Schrödinger equation which is integrable. The GPE has been used extensively to describe the dynamics of the condensate in three-dimensional systems.

Several studies have looked at the applicability of the mean-field or classical field description beyond the dynamics of the condensate. Kagan and Svistunov studied the evolution of an interacting Bose gas from a strongly non-equilibrium state towards condensation. They demonstrated that the classical-field description accurately describes a weakly interacting Bose gas *in the absence of a condensate* provided that the occupation numbers of the initially occupied state are much greater than unity (Kagan and Svistunov, 1997). Given this condition, the time evolution of a state can be accurately described by the diagonal elements of the statistical matrix in the coherent state representation.

Castin studies the classical field model for one-dimensional weakly interacting Bose gases (Castin, 2004). The classical field model is generated by replacing the quantum mechanical operator $\hat{\psi}(z)$ with a complex field $\psi(z)$. For the interacting Bose gas, the state of the classical field is governed by a single parameter,

$$\chi = \frac{\hbar^2 \rho^2}{mk_B T} \frac{\rho g}{k_B T}$$

where ρ is the mean density, T is the temperature, m is the mass, and g is the interaction parameter. Castin calculates the correlation functions $g_1(z) = \langle \hat{\psi}^\dagger(z) \hat{\psi}(0) \rangle$ and $g_2(z) =$

$\langle \hat{\Psi}^\dagger(z)\hat{\Psi}^\dagger(0)\hat{\Psi}(0)\hat{\Psi}(z) \rangle$. The contrast, $C \equiv g_2(0)/g_1^2(0)$ drops off quickly as χ increases and then slowly approaches unity for $\chi \gg 1$, indicating that density fluctuations are suppressed for large χ .

The conditions for the validity of the classical field model for $\chi \gg 1$ are summarized as :

1. large occupation numbers, $k_B T \gg \mu$
2. gas is degenerate, $\rho\lambda \gg 1$
3. weakly interacting regime, $\rho\xi \gg 1$

where $\xi = (\hbar/m\mu)^{1/2}$ is the healing length. Note that the condition that $\chi \gg 1$ automatically satisfies conditions (2) and (3).

In summary, the classical field model is a good approximation for weakly-interacting particles of a degenerate gas for large occupation number, in which case fluctuations are suppressed.

Mishmash and Carr study the correspondence between the mean-field and the fully quantum BHM in the dynamics of atoms in 1D optical lattices (Mishmash and Carr, 2008). The mean-field BHM is equivalent to the discrete nonlinear Schrödinger equation (DNLS). They numerically investigate the analogs of dark soliton of DLNS in BHM and use the time-evolving block decimation algorithm (TEBD) developed by Vidal (Vidal, 2004) to carry out the full quantum calculations.

1.6.5 Chaos and Integrability in Quantum Systems

Access to one-dimensional systems of ultracold atoms in optical lattices has led to realization of some known integrable models and observed effects of integrability in the dynamics of these models. We focus on the effects of integrability in bosonic systems in

optical lattices. The Lieb-Liniger model is a completely integrable quantum description of one-dimensional bosons with two-body δ -interactions (Lieb, 1963; Lieb and Liniger, 1963). The Hamiltonian is

$$\hat{H} = - \sum_{i=1}^N \frac{\partial^2}{\partial x_i^2} + 2c \sum_{\langle i,j \rangle} \delta(x_i - x_j), \quad (1.13)$$

where the interaction, governed by the parameter c is repulsive. The Lieb-Liniger model has been solved via Bethe Ansatz. In the limit of infinitely strong δ -repulsions, $c \rightarrow \infty$, the hard-core bosons, also known as a Tonks-Girardeau gas, map to non-interacting fermions (Girardeau, 1960). While these models were proposed a half-century ago, the Tonks-Girardeau gas was only recently realized experimentally in Rb⁸⁷ atoms that were strongly confined in two directions in an optical lattice to create one-dimensional tubes (Paredes *et al.*, 2004). By applying a shallow lattice in the longitudinal direction, the effective mass and thus interaction strength were increased in order to reach the Tonks-Girardeau regime.

Later experiments observed the effects of integrability on thermalization in a one-dimensional Bose gas. Kinoshita *et al.* (2006) demonstrate the first experimental evidence for the lack of thermalization in a many-body system with a large number of degrees of freedom for bosons in optical lattices. A gas of interacting bosons was prepared out-of-equilibrium by applying a laser pulse to a one-dimensional Bose-Einstein condensate in an optical lattice. For both strongly- and weakly-interacting bosons, the expanded momentum distribution retains the initial double peak structure. Even with the background harmonic potential, the system is integrable in the limit of infinite-strength repulsion. It was expected that a system with finite interactions, which is believed to be non-integrable in the presence of a harmonic trap, would reach thermal equilibrium. However, the absence of thermalization occurred even for finite interactions. Figure 1.5

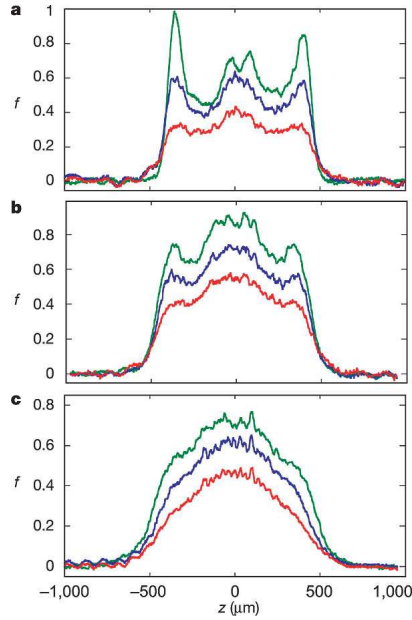


Figure 1.5: $f(p_{\text{ex}})$, momentum distribution for (a) $\gamma_0=4$, $\tau=34$ ms. $t_{\text{blue}} = 15\tau$, $t_{\text{red}} = 30\tau$ (b) $\gamma_0=1$, $\tau=13$ ms. $t_{\text{blue}} = 15\tau$, $t_{\text{red}} = 40\tau$ (c) $\gamma_0=0.62$, $\tau=13$ ms. $t_{\text{blue}} = 15\tau$, $t_{\text{red}} = 40\tau$. Green is the initial momentum distribution averaged over the first period. (Kinoshita *et al.*, 2006)

shows the expanded momentum distribution for three different coupling strengths. From the three peak structure in Fig. 1.5(a)-(b) it is clear that the gas has not thermalized for the Tonks-Girardeau limit ($\gamma_0 = 4$) and the intermediate regime ($\gamma_0 = 1$) even after thousands of collisions have occurred between atoms.

1.6.6 Constrained equilibrium

One question that arises from these experiments on hard-core bosons is: do integrable systems, which don't relax to the usual thermodynamic equilibrium distribution attain some other steady state? Numerical studies on one-dimensional hard-core bosons in a lattice addressed the relaxation dynamics of a fully-integrable quantum system (Rigol *et al.*, 2007).

The method to derive the steady-state distribution is to maximize the entropy subject to the constraints of the system, which include all of the conserved quantities (Jaynes, 1957a,b). In this approach the many-body density matrix is given by

$$\hat{\rho} = Z^{-1} \exp \left[- \sum_m \lambda_m \hat{I}_m \right]$$

where $\{\hat{I}_m\}$, $\{\lambda_m\}$ are the Lagrange multipliers which are determined by the initial conditions. This distribution is called the generalized Gibbs ensemble or fully-constrained thermodynamic ensemble.

One-dimensional hard-core bosons on a lattice can be mapped to free-fermions via a Jordan-Wigner transformation. The conserved quantities are moments of the fermionic momentum distribution. Rigol *et al.* solve analytically for the density matrix with the constraints from the fermionic momentum distribution. The results of numerical simulations confirmed that when the system is prepared in the ground state of a small box and then allowed to expand in a larger box, it reaches a steady state, which is in agreement with the analytic results for the fully constrained system, rather than the grand canonical thermodynamic distribution. Additionally for an initial state with two momentum peaks, the two peaks structure remains after many oscillations, in agreement with the experiment performed by Kinoshita *et al.* (2006).

1.7 Outline of Thesis

In this work we present a comprehensive study of chaos and thermalization in the 1D Bose-Hubbard model within the classical-field approximation. We study the threshold for chaos and its relation to thermalization. Two quantitative measures of thermalizability are compared: the Finite-time Maximal Lyapunov exponents (FTMLE) and the normalized spectral entropy (NSE). The FTMLE, averaged over phase space, converges

to the maximal Lyapunov Exponent, the standard measure of chaos. A positive MLE indicates that points that are initially close in phase-space diverge exponentially, rather than linearly. The spectral entropy measures the distance between the time-averaged momentum distribution of the numerical results and the momentum distribution predicted by thermodynamics, within the independent mode approximation. We investigate the dependence of the averaged FTMLE and normalized spectral entropy on a dimensionless nonlinearity parameter and the energy-per-particle, both of which are finite in the thermodynamic limit. The BHM is found to have a threshold for chaos which depends on the nonlinearity and the energy-per-particle. We study the size scaling of the Lyapunov exponent and normalized spectral entropy.

Furthermore we study resonances in the Bose-Hubbard model to find the Chirikov criterion for chaos. The criterion predicted by the Chirikov criterion is different from the one inferred from numerical calculations, signifying the failure of the standard Chirikov's approach.

There are at least three near-by integrable models: the Ablowitz-Ladik lattice, the continuous nonlinear Schrödinger equation and the noninteracting model. We outline the method of Inverse Scattering Transform and generate all of the integrals of motion of the closely related, fully integrable model of Ablowitz-Ladik. Furthermore, we discuss the possible role of these conserved quantities in relaxation in the BHM. We conjecture that the presense of quasi-conserved quantities may alter the scaling of the chaos criterion.

Chapter 2

Thermalization and Chaos in the 1D

Bose-Hubbard Model

2.1 Introduction

One of the fundamental assertions of statistical mechanics is that the time average of a physical observable is equivalent to the average over phase-space, with microcanonical measure. A system for which this is true is said to be ergodic and one can calculate dynamical properties of the system from static phase-space averages. While this is believed to be true, because of the success of statistical mechanics in accurately predicting experimental results, many open questions remain. Is ergodicity sufficient to ensure the accuracy of statistical mechanical predictions for times that are relevant for observations?

2.2 BHM: Hamiltonian and Equations of Motion

We study the dynamics of an interacting one-dimensional Bose gas on a lattice (1D Bose-Hubbard model (BHM)) (Jaksch *et al.*, 1998) with periodic boundary conditions in the classical field approximation. The Hamiltonian of the system of interest can be studied in many different forms through canonical transformations. Each equivalent representation has a different Hamiltonian, canonical coordinates and equations of motion. A well-chosen canonical transformation can pose the problem in a way which is more

intuitive. Here we present three different representations: The real-space representation, the momentum-space representation in terms of classical fields and the action-angle representation.

2.2.1 Real-Space Hamiltonian

In real space, the Hamiltonian is

$$H = -J \sum_s \tilde{\Psi}_s^* (\tilde{\Psi}_{s+1} + \tilde{\Psi}_{s-1}) + \frac{\mu_0 N_s}{2} \sum_s |\tilde{\Psi}_s|^4. \quad (2.1)$$

The equations of motion are given by

$$\frac{\partial}{\partial t} \tilde{\Psi}_s = -\frac{i}{\hbar} \frac{\partial H}{\partial \tilde{\Psi}_s^*} = -i \left[-J (\tilde{\Psi}_{s+1} + \tilde{\Psi}_{s-1} - 2\tilde{\Psi}_s) + \mu_0 N_s |\tilde{\Psi}_s|^2 \tilde{\Psi}_s \right] \quad (2.2)$$

$$\frac{\partial}{\partial t} \tilde{\Psi}_s^* = \frac{i}{\hbar} \frac{\partial H}{\partial \tilde{\Psi}_s} = i \left[-J (\tilde{\Psi}_{s+1}^* + \tilde{\Psi}_{s-1}^* - 2\tilde{\Psi}_s^*) + \mu_0 N_s |\tilde{\Psi}_s|^2 \tilde{\Psi}_s^* \right], \quad (2.3)$$

and the canonical pairs are $Q_s = \psi_s$, $P_s = i\hbar\psi_s^*$. These equations of motion are equivalent to the discrete nonlinear Schrödinger equation (DNLS). The time-evolution of the fields is carried out in real-space in all of the calculations.

2.2.2 Momentum-Space Representation

Another set of canonical coordinates, the momentum-space fields, $\Psi_n = \Psi(k_n)$, are related to the real-space field $\tilde{\Psi}_s = \tilde{\Psi}(x_s)$, by

$$\begin{aligned} \Psi_n &= \frac{1}{\sqrt{N_s}} \sum_{s=1}^{N_s} \tilde{\Psi}_s e^{-ik_n \cdot x_s} \\ \tilde{\Psi}_s &= \frac{1}{\sqrt{N_s}} \sum_{n=1}^{N_s} \Psi_n e^{ik_n \cdot x_s}. \end{aligned} \quad (2.4)$$

where $k_n = 2\pi n/L$ and $x_s = sa$.

In the momentum-space representation, the Hamiltonian is

$$H = \sum_m \left(\hbar\omega_m |\Psi_m|^2 - \frac{\mu_0}{2} |\Psi_m|^4 \right) + \frac{\mu_0}{2} \sum_{l,i,j} \Psi_l^* \Psi_i^* \Psi_j \Psi_{l+i-j} \quad (2.5)$$

where the sum carries the restrictions: $j \neq l, i$. Several canonical transformations have been performed in order to write the Hamiltonian in this form.

The canonical pairs are $Q_n = \Psi_n$, $P_n = i\hbar\Psi_n^*$ and the equations of motion are given by

$$\frac{\partial}{\partial t} \Psi_n = -\frac{i}{\hbar} \frac{\partial H}{\partial \Psi_n^*} = -i \left(\omega_n - \frac{\mu_0}{\hbar} |\Psi_n|^2 \right) \Psi_n - i \frac{\mu_0}{\hbar} \sum_{i,j} \Psi_i^* \Psi_j \Psi_{n+i-j} \quad (2.6)$$

$$\frac{\partial}{\partial t} \Psi_n^* = -\frac{i}{\hbar} \frac{\partial H}{\partial \Psi_n} = -i \left(\omega_n - \frac{\mu_0}{\hbar} |\Psi_n|^2 \right) \Psi_n^* - i \frac{\mu_0}{\hbar} \sum_{i,j} \Psi_i^* \Psi_j \Psi_{n+i-j} \quad (2.7)$$

with the restrictions $j \neq n, i$ on the sums and the indices span the range $n, i, j = 0, \pm 1, \pm 2, \dots, \pm \frac{N_s-1}{2}$ (N_s is supposed to be odd).

The bare frequency of each momentum mode is given by

$$\hbar\omega_n = \frac{\hbar^2}{ma^2} \left(1 - \cos \left(\frac{2\pi n}{N_s} \right) \right) = 2J \left(1 - \cos \left(\frac{2\pi n}{N_s} \right) \right). \quad (2.8)$$

The coupling constant is $\mu_0 = UN_a/N_s$. Here J and U are the nearest-neighbor site-hopping and on-site repulsion constants of the standard Bose-Hubbard model respectively, and N_a is the number of atoms.

Time propagation is performed in real space, while the output and analysis of the numerical calculations focus on the momentum fields.

Table 2.1: List of Parameters and Variables

a = lattice spacing
J = B-H nearest-neighbor kinetic energy
κ = nonlinearity parameter
L = length of lattice
μ_0 = coupling constant
N_s = number of lattice sites = number of momentum modes
N_a = number of atoms
τ_{tal} = Talbot time
U = B-H on-site repulsion energy
$\hbar\tilde{\omega}_1$ = ground state energy of non-interacting model with quadratic dispersion
ξ = size-dependent nonlinearity parameter

2.2.3 Action-Angle Representation

Equivalently, the momentum-space Hamiltonian can be written in terms of action-angle variables, by performing several canonical transformation on the momentum-space representation. It is this action-angle representation that will be the starting point of the resonant approximations and studies of individual resonances. The Hamiltonian is

$$H = \sum_m \left(\omega_m I_m - \frac{\mu_0}{2\hbar^2} I_m^2 \right) + \frac{\mu_0}{2\hbar^2} \sum_{m,l,i,j} (I_m I_l I_i I_j)^{1/2} e^{i(\theta_m + \theta_l - \theta_i - \theta_j)} \quad (2.9)$$

where the sum carries the restrictions: $m + l = i + j$; $m \neq i, j$; $l \neq i, j$. The momentum wavefunction canonical variables, $\{(\psi_k, i\hbar\psi_k^*)\}$ are related to the action-angle canonical variables $\{(I_k, \theta_k)\}$ by $\psi_k = \sqrt{\frac{I_k}{\hbar}} e^{-i\theta_k}$, $\psi_k^* = \sqrt{\frac{I_k}{\hbar}} e^{i\theta_k}$. In this form, the Hamiltonian can

be seen as the sum of an integrable term and a perturbation, $H(\{I_k, \theta_k\}) = H_0(\{I_k\}) + V(\{I_k, \theta_k\})$, where the integrable Hamiltonian is

$$H_0 = \sum_m \left(\omega_m I_m - \frac{\mu_0}{2\hbar^2} I_m^2 \right) = \sum_m \left(\hbar\omega_m |\psi_m|^2 - \frac{\mu_0}{2} |\psi_m|^4 \right). \quad (2.10)$$

Throughout the wavefunction ψ_n is normalized to unity: $\sum_n |\psi_n|^2 = 1$.

Dimensionless nonlinearity parameter We define the dimensionless nonlinearity parameter,

$$\kappa \equiv \frac{\mu_0}{J} \equiv \frac{U(N_a/N_s)^2}{J(N_a/N_s)} \quad (2.11)$$

whose physical meaning is the ratio between the typical interaction energy per site $U(N_a/N_s)^2$ and the kinetic energy per site JN_a/N_s . Note that this parameter governs both the strength of the nonlinearity and the strength of the perturbation from the integrable Hamiltonian (2.10).

In Tables 2.1 and 2.2, variables are listed and the relationship between relevant parameters are summarized.

2.2.4 Validity of the Classical-Field Theory

Based on the studies of the validity of the classical-field theory for Bose gases (Castin, 2004; Kagan and Svistunov, 1997) discussed earlier, the classical-field approximation will apply for the lattice site occupations satisfying

$$\frac{N_a}{N_s} \gg \max(\kappa, 1) \max \left[\left(\frac{N_s}{\Delta n} \right), 1 \right],$$

Table 2.2: Relationship between Parameters

$\hbar\tilde{\omega}_1 = \frac{\hbar^2}{2m} \left(\frac{2\pi}{L} \right)^2 = J \left(\frac{2\pi}{N_s} \right)^2$
$\tau_{\text{tal}} = \frac{2\pi}{\tilde{\omega}_1}$
$\mu_0 = \frac{gN_a}{L}$
$J = \frac{\hbar^2}{2ma^2}$
$U = \frac{g}{a} = \mu_0 \frac{N_s}{N_a}$
$U/J = \frac{2mag}{\hbar^2} = \frac{2mL^2}{\hbar^2 N_s N_a} \mu_0$
$\kappa = \frac{\mu_0}{J} \equiv \frac{U(N_a/N_s)^2}{J(N_a/N_s)}$
$\xi \equiv \frac{\mu_0}{\hbar\tilde{\omega}_1} = \kappa \left(\frac{N_s}{2\pi} \right)^2$
$\hbar\omega_n = \frac{\hbar^2}{ma^2} \left[1 - \cos \left(\frac{2\pi n}{N_s} \right) \right] = 2J \left[1 - \cos \left(\frac{2\pi n}{N_s} \right) \right]$

where Δn is the typical width of the momentum distribution. We note that the Mott regime, $N_a = \text{integer} \times N_s$, $\Delta n = N_s$, $U/J \geq 2.2N_a/N_s$ (Hamer and Kogut, 1979), lies well outside of the above criteria.

2.2.5 Nearby Integrable Models

There are several known intergrable models that are limiting cases of the BHM. These include

1. **Continuous Nonlinear Schrödinger Equation:** In the continuum limit, the 1D BHM becomes

$$H = \int_0^L dz \Psi^* \left\{ -\frac{\hbar^2}{2m} \Delta \right\} \Psi + \int_0^L dz \frac{1}{2} g |\Psi|^4.$$

2. **Linear Model:** In the non-interacting limit, $\kappa \rightarrow 0$, the 1D BHM becomes a sum of harmonic oscillators

$$H = \sum_m \hbar \omega_m |\psi_m|^2.$$

3. **Independent Mode:** If the interacting term vanishes, the 1D BHM becomes a sum of decoupled nonlinear oscillators,

$$H = \sum_m \hbar \omega_m |\psi_m|^2 - \frac{\mu_0}{2} |\psi_m|^4$$

with nonlinear frequencies given by $\Omega_m = \hbar \omega_m - \frac{\mu_0}{2} |\psi_m|^2$.

4. **Ablowitz-Ladik Lattice:** An alternate discretization of the NLS yields the Ablowitz-Ladik lattice, with Hamiltonian,

$$H = - \sum_n (q_n q_{n+1}^* + q_n^* q_{n+1}) - \frac{4}{\sigma} \sum_n \ln \left(1 - \frac{\sigma}{2} |q_n|^2 \right),$$

which will be discussed further in later chapters.

2.3 Time Dynamics

First we study the time dynamics of the 1D BHM on a lattice with $N_s = 21$ modes. The system is prepared in a state that is narrowly distributed in momentum space and evolves according to the classical equations of motion. Initially the lowest three momentum

modes are occupied, the minimum number of modes required by selection rules for non-trivial processes leading to population of initially unoccupied modes. In Fig. 2.1,

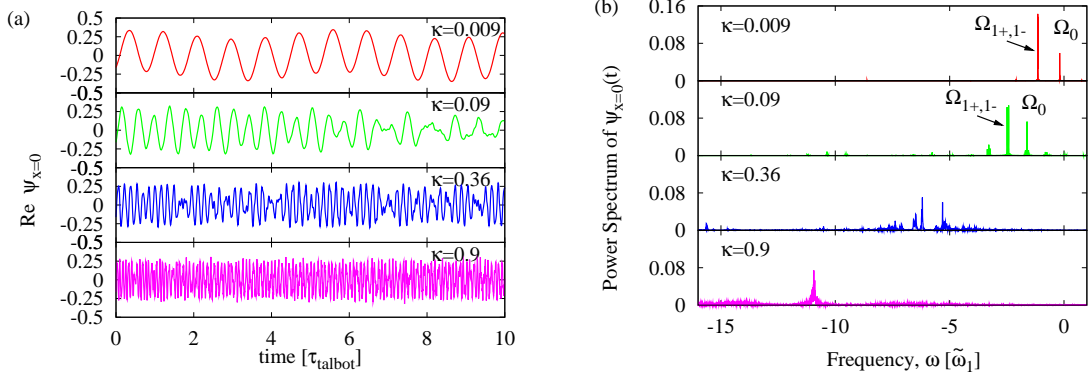


Figure 2.1: Time evolution of the wavefunction at the center of the box for a typical run for $\kappa = 0.009, 0.09, 0.36, 0.9$ with identical initial conditions. (a) Time dynamics of the real part of the wavefunction, $\text{Re } \psi_{x=0}(t)$. (b) Frequencies of the real-space wavefunction, $|\text{FT}[\psi_{x=0}(t)]|^2$. For $\kappa = 0.009, 0.09$ the descendants of the unperturbed frequencies generated by the first, “integrable” term of the Hamiltonian (2.5) are labeled.

the time dynamics and power spectrum of the wavefunction at the center of the box, $\psi_{x=0}(t)$, are plotted for various interaction strengths for a typical initial state. As seen in Fig. 2.1(a), the time evolutions of the zero momentum mode is quasi-periodic for weak interactions, with a few easily identifiable frequencies entering the dynamics, which is confirmed by the power spectrum in Fig. 2.1(b). As the nonlinearity increases, more frequencies determine the dynamics and for sufficiently large nonlinearity the motion loses its quasi-periodic character and appears to be chaotic.

The clear distinction between quasi-periodic and seemingly chaotic behavior of the time dynamics leads to the following questions:

1. Is the motion really chaotic?
2. If it is, where is the chaos threshold as one increases the nonlinearity κ ?
3. When chaotic, does the system reach thermal equilibrium?

In order to answer these questions, it is necessary to define appropriate measures of chaos and thermalization.

2.4 Chaos: Calculating Lyapunov Exponents

The standard signature of the chaotic nature of a region in phase-space is that the separation between trajectories that are initially close grows exponentially with time, for typical trajectories, as captured by a positive maximal Lyapunov exponent (MLE). In regular regions the separation grows linearly (Chirikov, 1979), resulting in zero MLE. As we increase κ in our system, we expect the phase space to change from being dominated by regular regions for small κ to being dominated by chaotic regions for large κ . In the present section, we use the MLEs to quantify this transition to chaos, which, as we will see in the subsequent section, coincides with a relatively broad change from unthermalizability to complete thermalizability.

Consider two trajectories $\mathbf{x}(t)$ and $\tilde{\mathbf{x}}(t)$ with initial points \mathbf{x}_0 and $\tilde{\mathbf{x}}_0$, respectively. The separation $\delta\mathbf{x}(t) = \tilde{\mathbf{x}}(t) - \mathbf{x}(t)$ initially satisfies a linear differential equation, and the duration of this linear regime grows without bound as the initial separation $\tilde{\mathbf{x}}_0 - \mathbf{x}_0$ goes to zero. The finite-time maximal Lyapunov exponent (FTMLE) corresponding to the phase-space point \mathbf{x}_0 (Eckhardt and Yao, 1993; Voglis and Contopoulos, 1994) is given by

$$\lambda_{t_{\text{fin}}}(\mathbf{x}_0) = \lim_{\tilde{\mathbf{x}}_0 \rightarrow \mathbf{x}_0} \frac{1}{t_{\text{fin}}} \ln \frac{\|\tilde{\mathbf{x}}(t_{\text{fin}}) - \mathbf{x}(t_{\text{fin}})\|}{\|\tilde{\mathbf{x}}_0 - \mathbf{x}_0\|}. \quad (2.12)$$

The limit $t_{\text{fin}} \rightarrow \infty$ gives the MLE, $\lambda_{\infty}(\mathbf{x}_0)$, but the FTMLE are themselves of intrinsic interest (Eckhardt and Yao, 1993; Voglis and Contopoulos, 1994; Contopoulos *et al.*, 1978; Contopoulos and Voglis, 1997). We chose a convenient quantum mechanical

metric, $\|\tilde{\mathbf{x}} - \mathbf{x}\|^2 = \sum_n |\tilde{\psi}_n - \psi_n|^2$. This metric becomes Euclidian under the canonical transformation

$$\begin{aligned} Q_n &= (2\hbar)^{1/2} \text{Re}(\psi_n) \\ P_n &= (2\hbar)^{1/2} \text{Im}(\psi_n) \\ \|\tilde{\mathbf{x}} - \mathbf{x}\|^2 &= \frac{1}{2\hbar} \sum_n [(Q'_n - Q_n)^2 + (P'_n - P_n)^2] \end{aligned}$$

where the sum runs from $n = -(N_s - 1)/2$ to $n = (N_s - 1)/2$.

2.5 Thermalization: Calculating Spectral Entropy

In order to measure thermalization, it is necessary to make thermodynamic predictions and compare the dynamics from the propagation of the equations of motion, with the thermodynamic state. In this section a method for calculating the thermodynamic state, within the Hartree-Fock approximation, is laid out. A full account is given in Appendix A. Additionally the spectral entropy is defined, which is a quantitative measure of the difference between the time-averaged dynamical state and the expected thermodynamic state.

2.5.1 Conserved Quantities

A treatment of the thermodynamic state must take into account all conserved quantities. The known conserved quantities of the 1D BHM are the energy and norm. Conservation of norm, $\sum_{n=1}^N |\psi_n|^2$, is associated with $U(1)$ symmetry in the real/imaginary plane represented by the transformation $\{\psi_n, \psi_n^*\} \rightarrow \{\psi_n e^{i\theta}, \psi_n^* e^{-i\theta}\}$. Unlike the continuous NLSE, the total momentum is not conserved.

2.5.2 Hartree-Fock

Within Hartree-Fock the form of the density distribution function is taken to be Gaussian and the thermal expectation value of the Grand Potential,

$$\langle F \rangle = \langle H \rangle - T \langle S \rangle - \mu \langle N_a \rangle, \quad (2.13)$$

is minimized, where N_a is the norm. The density distribution function with two-body interactions has the form,

$$\sigma_{HF} = \frac{1}{Z} \exp \left(\sum_{n,n'} -\hbar \alpha_{n,n'} \psi_n \psi_{n'}^* \right) = \frac{1}{Z} \exp \left(- \sum_n \alpha_n I_n \right). \quad (2.14)$$

We use the independent mode approximation so that in the second step, the off-diagonal elements are taken to be zero. The α_n coefficients are unknown and are determined by the condition of minimizing the grand potential. The density distribution function is normalized, so that the integration of σ_{HF} over all of phase space is 1, by

$$Z = \frac{1}{(2\pi\hbar)^N} \int d^N \theta \int d^N I e^{-\sum_n \alpha_n I_n} = \prod_{i=1}^N \frac{1}{\hbar \alpha_i}. \quad (2.15)$$

The expectation value of each term in the Grand Potential is calculated, using the Hartree-Fock density distribution function σ_{HF} . The expectation value of a generic observable is given by

$$\langle O \rangle = \frac{1}{(2\pi\hbar)^N} \int d^N \theta \int d^N I O(\{I_n, \theta_n\}) \sigma_{HF} \quad (2.16)$$

$$= \frac{1}{(2\pi)^N} \prod_{i=1}^N \alpha_i \int d^N \theta \int d^N I O e^{-\sum_n \alpha_n I_n} \quad (2.17)$$

The expectation values of the relevant observables are listed below.

Norm

$$\langle N_a \rangle = \left\langle \frac{1}{\hbar} \sum_n I_n \right\rangle = \sum_{n=1}^N \frac{1}{\hbar \alpha_n} \quad (2.18)$$

Hamiltonian - Kinetic Term

$$\langle H_0 \rangle = \left\langle \sum_n I_n \omega_n \right\rangle = \sum_{n=1}^N \frac{\omega_n}{\alpha_n} \quad (2.19)$$

Hamiltonian - Interaction Term

$$\langle H_I \rangle = \left\langle \frac{\mu_0}{2\hbar^2} \sum_{m,p,q,r} (I_m I_p I_q I_r)^{1/2} \delta_{m+p,q+r} e^{-i(\theta_m + \theta_p - \theta_q - \theta_r)} \right\rangle = \frac{\mu_0}{\hbar^2} \sum_{m,p} \frac{1}{\alpha_m} \frac{1}{\alpha_p} \quad (2.20)$$

Entropy

$$S = - \frac{1}{(2\pi\hbar)^N} \int d^N \theta \int d^N I \sigma_{HF} \log \sigma_{HF} = N_s - \sum_j \log(\hbar \alpha_j) \quad (2.21)$$

2.5.3 Minimization of the Grand Potential

The thermal expectation value of the Grand Potential within Hartree-Fock is given by

$$\langle F \rangle = \sum_m \frac{\omega_m}{\alpha_m} + \frac{\mu_0}{\hbar^2} \sum_{m,p} \frac{1}{\alpha_m} \frac{1}{\alpha_p} - T \left(N_s - \sum_m \log(\hbar \alpha_m) \right) - \mu \sum_m \frac{1}{\hbar \alpha_m} \quad (2.22)$$

Taking the variation with respect to α_n , and setting it equal to zero gives

$$\frac{\delta \langle F \rangle}{\delta \alpha_n} = - \frac{\omega_n}{\alpha_n^2} - 2 \frac{\mu_0}{\hbar^2} \frac{1}{\alpha_n^2} \sum_m \frac{1}{\alpha_m} + \frac{T}{\alpha_n} + \frac{\mu}{\hbar \alpha_n^2} = 0. \quad (2.23)$$

Using $\sum_m \alpha_m^{-1} = \hbar N_a$ and solving for α_n ,

$$\alpha_n = \frac{1}{\hbar T} [\hbar \omega_n + 2\mu_0 N_a - \mu] \quad (2.24)$$

The thermal expectation values of the occupation of momentum mode n become

$$\langle I_n \rangle = \frac{1}{\alpha_n} = \frac{\hbar T}{\hbar \omega_n + 2\mu_0 N_a - \mu}. \quad (2.25)$$

In general, the coefficients μ and T are unknown and are determined by imposing constraints on the norm and energy, which come from the dynamical code. The constraints are

$$\begin{aligned} N_a = \langle N_a \rangle &= \frac{1}{\hbar} \sum_n \langle I_n \rangle \\ E_T = \langle H \rangle &= \sum_n \omega_n \langle I_n \rangle + \frac{\mu_0}{\hbar^2} \sum_{m,n} \langle I_m \rangle \langle I_n \rangle = \sum_n \omega_n \langle I_n \rangle + \mu_0 N_a^2 \end{aligned} \quad (2.26)$$

Beginning with the expression for $\langle I_n \rangle$, we can solve for T in terms of μ , N_a and energy,

$$T = \omega_n \langle I_n \rangle + 2 \frac{\mu_0}{\hbar} N_a \langle I_n \rangle - \frac{\mu}{\hbar} \langle I_n \rangle. \quad (2.27)$$

Summing over n ,

$$T = \frac{1}{N_s} [E_k + 2\mu_0 N_a^2 - \mu N_a] \quad (2.28)$$

where $E_k \equiv \sum_n \omega_n \langle I_n \rangle$. This expression for T can be substituted back into the constraints to reduce the system to two equations with two unknowns. Using the expression for temperature and normalization condition, a single constraint remains to be solved,

$$\frac{1}{N_s} \sum_n \frac{[E_k + 2\mu_0 N_a^2 - \mu N_a]}{[\hbar \omega_n + 2\mu_0 N_a - \mu]} - N_a = 0. \quad (2.29)$$

The Hartree-Fock approximation is known to overestimate the interaction energy in the regime of strong interactions. For sufficiently large μ_0 , the Hartree-Fock interaction energy, $\mu_0 N_a^2$ becomes greater than the total energy resulting in negative kinetic energy,

where the kinetic energy is $E_k = E_T - \mu_0 N_a^2$. For this reason, we determine the temperature T and the chemical potential μ using the time-averaged numerical kinetic energy (along with the norm) instead of the total energy. The quantity E_k in the thermal distribution is fixed to the time-averaged kinetic energy of the final state from the dynamical code. We fix the norm to its numerical value, and subsequently solve iteratively for the norm to find all parameters. In this way, the total energy is never used in the constraints.

Additionally the solutions must satisfy the physical constraint that $I_n \geq 0$ for all n , which leads to bounds on μ . For $T > 0$, the condition such that the denominator is greater than zero for all n , is $\hbar\omega_n + 2\mu_0 N_a - \mu > 0$, which leads to an upper bound for μ , $\mu < 2\mu_0 N_a$. There is a critical kinetic energy that corresponds to infinite temperature, which leads to equal population of all the modes, $\langle I_n \rangle = \hbar N_a / N_s$. The critical kinetic energy, which separates the positive and negative temperature regime can be calculated as $E_{k-cr} = \sum_n \frac{N_a}{N_s} \hbar\omega_n = \frac{N_a}{N_s} \sum_n 2J [1 - \cos(\frac{2\pi n}{N})] = 2J N_a$. For $E_k > E_{k-cr}$ the temperature is negative, and the lower bound on μ is $\hbar\omega_n + 2\mu_0 N_a - \mu < 0$ for all n or $\mu > 4J + 2\mu_0 N_a$. Close to the critical kinetic energy, both the temperature and the chemical potential diverge. By expanding the norm in powers of $\omega_n / (\mu - 2\mu_0 N_a)$, an estimate for the chemical potential when $E_k = E_{k-cr} \pm \varepsilon$ is $\mu \approx 2\mu_0 + E_{k-cr} \pm E_{k-cr}^2 / (2\varepsilon)$. The temperature and the chemical potential were computed individually for each initial condition used.

In Fig. 2.2, the initial and time-averaged momentum distributions of a representative state are plotted for $\kappa = 0.09, 0.36$ and 0.9 , along with the thermal Hartree-Fock predictions, $\langle |\psi_n|^2 \rangle = (T / N_a) / (\hbar\omega_n + 2\mu_0 N_a - \mu)$.

2.5.4 Spectral Entropy

For coupled anharmonic oscillators, as in the FPU study, energy equipartition among the normal momentum modes signified thermalization. In the BHM, the additional

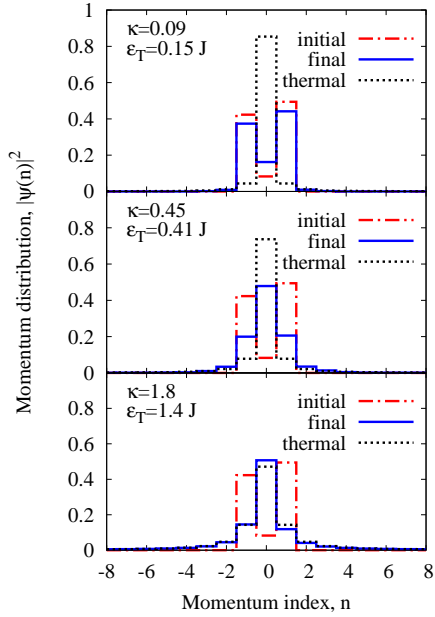


Figure 2.2: Initial, final and Hartree-Fock thermal momentum distributions for $\kappa = 0.09, 0.45, 1.8$, starting from the same initial state. $N_s = 21$. The initial state is a representative state and the final state is time-averaged. ε_T is the total energy per particle.

conservation of the norm modifies the quantity that is equipartitioned. To determine the best measure for the equipartition we use the variational Hartree-Fock Hamiltonian (Castin, 2001; Ohberg and Stenholm, 1997), $H^{\text{HF}} = \sum_n \hbar\omega_n^{\text{HF}} |\psi_n|^2$, where the set of Hartree-Fock energies $\{\hbar\omega_n^{\text{HF}}\}$ was regarded as the variational field. This procedure gives $\hbar\omega_n^{\text{HF}} = \hbar\omega_n + 2\mu_0 N_a - \mu$, where μ is the chemical potential.

The new quantity to be equipartitioned is the distribution of the Hartree-Fock energy,

$$q_n(t) = \frac{|\psi_n(t)|^2 \hbar\omega_n^{\text{HF}}}{\sum_{n'} |\psi_{n'}(t)|^2 \hbar\omega_{n'}^{\text{HF}}} \quad (2.30)$$

A quantitative measure of the distance from thermodynamic equilibrium is the spectral entropy

$$S(t) = - \sum_n q_n(t) \ln q_n(t). \quad (2.31)$$

In thermal equilibrium, q_n is equipartioned, maximizing the spectral entropy at a value $S_{\max} = \log(N_s)$. A more convenient quantity to study is the normalized spectral entropy (Livi *et al.*, 1985),

$$\eta(t) = \frac{S_{\max} - S(t)}{S_{\max} - S(0)}, \quad (2.32)$$

which is unity at $t = 0$ and vanishes as the system approaches thermal equilibrium.

2.6 Results: N=21 Sites, Three-Mode Initial Conditions

Initially, we study the FTMLE for a class of initial conditions where only the $k = 0, \pm 1$ modes are occupied. In this subspace we sample uniformly from the intersection of the microcanonical shells in energy and norm; the energy is chosen to be the infinite-temperature energy of the subsystem, and the norm is 1. For each value of κ , we sample 100 points, which we set as the initial points \mathbf{x}_0 . To each initial point we add a small random vector, as little as machine precision allows, to obtain the corresponding $\tilde{\mathbf{x}}_0$'s. Each pair we propagate for a time t_{fin} , short enough to ensure linearity of the evolution of $\delta\mathbf{x}(t)$ but long enough to be able to clearly distinguish chaotic trajectories from regular ones on a plot of $\ln \delta\mathbf{x}(t)$ versus t : the former are straight lines of positive slope, while the latter are logarithm-like (Contopoulos *et al.*, 1978). We also verify that the average of the FTMLE's over the ensemble of initial conditions does not depend on t_{fin} as long as both criteria above are satisfied. In Fig. 2.3 the averaged FTMLEs are plotted as a function of the interaction strength. There is a distinct regime with zero Lyapunov exponent for small $\kappa \lesssim 0.5$ and a strongly chaotic regime for $\kappa \gtrsim 1$ where all initial conditions have positive exponent. Next we consider the relation between chaos and thermalization in the system.

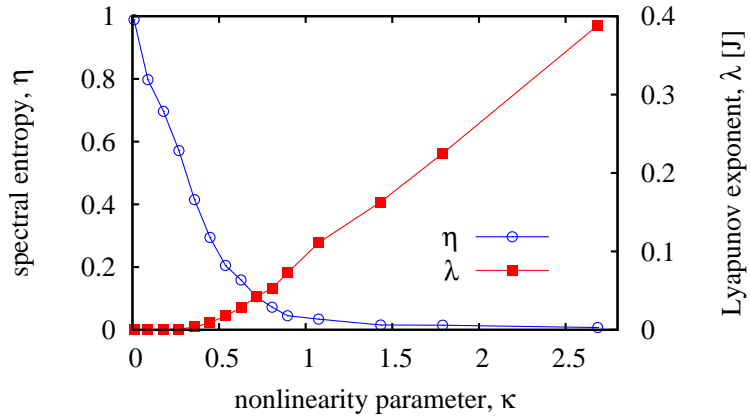


Figure 2.3: Ensemble-averaged finite-time maximal Lyapunov exponent, λ , and normalized spectral entropy, η , as a function of the nonlinearity, κ . $N_s = 21$.

In Fig. 2.3 the spectral entropy of the final time-averaged state, also averaged over 100 initial states (drawn from the same ensemble that was used for the Lyapunov exponent calculation) is plotted for each value of κ . For large nonlinearities, $\kappa \gtrsim 1$, the normalized spectral entropy goes to zero, indicating remarkable agreement between the final state and the thermal predictions. Note that this corresponds to chaos threshold observed previously. For $\kappa \lesssim .5$ the normalized spectral entropy is above .5 signifying that during the time evolution the state of the system remains close to the initial state. In the Fig. 2.4, the normalized spectral entropy is plotted versus the FTMLE for each of the 100 individual runs for $\kappa = 0.36, 0.54, 0.72, 0.9$. As seen in the plot, an individual initial state with larger FTMLE tends to have lower spectral entropy, i.e. to relax to a state which is closer to the thermal one. Beginning at $\kappa \approx 0.5$, where the averaged FTMLE is substantially non-zero, some of the initial states thermalize completely.

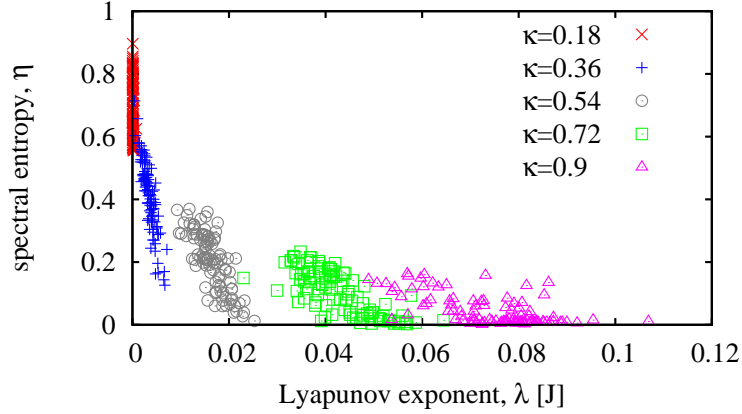


Figure 2.4: Normalized spectral entropy of the final time-averaged state versus finite-time maximal Lyapunov exponent for each of the 100 initial condition used to compute the averaged value for $\kappa = 0.36, 0.54, 0.72, 0.9$. $N_s = 21$.

Method of Calculating Spectral Entropy For an individual realization, we calculate μ_0 and T given the norm and the final kinetic energy. The spectral entropy is calculated for (1) the initial momentum distribution and (2) the final momentum distribution, $\langle |\psi_n(t)|^2 \rangle$, which is the time-averaged population of momentum mode n from the dynamical code.

2.6.1 Fluctuations

In order to confirm that the system is thermal when $\eta \rightarrow 0$, we investigate the scaling of fluctuations of the kinetic energy for large κ .

For a system with N particles and volume V in thermal equilibrium, the fluctuations of extensive observables scale with the size of the system as $V^{-1/2}$, in the thermodynamic limit, $N \rightarrow \infty, V \rightarrow \infty, N/V = \text{const}$. Consider an extensive quantity, O . The temporal fluctuations of O are given by

$$\sigma_O^2 = \langle O^2 \rangle - \langle O \rangle^2.$$

where $\langle O \rangle = \frac{1}{T} \int_{t-\Delta T/2}^{t+\Delta T/2} dt O(t)$, and the relative fluctuations are $\sigma_O / \langle O \rangle$. Now consider two identical systems, A and B , with corresponding extensive observables O_A and O_B , such that $O = O_A + O_B$. Then

$$\begin{aligned}
\sigma_O^2 &= \langle O^2 \rangle - \langle O \rangle^2. \\
&= \langle O_A^2 + O_B^2 + 2O_A O_B \rangle - \langle O_A + O_B \rangle^2 \\
&= \langle O_A^2 \rangle + \langle O_B^2 \rangle + 2\langle O_A O_B \rangle - \langle O_A \rangle^2 - \langle O_B \rangle^2 - 2\langle O_A \rangle \langle O_B \rangle \\
&= \sigma_{O_A}^2 + \sigma_{O_B}^2 + 2\langle O_A O_B \rangle - 2\langle O_A \rangle \langle O_B \rangle
\end{aligned}$$

For a system in thermal equilibrium, the two parts of the system are decorrelated, so that $\langle O_A O_B \rangle = \langle O_A \rangle \langle O_B \rangle$ and the last two terms cancel. For a general rescaling of the system $N' = \alpha N$ and the extensive observable $\langle O \rangle' = \alpha \langle O \rangle$, the fluctuations scale as $\sigma'_O = \sqrt{\alpha} \sigma_O$ and the relative fluctuations scale as $\sigma'_O / \langle O \rangle' = \alpha^{-1/2} \sigma_O / \langle O \rangle$. In contrast, consider the case where two identical systems in identical initial states are concatenated in a regime where the behavior is regular. In this case, there will be strong correlations between the two parts of the system. In the extreme case of $O_A(t) = O_B(t)$, then $\sigma_O = 2\sigma_{O_A} = 2\sigma_{O_B}$ and the relative fluctuations $\sigma'_O / \langle O \rangle'$ will be constant, independent of the size of the system.

For the system under consideration, the thermodynamic limit is taken by scaling the number of atoms and length as $N'_a = \alpha N_a$, $N'_s = \alpha N_s$, while the interaction parameter μ_0 and the lattice spacing, a , remain constant ($U, J = \text{constant}$ as well). In order to simulate the thermodynamic limit, the initial conditions are generated by concatenating α duplicates of the real-space wavefunction of the reference lattice. This is equivalent to generating an initial state with momentum modes ψ'_k , given by $\psi'_0 = \psi_0$, $\psi'_{\pm\alpha} = \psi_{\pm 1}$, from the initial state in the N_{s0} lattice, ψ_k . Generating the initial conditions in this way preserves the average energy per particle, in units of $J = \hbar^2 / 2ma^2$. A small

Table 2.3: Thermodynamic Limit and Scaling

$\hbar\tilde{\omega}'_1 = \frac{\hbar^2}{2m} \left(\frac{2\pi}{L'} \right)^2 = \frac{\hbar\tilde{\omega}_1}{\alpha^2}$
$\tau'_{\text{talbot}} = \frac{2\pi}{\tilde{\omega}'_1} = \alpha^2 \tau_{\text{talbot}}$
$\mu'_0 = \frac{gN_a}{L} = \mu_0$
$J' = \frac{\hbar^2}{2ma^2} = J$
$U' = \frac{g}{a} = U$
$U'/J' = U/J$
$\xi' = \frac{\mu_0}{\hbar\tilde{\omega}'_1} = \frac{N_a N_s U}{4\pi^2 J} = \alpha^2 \xi$
$\hbar\omega'_n = 2J' \left\{ 1 - \cos \left(\frac{2\pi n}{N'_s} \right) \right\} = 2J \left\{ 1 - \cos \left(\frac{2\pi n}{\alpha N_s} \right) \right\}$

perturbation is added to the initial wavefunction to break the symmetry associated with the translational invariance.

For the thermodynamic limit, we want to take the case where $N_a \rightarrow \infty, L \rightarrow \infty$, with $N_a/L = \text{const}$, with the lattice spacing, a , and interaction strength, g , remaining constant. Consider the case where $L' = \alpha L, N'_a = \alpha N_a$. The scaling of relevant parameters is given in Table 2.3.

We study the standard deviation of the fluctuations for systems with $N_s = 21$ sites and $\alpha=2,3,4$. To compare fluctuations for different lengths, we calculate:

$$\bar{\sigma}(N_s, N_{s0}) \equiv \frac{\sigma_{E_k(N_s)} / \overline{E_k(N_s)}}{\sigma_{E_k(N_{s0})} / \overline{E_k(N_{s0})}} \quad (2.33)$$

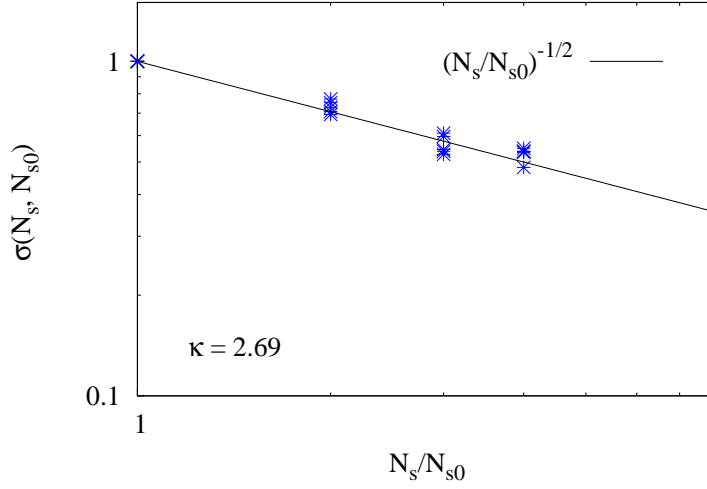


Figure 2.5: Relative fluctuations in kinetic energy. Normalized standard deviation/mean for $N_s=21, 42, 63, 84$ lattice sites and $N_0 = 21$. Data points are for five sample runs with equivalent initial conditions for different lattice sizes and $\kappa = 2.69$.

where $\sigma_E(N_s)$ and $\overline{E_k(N_s)}$ are the standard deviation and time average of the kinetic energy for a chain with N_s lattice sites. The reference lattice size is $N_{s0} = 21$ and the calculation begins after the system has already thermalized. In Fig. 2.5 we plot $\bar{\sigma}(N_s, N_{s0})$ as a function of $\alpha = N_s/N_{s0}$ for various lattice sizes on a log-log scale for $\kappa = 2.69$. As can be seen clearly from the plot, the fluctuations scale as $N_s^{-1/2}$, indicating that the fluctuations are indeed thermal.

2.7 Chaos Threshold for Different Lattice Sizes

Let us start from the notion that the parameter κ introduced in (2.11) is the only dimensionless combination of the parameters of the problem that remains finite in the thermodynamic limit, $N_s \rightarrow \infty, N_a/N_s = \text{const}, J = \text{const}, U = \text{const}$. Curiously, the chaos threshold for $N_s = 21$ is at $\kappa \approx .5$, *i.e.* $\kappa \sim 1$. Another observation comes from a related

work (Villain and Lewenstein, 2000) on chaos threshold in NLSE with hard-wall boundary conditions. The authors find that the boundary between regular and chaotic motions of momentum mode, n , is given by $(\mu_0|\psi_n|^2)/(\hbar\omega_1 n) \sim 1$, where $\hbar\omega_1$ is the lowest excitation energy, *e.g.* the energy of the first excited mode in the case of the Hamiltonian (2.5). Assuming that the shape of the momentum distribution $|\psi_n|^2$ as a function of n/N_s should be fixed in the thermodynamic limit, the left-hand side of the above relationship also remains finite. These observations lead to a conjecture that the chaos criterion involves only intensive parameters and observables, *i.e. those that are finite in the thermodynamic limit*. Our test for the above conjecture is based on the fact that for a chaotic

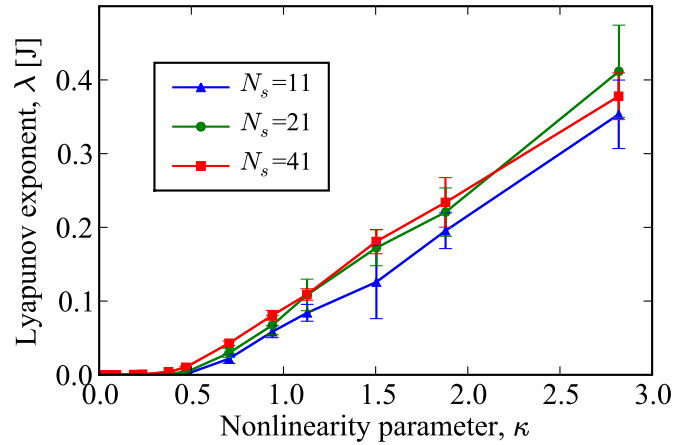


Figure 2.6: Averaged Finite Time Lyapunov exponent, $\lambda[J]$, for three different system sizes, $N_s = 11, 21, 41$. For each κ , the same energy-per-particle was used for each lattice size. The error bars represent one standard deviation.

motion the majority of the trajectories cover the whole available phase space, and as a result the LE becomes (for a given set of parameters) a function of the energy only. This implies that for the same energy-per-particle and the same nonlinearity parameter, κ , Lyapunov exponents for different lattice sizes should be similar. In Fig. 2.6 the time-averaged finite-time maximal Lyapunov exponent is plotted for three different lattices,

$N_s = 11, 21, \text{ and } 41$. For each κ , the same energy-per-particle (in units of J) is used for all three lattices.

From the plot it is indeed evident that the LE is universal with respect to the size of the lattice and that the values of the LE for $N_s = 11$ already give a very good estimate of both the value of the LE and the threshold.

2.8 Two Parametric Theory of the Chaos Threshold

The universality observed above suggests the most relevant pair of variables for mapping the chaos threshold, namely κ and the total energy-per-particle, ε_T/J . In order to test these parameters, we independently vary the nonlinearity, κ and the energy-per-particle, ε_T . For each κ and ε_T , we generate ten initial states with microcanonical weight in the reduced phase space of three ($n = 0, \pm 1$) or five ($n = 0, \pm 1, \pm 2$) momentum modes. It is necessary to generate initial states with five momentum modes $n = 0, \pm 1, \pm 2$ because there is an upper limit on the energy of an initial state with only three modes occupied. The finite-time maximal Lyapunov exponent and normalized spectral entropy are calculated for each of the ten realizations and averaged over this ensemble. For the rest of this work we will use the term Lyapunov exponent (LE) to denote the ensemble-averaged finite time maximal Lyapunov exponent and normalized spectral entropy (NSE) to denote the ensemble-averaged normalized spectral entropy, unless otherwise specified. The total data represents over 3200 runs.

In Fig. 2.7(a) contour lines of the LE for $N_s = 11$ are plotted versus the nonlinearity parameter and total energy-per-particle. One can observe an initial plateau in the LE for $\lambda \lesssim \lambda_c = 0.02$, given by the solid line. The threshold depends on both the nonlinearity and the total energy-per-particle. Based on the parameter regime investigated, it appears

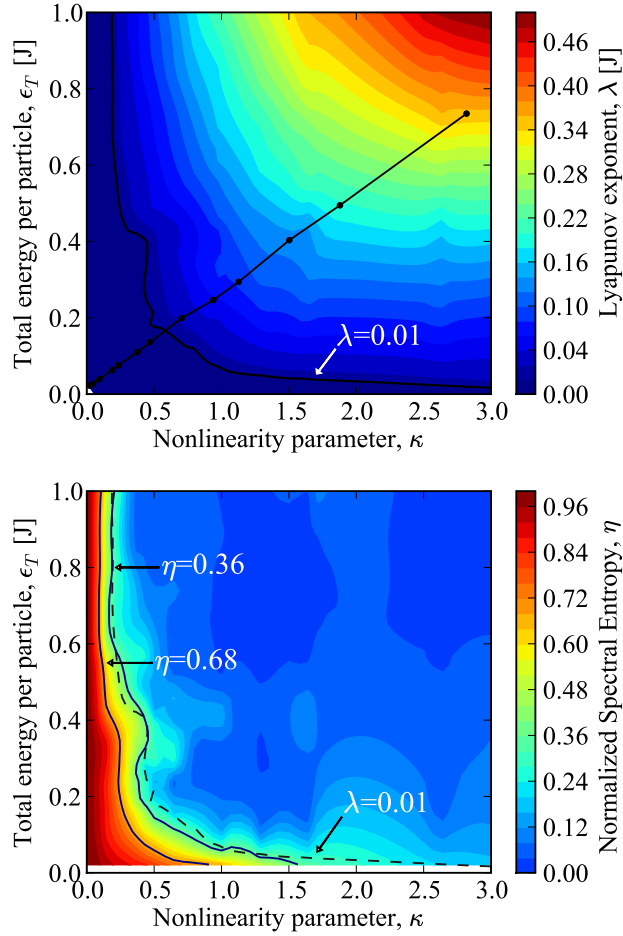


Figure 2.7: (a) Contour lines of the averaged FTMLE versus the nonlinearity, κ , and energy-per-particle, $\epsilon_T = (H - H_0)/N_a$, where H is the Hamiltonian (2.5), and $H_0 = -2J + (1/2)\mu_0$ is the ground state value of H . The solid contour line corresponds to $\lambda_c = 0.01$. The diagonal solid line represents the set of energies and nonlinearities used in Fig. 2.6. (b) Contour lines of the averaged normalized spectral entropy versus the nonlinearity, κ and energy-per-particle. Solid contour lines correspond to $\eta = 0.68$ and $\eta = 0.36$. For reference, the threshold line from the FTMLE in (a) is plotted (dashed line). $N_s = 11$.

that the threshold persists for small κ no matter how much energy is present. For small energies it is unclear whether the threshold will persist or vanish for $\kappa \gg 1$.

After crossing the critical line the LE increases with uniform slope. The critical line resembles a hyperbola with the point of closest approach to the origin at $(\kappa, \epsilon_T) \sim$

$(0.5, 0.2J)$, so that the hopping parameter J appears to be a relevant energy scale. This is probably not an accident: for $\epsilon_T \gg J$ the dispersion law ω_n begins to deviate from the (quadratic) dispersion law of the continuous NLSE with periodic boundary conditions, which is integrable.

The normalized spectral entropy was calculated for the same set of data runs and is plotted in Fig. 2.7(b). There are two solid contour lines, at $\eta = 0.68$ and $\eta = 0.36$. The second contour line at $\eta = 0.36$ follows closely the dotted line, which is the threshold from the Lyapunov exponent. It is apparent that the two plots have the same general features, and that there is a strong correspondence between the presence of chaos and thermalization in the BHM.

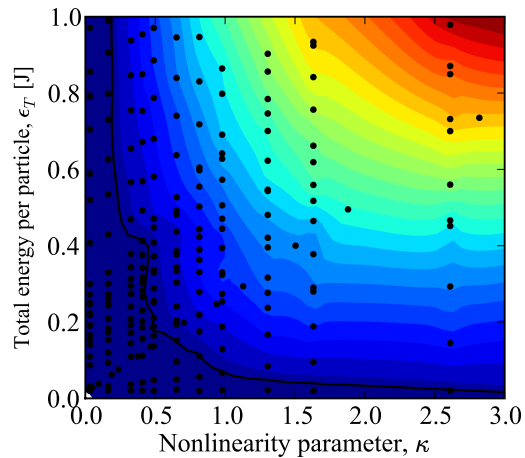


Figure 2.8: Data points used for interpolation for contour plots in Fig. 2.7 superimposed on data for Lyapunov exponent.

A few features deserve discussion.

In the region of $\eta \gtrsim 0.68, \lambda = 0$, which is enclosed by the first contour line in the NSE and the x- and y-axes, the system relaxes to a state that is closer to the thermal state even though the Lyapunov exponent is zero. The time dependence of the spectral entropy reveals that this relaxation takes place very quickly, after which the spectral

entropy remains flat for many fundamental cycles, indicating that no further relaxation will take place (See Fig. 2.11). This raises a few questions: To what state does the system relax in this region? It is possible to describe it by a constrained ensemble, where the constrained quantities are the conserved quantities of near-by integrable systems? We will return to these questions later.

For $\lambda \gg \lambda_c$, the region of strong chaos, the majority of initial states relax to the thermal state and all final states are close to the thermal. It is likely in this region, that full relaxation is not seen due to slow relaxation times and the spectral entropy would vanish for longer propagation times.

We consider the two limits, $\kappa \rightarrow 0, \epsilon_T \sim J$ and $\epsilon_T/J \rightarrow 0, \kappa \approx 3$. In the limit of small κ , the chaos threshold and NSE contour line $\eta = 0.36$ overlap and for $\kappa \rightarrow 0, \epsilon_T \gtrsim 0.6J$ converge to a value that is independent of the total energy-per-particle. For the parameter region explored there is no indication that the threshold will vanish, even for very large energies. This suggests a dependence on the ratio of the nonlinear to linear terms, similar to the critical Reynolds number found in FPU (Livi *et al.*, 1985). In the opposite limit of $\epsilon_T/J \rightarrow 0, \kappa \gtrsim 1.5$ the behavior is quite different. While the Lyapunov exponent is zero, there is significant relaxation in the momentum distribution. It is important to note that in the limit that $\epsilon_T \rightarrow 0$ the initial state approaches the state where only the $n = 0$ mode is populated, which is also the thermal state and thus the normalized spectral entropy is not well-defined in that limit. For this reason, data is plotted for $\epsilon_T > 0.02J$, the lowest energies simulated. However even for $\epsilon_T \sim 0.02J$, relaxation is visible in the momentum distributions.

In Fig. 2.9 the standard deviation of the normalized spectral entropy is plotted along with the contour lines at $\eta = 0.36$ and $\eta = 0.68$ from Fig. 2.7(b). The contour line at $\eta = 0.36$ follows closely the chaos threshold from Fig. 2.7(a). Far above the threshold, where the $\eta \rightarrow 0$, the standard deviation is also small indicating that most of the states

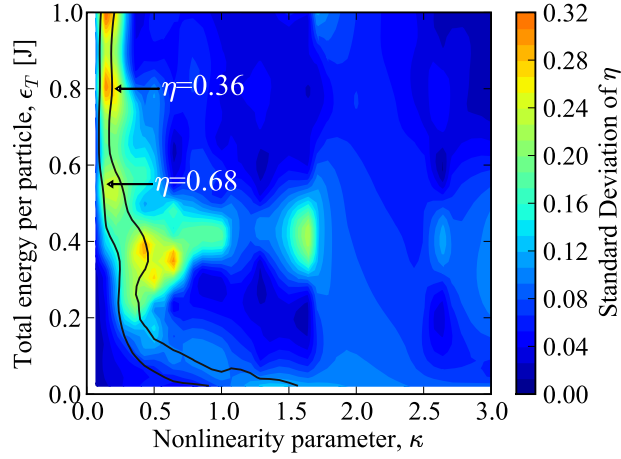


Figure 2.9: Contour lines of the standard deviation of the NSE versus the nonlinearity, κ and energy-per-particle. Solid contour line corresponds to at $\eta = 0.36$ and $\eta = 0.68$ from Fig. 2.7(b). $N_s = 11$.

thermalize, as expected. Below $\eta = 0.68$, (in the region bounded by the axes), relaxation is minimal and the standard deviation is small, indicating that most initial states will not thermalize. In the vicinity of the threshold ($\lambda = \lambda_c$, which is close to $\eta = 0.36$), the standard deviation is larger. We conjecture that this is because there is a large spread in the amount of relaxation expected for different initial states with the same parameters and/or that some states have not fully relaxed due to insufficient propagation times as a result of multiple relaxation time scales.

In Fig. 2.10 the normalized spectral entropy is plotted for three different lattice lengths, $N_s = 11, 21, 41$ for the same energy-per-particle at each κ , using the same energy values as in Fig. 2.6. While the main features are similar for the different lattice sizes, the size scaling of the NSE is not as universal as the scaling of Lyapunov exponent. For small κ 's with the same energy-per-particle, more relaxation is seen in larger lattices. This suggests that the number of modes involved in the dynamics may play a role in relaxation. In addition the standard deviation of the NSE is larger than for the Lyapunov exponents. In contrast to the size scaling of the Lyapunov exponents, the variance of

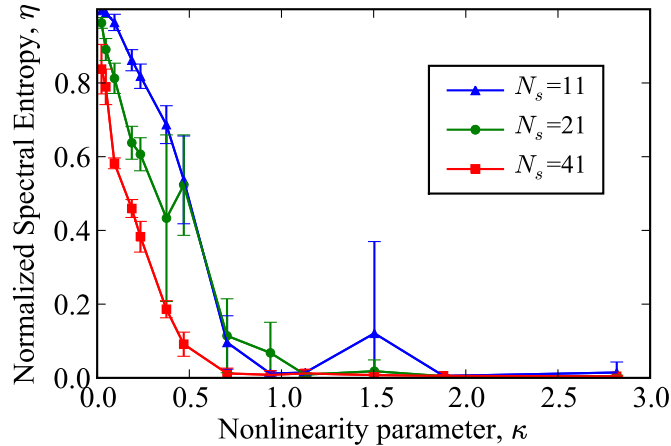


Figure 2.10: Averaged normalized spectral entropy, η , for three different system sizes, $N_s = 11, 21, 41$. For each κ , the same energy-per-particle was used for each lattice size.

the NSE increases with smaller chains. We conjecture that the large variance can be attributed to multiple relaxation scales. For example, for $N_s = 11, \kappa = 1.5$, individual states reveal that while most relax fully to the thermal state there is a single state that remains very far from thermal, which is the cause of the large variance.

The large variance of the spectral entropy is the reason that there are more features in the contour plot of the normalized spectral entropy compared with the contour plot of the Lyapunov exponent. Repeating the simulations for longer times would likely smooth some of the features of the NSE contour plot, and decrease the variance in regions where it is currently large.

2.8.1 Thermalization Times and Slow Relaxation

The time dependence of the normalized spectral entropy is plotted in Fig. 2.11 for $\kappa = 0.09$ and $\varepsilon_T = 0.081J$, which is in the non-chaotic region. The initial, thermal and final momentum distributions are plotted in the inset. The time-dependent spectral entropy is calculated from a running average over the momentum distribution and plotted in units

of τ_{tal} , the talbot time, which is the period associated with the lowest frequency of the non-interacting system with quadratic dispersion. After an initial relaxation during the first talbot time, the spectral entropy saturates and remains flat for close to $1000\tau_{\text{tal}}$. The momentum distributions confirm that there is some relaxation, but that the state remains far from the thermal state.

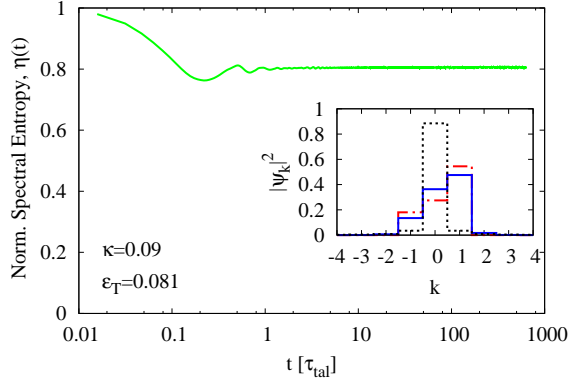


Figure 2.11: Sample time dependence of normalized spectral entropy, η . $\kappa = 0.09$, $\varepsilon_T = 0.081J$, $N_s = 21$. Inset: Initial (dashed red), final (solid blue) and thermal (dotted black) momentum distributions.

In Fig. 2.12 the time dependence of the normalized spectral entropy is plotted for two different initial states that both have $\kappa = 0.54$ and total energy $\varepsilon_T = 0.19J$. In Fig. 2.12(a) the normalized spectral entropy vanishes indicating that the state relaxes to the thermal state, which is also seen in the final momentum distribution. The normalized spectral entropy drops in several stages suggesting that there are multiple relaxations time scales. In Fig. 2.12(b), the state does not fully relax during the observed propagation time. After the initial relaxation, which is very similar to the previous case, the normalized spectral entropy slowly relaxes further but does not vanish in the observed time. Both states have a positive finite-time maximal Lyapunov exponent and thus are in the chaotic regime. These observations brings up several questions. Given states in the chaotic sea with the same total energy and strength of nonlinearity, why do some

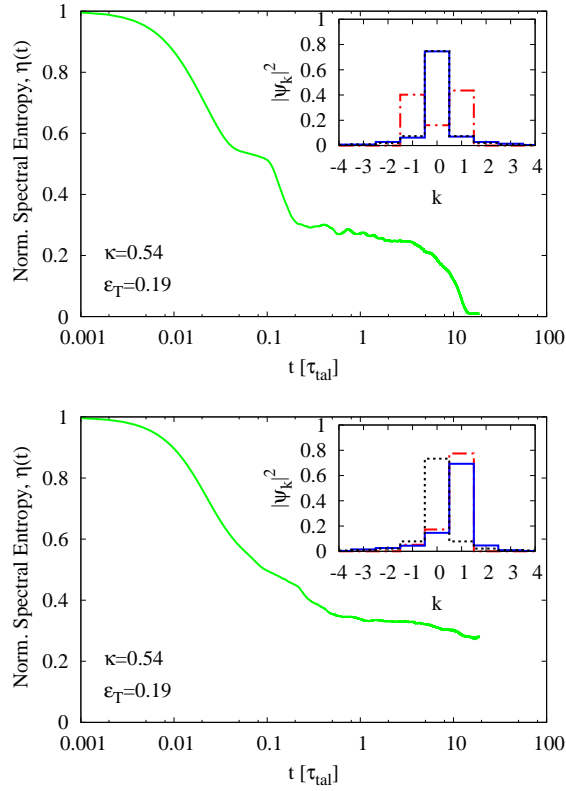


Figure 2.12: Sample time dependence of normalized spectral entropy, η , for two different initial states. $\kappa = 0.54, \varepsilon_T = 0.19J$ for both. $N_s = 21$. Inset: Initial (dashed red), final (solid blue) and thermal (dotted black) momentum distributions.

fully relax while other do not? Will these states fully thermalize for longer propagation times? What are the relevant time scales? What governs the slow relaxation times?

Comparing the momentum distributions for both plots, the initial momentum distribution is almost symmetric in Fig. 2.12(a) so that the total quasi-momentum of the initial state is close to zero. Total quasi-momentum is not a conserved quantity of the BHM, although it is a conserved quantity of the noninteracting model, the continuous model (in which case it becomes the true momentum) and the Ablowitz-Ladik discretization of the NLS. The total quasi-momentum is zero in the thermal state. For small κ 's, there is very little redistribution among the momentum modes and thus the total quasi-momentum

is well conserved. We call the total quasi-momentum a “quasi-conserved quantity” because it is not actually conserved in the BHM, but it is conserved in the nearby integrable models and thus is expected to be conserved in the BHM when it is “close” to one of the integrable limits. Proposed future work includes the investigation of the role of the conserved quantities of the nearby integrable models in the dynamics of the BHM.

While these plots are sample runs, the pattern just described is observed in other individual runs for different values of κ and ε_T in the chaotic region. Relaxation occurs on multiple time scales and the propagation times used in the simulations are long enough for the fast relaxation, but are not always long enough for the slow relaxation. For a given set of parameters, (κ, ε_T) there are different slow relaxation times for different initial states. Insufficient propagation times are one possible reason for large variation of the individual NSE’s observed in Fig. 2.9. In the strongly chaotic regime, it is expected that the normalized spectral entropy will converge to zero for longer propagation times. However it is also possible that for $\lambda \approx \lambda_c$, ($\eta \approx 0.36$) some initial states will not fully relax, even for very long times. Furthermore, for $0.68 \gtrsim \eta \gtrsim 0.36$ it is likely that the variance will remain large. It is clear from Fig. 2.11 that some states do not relax, even for very long times.

In summary, we have observed a threshold for chaos in the BHM, which depends on two parameters, the strength of the nonlinearity, κ and the total energy-per-particle, ε_T/J . Far above the threshold, the state relaxes to the one predicted by statistical mechanics. Below the chaos threshold, we observe relaxation to a non-thermal steady-state. For small nonlinearities, κ ’s the chaos threshold and absence of thermalization persist even for large energy-per-particle, $\varepsilon_T \sim J$. For regions just above the threshold, there are multiple relaxation times, with different initial states relaxing on different time scales. These observations bring up several questions: What is the origin of the chaos

threshold? What governs the long relaxation times? Is the nonthermal steady-state affected by the conserved quantities of the nearby integrable systems?

Chapter 3

Resonance Model and Failure of Chirikov's Criterion

In this chapter we study a Hamiltonian coupling a single set of modes for initial states with few modes occupied. First we use a perturbation theory expansion that is valid for small nonlinearities. Second we study nonlinear resonances of the one-dimensional mean-field Bose-Hubbard model to predict the chaos criterion by Chirikov's method of overlapping resonances.

3.1 Perturbation Theory Study of BHM

To study a perturbation theory expansion we introduce the a prefactor ε in the driving term, which will be set to unity in the end.

The full Hamiltonian in the momentum-space wavefunction representation is:

$$H = \sum_m \left(\hbar\omega_m |\psi_m|^2 - \frac{\mu_0}{2} |\psi_m|^4 \right) + \varepsilon \frac{\mu_0}{2} \sum_{m', l', i', j'} \psi_{m'}^* \psi_{l'}^* \psi_{i'} \psi_{j'} \quad (3.1)$$

where the sum carries the restrictions: $m' + l' = i' + j'$; $m' \neq i', j'$; $l' \neq i', j'$. We define the unperturbed Hamiltonian as

$$H_0 = \sum_m \left(\hbar\omega_m |\psi_m|^2 - \frac{\mu_0}{2} |\psi_m|^4 \right), \quad (3.2)$$

which consists of decoupled nonlinear oscillators. The frequencies of the unperturbed Hamiltonian are

$$\Omega_n \equiv \omega_n - (\mu_0/\hbar)|\psi_n|^2 = \tilde{\omega}_1 n^2 - (\mu_0/\hbar)|\psi_n|^2.$$

The equations of motion of the full Hamiltonian are given by:

$$\frac{\partial}{\partial t}\psi_n = -\frac{i}{\hbar}\frac{\partial H}{\partial \psi_n^*} = -i\left(\omega_n - \frac{\mu_0}{\hbar}|\psi_n|^2\right)\psi_n - i\varepsilon\frac{\mu_0}{\hbar}\sum_{l,i,j;i \neq l,n}\psi_l^*\psi_i\psi_{n+l-i} \quad (3.3)$$

$$= -i\Omega_n\psi_n - i\varepsilon\frac{\mu_0}{\hbar}\sum_{l,i;i \neq n,l}\psi_l^*\psi_i\psi_{n+l-i} \quad (3.4)$$

Now we make the following assumption: (1) All modes except n are treated as independent oscillators with equations of motion given by the unperturbed Hamiltonian, $\dot{\psi}_l = -i\Omega_l\psi_l$ which has solutions of $\psi_l(t) = \bar{\psi}_l e^{-i\Omega_l t}$ and (2) the nonlinear frequency of mode n associated with the unperturbed Hamiltonian is fixed, $\Omega_n = \text{const}$. With these restrictions, the equations of motion of mode n become

$$\frac{\partial}{\partial t}\psi_n = -i\Omega_n\psi_n - i\varepsilon\frac{\mu_0}{\hbar}\sum_{l,j;j \neq n,l}\bar{\psi}_l\bar{\psi}_j\bar{\psi}_{n+l-j}e^{-i(\Omega_j+\Omega_{n+l-j}-\Omega_l)t}. \quad (3.5)$$

3.1.1 Dynamics of an Initially Unpopulated Mode

First we study the maximum value of initially unpopulated mode in the perturbation theory expansion. We consider the initial state where a block of modes from $[-N_{max}, N_{max}]$ are equally populated and study the time dynamics of mode $Q = N_{max} + 1$. In order to do this, we seek a solution of

$$\frac{d}{dt}\psi_n + i\Omega_n\psi_n = f(t) \quad (3.6)$$

We want to find an integrating factor $h(t)$, satisfying $\dot{h}(t) = i\Omega_n h(t)$ such that

$$\frac{d}{dt}[\psi_n(t)h(t)] = h(t)\frac{d}{dt}\psi_n + i\Omega_n h(t)\psi_n = f(t)h(t). \quad (3.7)$$

The solution is $h(t) = \exp(i\Omega_n t)$. Let $f(t) = \sum_{\alpha} g(\alpha) \exp(i\Delta_{\alpha} t)$ where

$$\begin{aligned} \sum_{\alpha} &= \sum_{l,j;j \neq n,l} \\ g(\alpha) &= -\frac{\mu_0}{\hbar} \bar{\psi}_l \bar{\psi}_j \bar{\psi}_{n+l-j} \\ \Delta_{\alpha} &= \Omega_l - \Omega_j - \Omega_{n+l-j}. \end{aligned} \quad (3.8)$$

Next we integrate over time

$$\begin{aligned} \int_0^{\tau} dt \frac{d}{dt} \left(\psi_n(t) e^{i\Omega_n t} \right) &= \int_0^{\tau} dt \sum_{\alpha} g(\alpha) e^{i(\Omega_n + \Delta_{\alpha})t} \\ \psi_n(\tau) e^{i\Omega_n \tau} - \psi_n(0) &= \sum_{\alpha} \frac{g(\alpha)}{i(\Omega_n + \Delta_{\alpha})} \left(e^{i(\Omega_n + \Delta_{\alpha})\tau} - 1 \right) \\ \psi_n(t) &= \sum_{\alpha} \frac{g(\alpha)}{i(\Omega_n + \Delta_{\alpha})} \left(e^{i\Delta_{\alpha} t} - e^{-i\Omega_n t} \right) \end{aligned} \quad (3.9)$$

The time-averaged value of $\psi_n(t)$ is given by

$$\begin{aligned} \overline{|\psi_n|^2} &= \lim_{T \rightarrow \infty} \frac{1}{T} \int_0^T dt |\psi_n(t)|^2 \\ &= \lim_{T \rightarrow \infty} \frac{1}{T} \int_0^T dt \sum_{\alpha, \beta} \frac{g(\alpha)g(\beta)}{(\Omega_n + \Delta_{\alpha})(\Omega_n + \Delta_{\beta})} \left(e^{i(\Delta_{\alpha} - \Delta_{\beta})t} - e^{i(\Delta_{\alpha} - \Omega_n)t} - e^{-i(\Delta_{\beta} - \Omega_n)t} - 1 \right) \\ &= \sum_{\alpha, \beta} \frac{g(\alpha)g(\beta)}{(\Omega_n + \Delta_{\alpha})(\Omega_n + \Delta_{\beta})} [\delta(\Delta_{\alpha} - \Delta_{\beta}) - \delta(\Delta_{\alpha} - \Omega_n) - \delta(\Delta_{\beta} - \Omega_n) - 1] \\ &= \sum_{\alpha, \beta} \frac{g(\alpha)g(\beta)}{(\Omega_n + \Delta_{\alpha})(\Omega_n + \Delta_{\beta})} [\delta(\Delta_{\alpha} - \Delta_{\beta}) - 1], \end{aligned} \quad (3.10)$$

We introduce the dimensionless variables,

$$\boxed{\xi = \frac{\mu_0}{\hbar \tilde{\omega}_1}}, \quad \left(\xi = \kappa \left(\frac{N_s}{2\pi} \right)^2 \right)$$

which is directly proportional to the nonlinearity parameter, κ , but scales with the size of the system in the thermodynamic limit. We also introduce a new time scale, $\tau = \tilde{\omega}_1 t$.

Occupation of mode $N_{max} + 1$ for Quadratic Dispersion We are interested in the population of mode $Q \equiv N_{max} + 1$ when initially modes $(-N_{max}, N_{max})$ are equally occupied with population $\bar{\psi}$.

When only low momentum modes are excited, the true cosine dispersion laws can be approximated by a quadratic dispersion relation, $\omega_n = \tilde{\omega}_1 n^2$ and the unperturbed frequencies can be written as $\Omega_l = \omega_l(l^2 - \xi|\bar{\psi}|^2)$. Dropping terms $O(\xi)$ in the denominator, the equation of motion for ψ_Q can be written as

$$\begin{aligned} \psi_Q(t) &= -\varepsilon \xi \tilde{\omega}_1 e^{-i\Omega_Q t} \bar{\psi}^3 \sum_{|j|, |l| < Q; j \neq l} \frac{e^{i(\Omega_Q + \Omega_l - \Omega_j - \Omega_{Q+l-j})t} - 1}{\Omega_Q + \Omega_l - \Omega_j - \Omega_{Q+l-j}} \\ \psi_Q(\tau) &= -\varepsilon \xi \bar{\psi}^3 \sum_{|j|, |l| < Q; j \neq l} \frac{e^{i(l^2 - j^2 - (Q+l-j)^2)\tau} - e^{-iQ^2\tau}}{Q^2 + l^2 - j^2 - (Q+l-j)^2} \\ \psi_Q(\tau) &= -\varepsilon \xi \bar{\psi}^3 \sum_{|j|, |l| < Q} \bar{\psi}_j \bar{\psi}_{Q+l-j} \frac{e^{i(2(i-Q)(j-Q) - Q^2)\tau} - e^{-iQ^2\tau}}{2(i-Q)(j-Q)} \end{aligned} \quad (3.11)$$

where we make the substitution $l = j + i - Q$ in the last expression. Consider the case where modes $0, \pm 1$ are initially occupied with equal occupation, $\bar{\psi}$ and $Q = 2$. The

nonzero terms in the sum correspond to modes $(2, 0 \leftrightarrow 1, 1)$, $(2, -1 \leftrightarrow 1, 0)$, $(2, -1 \leftrightarrow 0, 1)$. The time evolution becomes:

$$\begin{aligned}\Psi_2(t) &= -e^{-i\Omega_2 t} \frac{\mu_0 \bar{\Psi}^3}{\hbar} \left[\frac{e^{i(\Omega_2 + \Omega_0 - 2\Omega_1)t} - 1}{\Omega_2 + \Omega_0 - 2\Omega_1} + 2 \frac{e^{i(\Omega_2 + \Omega_{-1} - \Omega_0 - \Omega_1)t} - 1}{\Omega_2 + \Omega_{-1} - \Omega_0 - \Omega_1} \right] \\ \Psi_2(\tau) &= \xi \bar{\Psi}^3 e^{-i4\tau} \left(\frac{e^{i2\tau} - 1}{2} + 2 \frac{e^{i4\tau} - 1}{4} \right) = \xi \bar{\Psi}^3 \left(\frac{1 + e^{-i2\tau} - 2e^{-i4\tau}}{2} \right)\end{aligned}\quad (3.12)$$

So that for $N_{max} = 1$, the time evolution of $|\Psi_2(\tau)|^2$ is:

$$|\Psi_2(\tau)|^2 = \xi^2 \bar{\Psi}^6 \left(\frac{3 - \cos(2\tau) - 2\cos(4\tau)}{2} \right) \quad (3.13)$$

Occupation of mode $N_{max} + 1$ for Cosine Dispersion In the previous case, we assumed a quadratic dispersion, which corresponds to the free space. The true dispersion of the BHM, which is a lattice model, is cosine,

$$\omega_n = -\tilde{\omega}_1 \frac{N_s^2}{2\pi^2} \left(1 - N_s^2 \cos\left(\frac{2\pi n}{N_s}\right) \right) \quad (3.14)$$

and the time evolution of mode population $|\Psi_2(\tau)|^2$ becomes

$$\begin{aligned}\Psi_2(t) &= -\xi \bar{\Psi}^3 e^{iN_s^2 \cos(4\pi/N_s)t} \frac{\tilde{\omega}_1}{N_s^2} \left(\frac{e^{itN_s^2(\cos(4\pi/N_s)+1-2\cos(2\pi/N_s))} - 1}{-\cos(4\pi/N_s) - 1 + 2\cos(2\pi/N_s)} \right. \\ &\quad \left. + 2 \frac{e^{itN_s^2(\cos(4\pi/N_s)-1)} - 1}{-\cos(4\pi/N_s) + 1} \right)\end{aligned}$$

Defining $\Delta_1 \equiv N_s^2(\cos(4\pi/N_s) + 1 - 2\cos(2\pi/N_s))/\tilde{\omega}_1$, $\Delta_2 \equiv N_s^2(\cos(4\pi/N_s) - 1)/\tilde{\omega}_1$, the

$$|\Psi_2(\tau)|^2 = \xi^2 \bar{\Psi}^6 \left(\frac{e^{i\tau\Delta_1} - 1}{\Delta_1} + 2 \frac{e^{i\tau\Delta_2} - 1}{\Delta_2} \right) \left(\frac{e^{-i\tau\Delta_1} - 1}{\Delta_1} + 2 \frac{e^{-i\tau\Delta_2} - 1}{\Delta_2} \right) \quad (3.15)$$

$$\begin{aligned}
|\Psi_2(\tau)|^2 &= \xi^2 \bar{\Psi}^6 \left(\frac{e^{i\tau\Delta_1} - 1}{\Delta_1} + 2 \frac{e^{i\tau\Delta_2} - 1}{\Delta_2} \right) \left(\frac{e^{-i\tau\Delta_1} - 1}{\Delta_1} + 2 \frac{e^{-i\tau\Delta_2} - 1}{\Delta_2} \right) \\
&= \xi^2 \bar{\Psi}^6 \left(\frac{2(1 - \cos(\tau\Delta_1))}{\Delta_1^2} + 8 \frac{1 - \cos(\tau\Delta_2)}{\Delta_2^2} \right. \\
&\quad \left. + \frac{4(\cos(\tau(\Delta_1 - \Delta_2)) - \cos(\tau\Delta_1) - \cos(\tau\Delta_2) + 1)}{\Delta_1\Delta_2} \right)
\end{aligned} \tag{3.16}$$

This expression for the time evolution of the modes is expected to be accurate for small values of ξ . Comparison of these predictions with numerics shows very good agreement for small ξ .

3.1.2 Nonlinear Frequencies in the Real-Space Dynamics

For small values of ξ , the perturbation theory expansion accurately predicts the time-dynamics of the real-space wavefunctions. Next we consider the same model as the nonlinear coupling increases. In Fig. 3.1 we plot the modulus-squared of the Fourier transform of the real-space wavefunction at the center of the box, $\Psi_{x=0}(t)$, is plotted for $N_s = 21$ and $\xi = 0.1, 1, 2, 3$ for an initial state with momentum modes $\Psi_{n=0}, \Psi_{n=\pm 1}$ occupied. Using a non-interacting model (no coupling between modes, but nonlinear terms associated with each mode), the predicted value of each of the resonances is $\Omega_n = \omega_n - \frac{\mu_0}{\hbar^2} I_n$. Taking I_n as the time-averaged value of $I_n(t)$. The driving term is of the form $e^{i(\Omega_m + \Omega_n - \Omega_l)}$, so additional frequencies are expected to be linear combinations of three other frequencies.

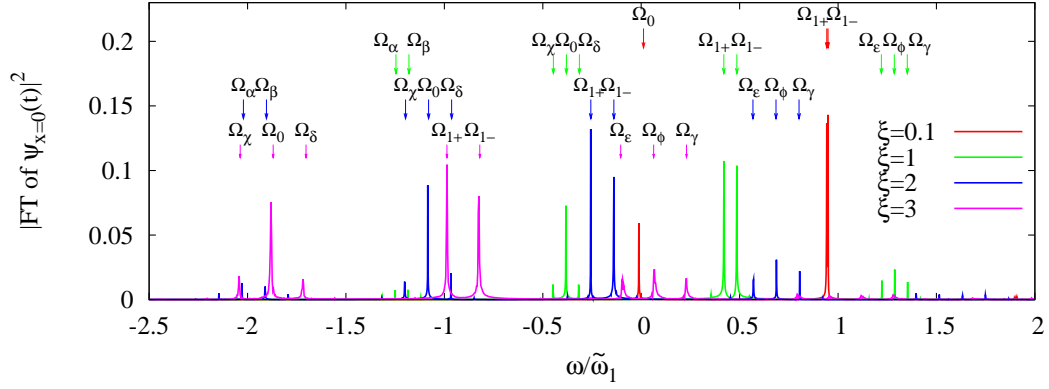


Figure 3.1: Frequencies of the real-space wavefunction at the center of the box, $|FT[\Psi_{x=0}(t)]|^2$ for $\xi = 0.1, 1, 2, 3$.

$$\Omega_\alpha = 2\Omega_0 - \Omega_{1-}$$

$$\Omega_\beta = 2\Omega_0 - \Omega_{1+}$$

$$\Omega_\chi = \Omega_0 + \Omega_{1+} - \Omega_{1-}$$

$$\Omega_\delta = \Omega_0 + \Omega_{1-} - \Omega_{1+}$$

$$\Omega_\epsilon = 2\Omega_{1+} - \Omega_0$$

$$\Omega_\phi = \Omega_0 - \Omega_{1+} - \Omega_{1-}$$

$$\Omega_\gamma = 2\Omega_{1-} - \Omega_0$$

3.2 Chirikov's Criterion

Next, we study the Bose-Hubbard Model in the Born-Oppenheimer approximation (BOA). In the BOA, the populations of all but one mode are fixed. The fixed modes rotate in phase-space with constant frequency. The motion of the free mode is coupled to the the fixed modes and motion is governed by the equations of motion.

In the next section, we deduce the Chirikov chaos criterion by studying single resonances within the Born Oppenheimer approximation. Within the resonant approximation it is assumed that near a resonance, the resonance dominates the motion, so that driving terms can be studied independently. Within the BOA, we assume that the action variable of the single mode under study is small compared to the other modes, p, q, r , and that the other modes can be well-described by the integrable Hamiltonian, H_0 that describes independent modes,

$$H_0 = \sum_m \left(\omega_m - \frac{\mu_0}{2\hbar^2} I_m \right) I_m.$$

Solving the equations of motion for the action variable, $\dot{I}_m = -\frac{\partial H_0}{\partial \theta_m}$ gives $I_m = \text{const} \equiv \bar{I}_m$, while the equation of motion for the angle variable, $\dot{\theta}_m = \frac{\partial H_0}{\partial I_m}$ gives

$$\theta_m = \left(\omega_m - \frac{\mu_0}{\hbar^2} \bar{I}_m \right) t \equiv \Omega_m(\bar{I}_m)t. \quad (3.17)$$

Thus the action variable of modes p, q, r is fixed and the angle rotates with constant frequency.

Summary of assumptions: Throughout this section, we assume that

1. Single resonance approximation: we isolate individual driving terms of the Hamiltonian and study the resonances of these models.
2. Born-Oppenheimer approximation: The population of all modes, except the one under study are fixed. The fixed modes have frequencies $\Omega_m = \left(\omega_m - \frac{\mu_0}{\hbar^2} \bar{I}_m \right)$.
3. Quadratic Dispersion: For low-energy modes the dispersion $\omega_n = 2\tilde{\omega}_1(N_s/2\pi)^2[1 - \cos(2\pi n/N_s)]$ can be approximated by a quadratic dispersion, $\omega_n = \tilde{\omega}_1 n^2$.

4. Equal population of fixed modes: The populations of the fixed modes are taken to be equal in order to reduce the number of parameters.

3.2.1 Classification of Resonances

We classify the single resonances into three categories. We use the notation $(p, q) \rightarrow (n, r)$, where the first two modes are the “feeding” modes and the second two modes are the “filling modes”. Mode n is the mode of interest, whose dynamics are governed by the resonant Hamiltonian, while p, q and r are three *different* modes with fixed action variables. Additionally, the momentum indices must satisfy $p + q = r + n$. The resonances are classified according to the order of the exponent of mode n in the driving term. The three classes of Hamiltonians are:

1. **First-order Resonance** $(p, q) \rightarrow (r, n)$

The two feeding modes p, q fill two different modes, r, n . The first-order resonant Hamiltonian is

$$H_n = \omega_n I_n - \frac{\mu_0}{2\hbar^2} I_n^2 + \frac{4\mu_0}{\hbar^2} (I_n I_p I_q I_r)^{1/2} \cos(\theta_n + \theta_r - \theta_p - \theta_q). \quad (3.18)$$

2. **1-R Resonance** $(p, p) \rightarrow (r, n)$

A single feeding mode p fills two different modes, r, n . The 1-R resonant Hamiltonian is

$$H_n = \omega_n I_n - \frac{\mu_0}{2\hbar^2} I_n^2 + \frac{2\mu_0}{\hbar^2} (I_n I_r I_p^2)^{1/2} \cos(\theta_n + \theta_r - 2\theta_p). \quad (3.19)$$

The 1-R resonance differs from the first-order resonance only in the prefactor in front of the driving term.

Table 3.1: Resonance Parameters

Order	Modes	Bare Detuning	Mean Occupation of Fixed Modes
First	$p, q \rightarrow r, n$ $p + q = r + n$	$\Delta_{01} \equiv p^2 + q^2 - r^2 - n^2$	$\bar{I}_1 \equiv (\bar{I}_p \bar{I}_q \bar{I}_r)^{3/2}$
1R	$p, p \rightarrow r, n$ $2p = r + n$	$\Delta_{01r} \equiv 2p^2 - r^2 - n^2$	$\bar{I}_{1r} \equiv (\bar{I}_p^2 \bar{I}_r)^{3/2}$
Second	$p, q \rightarrow n, n$ $p + q = 2n$	$\Delta_{02} \equiv p^2 + q^2 - 2n^2$	$\bar{I}_2 \equiv (\bar{I}_p \bar{I}_q)^{1/2}$

Order	Drive Frequency	Nonlinear Detuning
First	$v_1 \equiv \Omega_p + \Omega_q - \Omega_r$ $= \omega_p + \omega_q - \omega_r - \frac{2\mu_0}{\hbar}(\bar{I}_p + \bar{I}_p - \bar{I}_r)$	$\Delta_1 \equiv (v_1 - \omega_n)/\tilde{\omega}_1$ $= \Delta_{01} - \xi \bar{I}_1$
1R	$v_{1r} \equiv 2\Omega_p - \Omega_r$ $= 2\omega_p - \omega_r - \frac{2\mu_0}{\hbar}(2\bar{I}_p - \bar{I}_r)$	$\Delta_{1r} \equiv (v_{1r} - \omega_n)/\tilde{\omega}_1$ $= \Delta_{01r} - \xi \bar{I}_{1r}$
Second	$v_2 \equiv \Omega_p + \Omega_q$ $= \omega_p + \omega_q - \frac{2\mu_0}{\hbar}(\bar{I}_p + \bar{I}_q)$	$\Delta_2 \equiv (v_2 - 2\omega_n)/(2\tilde{\omega}_1)$ $= \Delta_{02}/2 - \xi \bar{I}_2$

3. Second-order Resonance $(p, q) \rightarrow (n, n)$

Two different feeding modes, p, q fill the same mode, n . The second order resonant Hamiltonian is

$$H_n = \omega_n I_n - \frac{\mu_0}{2\hbar^2} I_n^2 + \frac{2\mu_0}{\hbar^2} I_n (I_p I_q)^{1/2} \cos(2\theta_n - \theta_p - \theta_q) \quad (3.20)$$

In Table 3.1 the important parameters and definitions are listed for the three classes of resonances. The parameters include: the geometric mean of the fixed modes, \bar{I} , the bare detuning, Δ_0 , and the frequency of the drive v . For the nonlinear detuning, the second equality holds when all the fixed modes have the same population. For a generic driving term of each type, the bare detuning, Δ_0 is always negative for 1-R terms, always

Table 3.2: Bare Detuning: Generic Values

Order	Modes	Bare Detuning
First	$n + m, n + l \rightarrow n, n + l + m$	$\Delta_{01} \equiv (n + m)^2 + (n + l)^2$ $- (n + m + l)^2 - n^2$ $= -2ml$
1R	$n + m, n + m \rightarrow n, n + 2m$	$\Delta_{01r} \equiv 2(n + m)^2$ $- (n + 2m)^2 - n^2$ $= -2m^2$
Second	$n + m, n - m \rightarrow n, n$	$\Delta_{02} \equiv (n + m)^2 + (n - m)^2$ $- 2n^2$ $= 2m^2$

positive for 2nd order terms and can be positive or negative for 1st order terms (see Table 3.2). Next we will study the resonances in each class of Hamiltonians.

3.2.2 First-Order Resonances in BOA

Consider a first-order resonance where $n + r = p + q$; $p, q \neq n, r$. Fix the populations of the feeding modes, p, q and the filling mode r , so that the only variables are the population and angle of mode n . The frequencies of modes p, q, r are fixed to their values in the unperturbed Hamiltonian (3.2). Solving $\dot{\theta}_n = \frac{\partial H_0}{\partial I_n}$ for the angle gives

$$\theta_n = \left(\omega_n - \frac{\mu_0}{\hbar^2} \bar{I}_n \right) t \equiv \Omega_n(\bar{I}_n) t. \quad (3.21)$$

In this approximation, which we call the Born-Oppenheimer approximation (BOA), we keep the eight terms corresponding to $(p, q) \rightarrow (r, n)$ from the full Hamiltonian. The Hamiltonian for first-order resonances in the Born-Oppenheimer approximation is:

$$\begin{aligned} H_n &= \omega_n I_n - \frac{\mu_0}{2\hbar^2} I_n^2 + \frac{4\mu_0}{\hbar^2} (I_n I_p I_q I_r)^{1/2} \cos(\theta_n + \theta_r - \theta_p - \theta_q) \\ &= \omega_n I_n - \frac{\mu_0}{2\hbar^2} I_n^2 + \frac{4\mu_0}{\hbar^2} (I_n I_p I_q I_r)^{1/2} \cos(\theta_n - \nu t + \phi_1) \end{aligned} \quad (3.22)$$

where $\nu \equiv \Omega_p + \Omega_q - \Omega_r$. Now we let $\bar{I}_1 \equiv (\bar{I}_p \bar{I}_q \bar{I}_r)^{1/3}$, divide by $\tilde{\omega}_1$, set $\hbar = 1$ and use $\xi = \mu_0/(\hbar \tilde{\omega}_1)$ to get

$$h_n \equiv \frac{H_n}{\tilde{\omega}_1} = \frac{\omega_n}{\tilde{\omega}_1} I_n - \frac{\xi}{2} I_n^2 + 4\xi (\bar{I}_1)^{1/2} \cos(\theta_n - \nu t + \phi_1). \quad (3.23)$$

We seek a canonical transformation to a rotating reference frame $(I_n, \theta_n \rightarrow \tilde{I}_n, \tilde{\theta}_n)$, where the new angle, $\tilde{\theta}_n$ is slowly varying. Introducing the type 2 generating function

$$\Phi = (\theta_n - \nu t + \phi_1) \tilde{I}_n, \quad (3.24)$$

the new canonical variables are given by

$$I_n \equiv \frac{\partial \Phi}{\partial \theta_n} = \tilde{I}_n \quad (3.25)$$

$$\tilde{\theta}_n \equiv \frac{\partial \Phi}{\partial \tilde{I}_n} = \theta_n - \nu t + \phi_1. \quad (3.26)$$

$$(3.27)$$

The Hamiltonian, which transforms according to $\tilde{h}_n = h_n + \frac{\partial \Phi}{\partial t}$, becomes

$$\boxed{\tilde{h}_n = (\omega_n - \nu_1)/\tilde{\omega}_1 \tilde{I}_n - \frac{\xi}{2} \tilde{I}_n^2 + 4\xi \bar{I}_1^{3/2} \tilde{I}_n^{1/2} \cos \tilde{\theta}_n.} \quad (3.28)$$

The corresponding equations of motion are

$$\dot{\tilde{I}}_n = -\frac{\partial \tilde{h}_n}{\partial \tilde{\theta}_n} = 4\xi \tilde{I}_n^{1/2} (\bar{I}_1)^{3/2} \sin \tilde{\theta}_n \quad (3.29)$$

$$\dot{\tilde{\theta}}_n = \frac{\partial \tilde{h}_n}{\partial \tilde{I}_n} = -\Delta_1 - \xi \tilde{I}_n + 2\xi \frac{\bar{I}_1^{3/2}}{\tilde{I}_n^{1/2}} \cos \tilde{\theta}_n, \quad (3.30)$$

where $\Delta_1 \equiv \nu_1 - \omega_n$.

Resonance Condition

Resonance occurs at the stationary points, that is

$$\dot{\tilde{I}}_n \Big|_{(\tilde{I}_n^*, \tilde{\theta}_n^*)} = 0 \quad \Rightarrow \quad 4\xi (\tilde{I}_n^*)^{1/2} \bar{I}_1^{3/2} \sin \tilde{\theta}_n^* = 0 \quad (3.31)$$

$$\dot{\tilde{\theta}}_n \Big|_{(\tilde{I}_n^*, \tilde{\theta}_n^*)} = 0 \quad \Rightarrow \quad -\Delta_1 - \xi \tilde{I}_n^* + 2\xi \frac{\bar{I}_1^{3/2}}{(\tilde{I}_n^*)^{1/2}} \cos \tilde{\theta}_n^* = 0. \quad (3.32)$$

The first condition is satisfied by (a) $\tilde{I}_n^* = 0$ or (b) $\sin \tilde{\theta}_n^* = 0$. For $\tilde{I}_n = 0$ the phase is not well-defined and corresponds to a stationary point, even though (3.32) is not satisfied.

The resonances of this model will correspond to taking $\sin \tilde{\theta}_n^* = 0$ and solving (3.32) for \tilde{I}_n^* ,

$$-\Delta_1 \tilde{I}_n^{1/2} - \xi \tilde{I}_n^{3/2} = \mp 2\xi \bar{I}_1^{3/2}. \quad (3.33)$$

Squaring both sides and rearranging gives,

$$\tilde{I}_n^3 + 2\frac{\Delta_1}{\xi} \tilde{I}_n^2 + \frac{\Delta_1^2}{\xi^2} \tilde{I}_n - 4\bar{I}_1^3 = 0. \quad (3.34)$$

The solution to this cubic equation gives the fixed points,

$$\tilde{I}_{n1}^* = -\frac{2\Delta_1}{3\xi} + A + B \quad (3.35)$$

$$\tilde{I}_{n2}^* = -\frac{2\Delta_1}{3\xi} - \frac{1}{2}(A + B) + i\frac{\sqrt{3}}{2}(A - B) \quad (3.36)$$

$$\tilde{I}_{n3}^* = -\frac{2\Delta_1}{3\xi} - \frac{1}{2}(A + B) - i\frac{\sqrt{3}}{2}(A - B), \quad (3.37)$$

where

$$A = \left[\left(\frac{\Delta_1}{3\xi} \right)^3 + 2\bar{I}_1^3 + 2\bar{I}_1^{3/2} \left(\left(\frac{\Delta_1}{3\xi} \right)^3 + \bar{I}_1^3 \right)^{1/2} \right]^{1/3} \quad (3.38)$$

$$B = \left[\left(\frac{\Delta_1}{3\xi} \right)^3 + 2\bar{I}_1^3 - 2\bar{I}_1^{3/2} \left(\left(\frac{\Delta_1}{3\xi} \right)^3 + \bar{I}_1^3 \right)^{1/2} \right]^{1/3}. \quad (3.39)$$

The real and imaginary parts of the roots are plotted in Fig. 3.2 for $\bar{I}_1 = 1/3$ and $\Delta_{01} = -4$, which corresponds to $(n+2, n+1) \rightarrow (n, n+3)$, which is the negative detuning closest to zero. For the initial condition studied by the previous perturbation expansion, where a block of consecutive modes are initially occupied, the bare detuning is always negative. Thus, we still study the case of negative detuning although it is possible to have a first-order resonance with positive or negative values. The value of ξ the separates regions with three real solutions to one real solution is given by $\left(\frac{\Delta_1}{3\xi_c} \right)^3 + \bar{I}_1^3 = 0$ or

$$\frac{\Delta_1}{3\xi_c} = \frac{\Delta_{01} - \xi_c \bar{I}_1}{3\xi_c} = -\bar{I}_1 \quad \Rightarrow \quad \boxed{\xi_{c2} \equiv -\frac{\Delta_{01}}{2\bar{I}_1}} \quad (3.40)$$

As will be shown below there is another relevant critical value of ξ at lower values, so this critical value is defined as ξ_{c2} . There are three physical fixed points ($\tilde{I}_n^* \geq 0$ for $\xi \leq \xi_{c2}$ and one physical fixed point for $\xi > \xi_{c2}$).

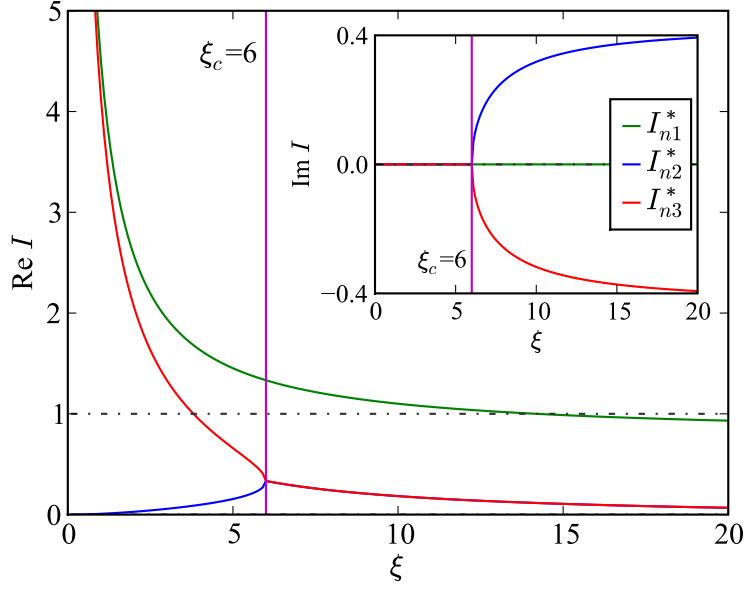


Figure 3.2: Real and imaginary parts of the fixed points of first-order Hamiltonian (3.28). $\Delta_{01} = -4$, $\bar{I}_1 = 1/3$.

Separatrix Width

There are two separatrices: one is associated with $\tilde{h}_n = 0$ another passes through the fixed point $(\tilde{I}_{n3}^*, \tilde{\theta}_n^* \pm \pi)$ and is defined by the contour $\tilde{h}_n = \tilde{h}_n(\tilde{I}_{n3}^*, \pm\pi)$.

In this section we calculate the maximum value of \tilde{I}_n for the separatrix defined by $\tilde{h}_n = 0$. The maximum value of the separatrix occurs at $\tilde{\theta}_n = \pm m\pi$ for integer m . We thus solve $\tilde{h}_n = 0$ for $\cos(\tilde{\theta}_n) = \pm 1$.

$$-\Delta_1 \tilde{I}_n - \frac{1}{2} \xi \tilde{I}_n^2 = \mp 2 \xi \tilde{I}_1^{3/2} \tilde{I}_n^{1/2}. \quad (3.41)$$

Squaring both sides and rearranging gives,

$$\tilde{I}_n^3 + 4 \frac{\Delta_1}{\xi} \tilde{I}_n^2 + 4 \frac{\Delta_1^2}{\xi^2} \tilde{I}_n - 64 \tilde{I}_1^3 = 0. \quad (3.42)$$

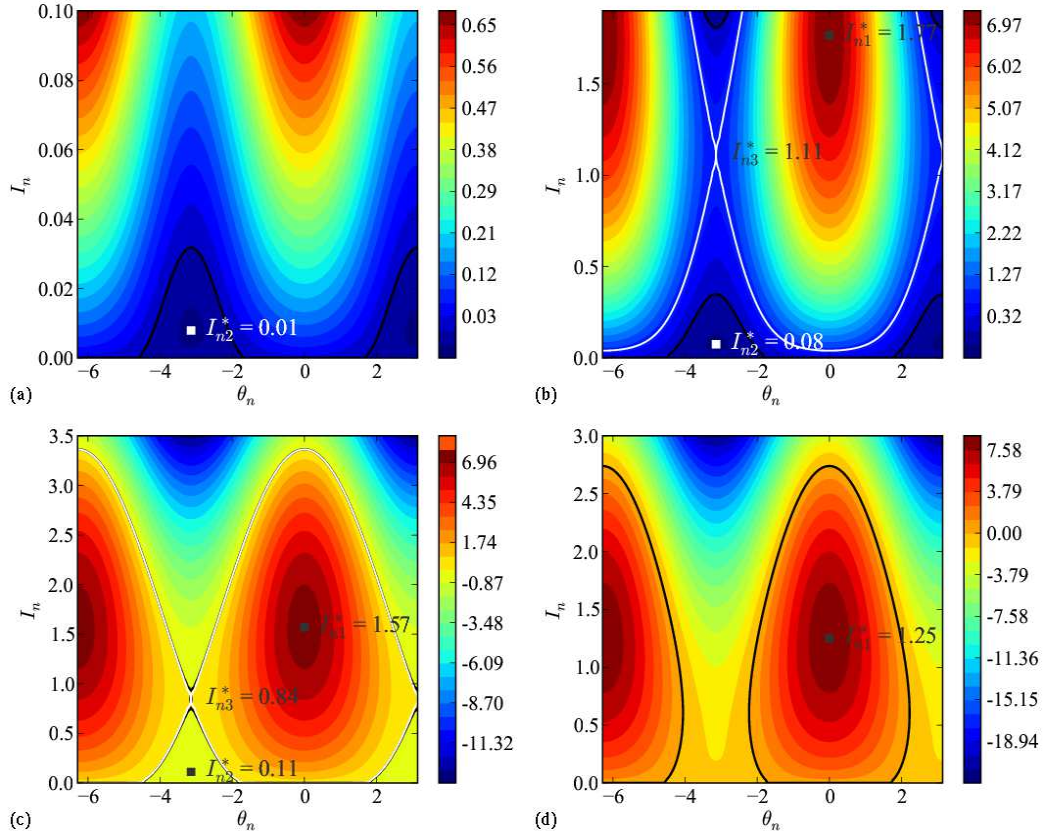


Figure 3.3: Action-angle phase-space plots for variables $\tilde{I}_n, \tilde{\theta}_n$ for the first-order resonant Hamiltonian (3.28). $(n+2, n+1) \rightarrow (n, n+3)$ ($\Delta_{01} = -4$). $\bar{I}_1 = 1/3$. (a) $\xi = 1$ (b) $\xi = 3.5$ (c) $\xi = \xi_{c1} = 4.3$ (d) $\xi = 7 > \xi_{c2}$. The black contour line corresponds to $\tilde{h}_n = 0$ and the white contour line to $\tilde{h}_n(\tilde{I}_n, \tilde{\theta}_n) = \tilde{h}_n(\tilde{I}_{n3}^*, -\pi)$.

Solving this cubic equation gives the roots,

$$\tilde{I}_{sep1} = -\frac{4\Delta_1}{3\xi} + A + B \quad (3.43)$$

$$\tilde{I}_{sep2} = -\frac{4\Delta_1}{3\xi} - \frac{1}{2}(A+B) + i\frac{\sqrt{3}}{2}(A-B) \quad (3.44)$$

$$\tilde{I}_{sep3} = -\frac{4\Delta_1}{3\xi} - \frac{1}{2}(A+B) - i\frac{\sqrt{3}}{2}(A-B) \quad (3.45)$$

where

$$A = \left[8 \left(\frac{\Delta_1}{3\xi} \right)^3 + 4\bar{I}_1^3 + 16\sqrt{2}\bar{I}_1^{3/2} \left(\left(\frac{\Delta_1}{3\xi} \right)^3 + 2\bar{I}_1^3 \right)^{1/2} \right]^{1/3} \quad (3.46)$$

$$B = \left[8 \left(\frac{\Delta_1}{3\xi} \right)^3 + 4\bar{I}_1^3 - 16\sqrt{2}\bar{I}_1^{3/2} \left(\left(\frac{\Delta_1}{3\xi} \right)^3 + 2\bar{I}_1^3 \right)^{1/2} \right]^{1/3}. \quad (3.47)$$

The second critical value of ξ is given by $\left(\frac{\Delta_1}{3\xi_c} \right)^3 + 2\bar{I}_1^3 = 0$ or

$$\frac{\Delta_1}{3\xi_c} = \frac{\Delta_{01} - \xi_c \bar{I}_1}{3\xi_c} = -\sqrt[3]{2}\bar{I}_1 \quad \Rightarrow \quad \boxed{\xi_{c1} \equiv -\frac{\Delta_{01}}{(1 + 3\sqrt[3]{2})\bar{I}_1}} \quad (3.48)$$

The maximum value of the separatrix occurs at $\tilde{\theta}_n = \pm\pi$, ($\cos(\tilde{\theta}_n) = -1$) for $\xi \leq \xi_{c1}$ and at $\tilde{\theta}_n = 0 \pm 2\pi$, ($\cos(\tilde{\theta}_n) = +1$) for $\xi \geq \xi_{c1}$. In Fig. 3.4 the real and imaginary parts of these solutions are plotted.

From the fixed points of the Hamiltonian, solutions of $\tilde{h}_n = 0$ and sample contour plots, the phase-space of the first-order Hamiltonian can be characterized as follows:

$\xi < \xi_{c1}$ There are two resonances. One is at $(\tilde{I}_n, \tilde{\theta}_n) = (\tilde{I}_{n2}^*, \pm\pi)$ with the separatrix defined by the contour at $\tilde{h}_n = 0$. This resonance can be seen in the phase-space diagrams of Fig. 3.3(a)-(b). The height of the separatrix is given by I_{sep2} which increases from zero at $\xi = 0$ to a maximum value $\tilde{I}_{n2-\max} = 2\sqrt[3]{2}\bar{I}_1$ at $\xi = \xi_{c2}$ as seen in Fig. 3.4. For $\bar{I}_1 = 1/3$ the maximum value is $\tilde{I}_{n2-\max} \approx 0.84$. The second resonance is given by $(\tilde{I}_{n1}^*, \tilde{\theta}_n = 0)$. The separatrix is defined by the contour that passes through the saddle point $(\tilde{I}_{n3}^*, \pm\pi)$. This resonance diverges as $\xi \rightarrow 0$ and remains above 1 in this parameter range is thus not physically accessible. However, the lower separatrix comes into the accessible phase space as seen in Fig. 3.3(b). Due to the normalization, the occupation of \tilde{I}_n is bounded by one.

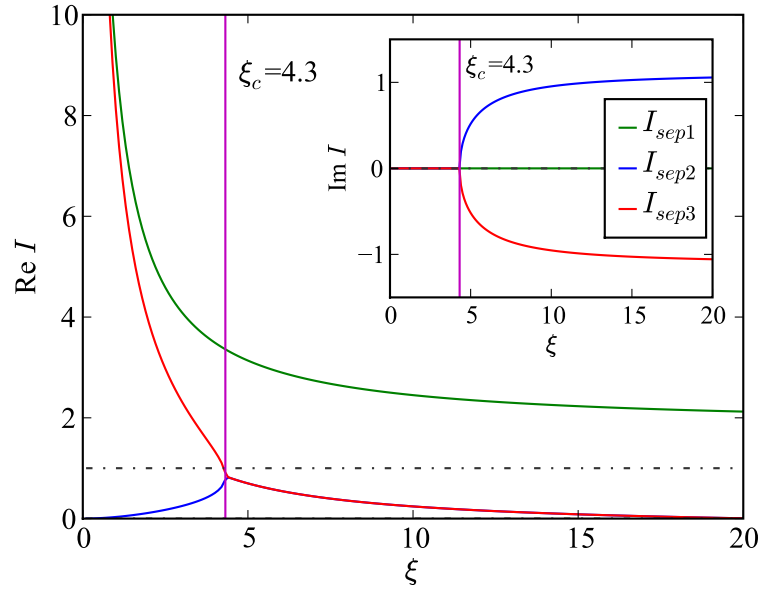


Figure 3.4: Real and imaginary parts of the solutions of $\tilde{h}_n = 0$ for the first-order Hamiltonian (3.28). $\Delta_{01} = -4(n+1, n+2) \rightarrow (n, n+3)$, $\bar{I}_1 = 1/3$. For $\xi \leq \xi_{c1}$, \tilde{I}_{sep2} gives the separatrix for the resonance at $(\tilde{I}_{n2}^*, \tilde{\theta}_n = \pm\pi)$. For $\xi \geq \xi_{c1}$, \tilde{I}_{sep1} gives the separatrix for the resonance at $(\tilde{I}_{n1}^*, \tilde{\theta}_n = 0)$.

Larger values of \tilde{I}_n are plotted in Fig. 3.3 to gain a deeper understanding of the phase space.

$\xi = \xi_{c1}$ At the first critical point, the separatrices of the two resonances overlap as shown in Fig. 3.3(c). At this critical point, the lower bound of the separatrix defined by $\tilde{h}_n = \tilde{h}_n(\tilde{I}_{n3}^*, -\pi)$ touches zero. Starting with an arbitrarily small occupation, the entire physical phase space becomes accessible to \tilde{I}_n once the two resonances touch.

$\xi_{c1} < \xi < \xi_{c2}$ The two resonances at $(\tilde{I}_{n1}^*, 0)$ and $(\tilde{I}_{n2}^*, \pm\pi)$ remain, with the separatrix of the first defined by $\tilde{h}_n = 0$ and the separatrix of the second resonance defined by $\tilde{h}_n = \tilde{h}_n(\tilde{I}_{n3}^*, -\pi)$. The association of the separatrices has switched from the case where $\xi < \xi_{c1}$.

$\xi \geq \xi_{c2}$ At the second critical point the fixed points $(\tilde{I}_{n2}^*, \pm\pi)$ and $(\tilde{I}_{n3}^*, \pm\pi)$ merge and annihilate and a single resonance at $(\tilde{I}_n, \tilde{\theta}_n) = (\tilde{I}_{n1}^*, 0)$ persists. Above ξ_c , there is a single resonance at $(\tilde{I}_n, \tilde{\theta}_n) = (\tilde{I}_{n1}^*, 0)$, as show in Fig. 3.3(d) and the separatrix is defined by the contour $\tilde{h}_n = 0$. The height of the separatrix is given by \tilde{I}_{sep1} in Fig. 3.4.

3.2.3 1-R Resonances in BOA. $\Omega_p = \Omega_q$

Consider a first-order resonance where the feeding modes are the same, $n + r = 2p$. In this case, we keep four terms from the full Hamiltonian, and the Hamiltonian for the first-order resonances (1-R) is

$$H_n = \omega_n I_n - \frac{\mu_0}{2\hbar^2} I_n^2 + \frac{2\mu_0}{\hbar^2} (I_n I_p^2 I_r)^{1/2} \cos(\theta_n + \theta_r - 2\theta_p) \quad (3.49)$$

After making the transformation to a rotating reference frame, introducing $\nu_{1r} = 2\Omega_p - \Omega_r$, fixing the populations of modes I_p, I_r , and dividing by ω_n , the Hamiltonian, $\tilde{h}_n \equiv \tilde{H}_n/\omega_n$ becomes

$$\boxed{\tilde{h}_n = -\Delta_{1r} \tilde{I}_n - \frac{\xi}{2} \tilde{I}_n^2 + 2\xi \tilde{I}_n^{1/2} \tilde{I}_{1r}^{3/2} \cos \tilde{\theta}_n} \quad (3.50)$$

where $\Delta_{1r} \equiv \nu_{1r} - \omega_n$. The corresponding equations of motion are

$$\dot{\tilde{I}}_n = -\frac{\partial \tilde{h}_n}{\partial \tilde{\theta}_n} = 2\xi \tilde{I}_n^{1/2} \tilde{I}_{1r}^{3/2} \sin \tilde{\theta}_n \quad (3.51)$$

$$\dot{\tilde{\theta}}_n = \frac{\partial \tilde{h}_n}{\partial \tilde{I}_n} = -\Delta - \xi \tilde{I}_n + 2\xi \left(\frac{\tilde{I}_{1r}^{3/2}}{\tilde{I}_n} \right)^{1/2} \cos \tilde{\theta}_n \quad (3.52)$$

The Hamiltonian for the 1R resonances differs from the first-order Hamiltonian only by prefactors. The resonances of the 1-R Hamiltonian will thus be very similar in form

to those of the first-order resonances, and can be determined from the previous analysis by a proper rescaling of \bar{I}_1 .

3.2.4 Second Order Resonances in BOA

For the second order case, we consider a single filling mode n and restrict the resonance to modes that satisfy $p + q = 2n$. The Hamiltonian for a single second order resonance in the Born Oppenheimer approximation is

$$\begin{aligned} H_n &= \omega_n I_n - \frac{\mu_0}{2\hbar^2} I_n^2 + \frac{2\mu_0}{\hbar^2} I_n (I_p I_q)^{1/2} \cos(2\theta_n - \theta_p - \theta_q) \\ &= \omega_n I_n - \frac{\mu_0}{2\hbar^2} I_n^2 + \frac{2\mu_0}{\hbar^2} I_n (\bar{I}_p \bar{I}_q)^{1/2} \cos(2\theta_n - \nu_2 t) \end{aligned} \quad (3.53)$$

where in the second line we set I_p and I_q to their unperturbed values and

$$\nu_2 \equiv \Omega_p(\bar{I}_p) + \Omega_q(\bar{I}_q) = \omega_p + \omega_q - \frac{\mu_0}{\hbar^2} (\bar{I}_p + \bar{I}_q).$$

Next we make a canonical transformation to a rotating reference frame $(I_n, \theta_n \rightarrow \tilde{I}_n, \tilde{\theta}_n)$, through the type 2 generating function

$$\Phi = \frac{1}{2}(2\theta_n - \nu_2 t + \phi_1)\tilde{I}_n. \quad (3.54)$$

The new canonical variables are determined by

$$I_n = \frac{\partial \Phi}{\partial \theta_n} = \tilde{I}_n \quad (3.55)$$

$$\tilde{\theta}_n = \frac{\partial \Phi}{\partial \tilde{I}_n} = \frac{1}{2}(2\theta_n - \nu_2 t + \phi_1), \quad (3.56)$$

and the Hamiltonian transforms according to $\tilde{H}_n(\tilde{I}_n, \tilde{\theta}_n) = H_n(I, \theta_n) + \frac{\partial \Phi}{\partial t}$ becomes

$$\boxed{\tilde{H}_n = \left(\omega_n - \frac{1}{2}v_2 \right) \tilde{I}_n - \frac{\mu_0}{2\hbar^2} \tilde{I}_n^2 + \frac{2\mu_0}{\hbar^2} \tilde{I}_n (\bar{I}_p \bar{I}_q)^{1/2} \cos 2\tilde{\theta}_n} \quad (3.57)$$

Next we divide by $\tilde{\omega}_1$, which is equivalent to rescaling time by a factor $\tau = \tilde{\omega}_1 t$, introduce $\xi \equiv \mu_0/\hbar\tilde{\omega}_1$ and set $\hbar = 1$. Furthermore, we define $\bar{I}_2 \equiv (\bar{I}_p \bar{I}_q)^{1/2}$ as the geometric mean of the filling modes \bar{I}_p, \bar{I}_q and $\Delta_2 \equiv (\frac{1}{2}v_2 - \omega_n)/\tilde{\omega}_1$.

$$\boxed{\tilde{h}_n \equiv \frac{\tilde{H}_n}{\tilde{\omega}_1} = -\Delta_2 \tilde{I}_n - \frac{\xi}{2} \tilde{I}_n^2 + 2\xi \tilde{I}_n \bar{I}_2 \cos 2\tilde{\theta}_n} \quad (3.58)$$

The corresponding equations of motion are

$$\dot{\tilde{I}}_n = -\frac{\partial \tilde{h}_n}{\partial \tilde{\theta}_n} = 4\xi \tilde{I}_n \bar{I}_2 \sin 2\tilde{\theta}_n \quad (3.59)$$

$$\dot{\tilde{\theta}}_n = \frac{\partial \tilde{h}_n}{\partial \tilde{I}_n} = -\Delta_2 - \xi \tilde{I}_n + 2\xi \bar{I}_2 \cos 2\tilde{\theta}_n. \quad (3.60)$$

If we furthermore assume that the filling modes have equal populations, $\bar{I}_p = \bar{I}_q = \bar{I}_2$ and that the dispersion is quadratic, $\omega_n = n^2 \tilde{\omega}_1$ then the detuning reduces to

$$\Delta_2 = \frac{1}{2\tilde{\omega}_1} (v - 2\omega_n) = \frac{1}{2\tilde{\omega}_1} [(p^2 + q^2 - 2n^2)\tilde{\omega}_1 - \xi (\bar{I}_p + \bar{I}_q)] \quad (3.61)$$

$$= \frac{\Delta_{02}}{2} - \xi \bar{I}_2. \quad (3.62)$$

Resonances Conditions

Unlike the first-order resonances there is a simple expression for the fixed points of the second order resonances. The conditions for the fixed points are $\dot{\tilde{I}}_n|_{(\tilde{I}_n^*, \tilde{\theta}_n^*)} = 0, \dot{\tilde{\theta}}_n|_{(\tilde{I}_n^*, \tilde{\theta}_n^*)} = 0$.

$$\dot{\tilde{I}}_n|_{(\tilde{I}_n^*, \tilde{\theta}_n^*)} = 0 \quad \Rightarrow \quad \boxed{4\xi\tilde{I}_n^*\bar{I}_2 \sin 2\tilde{\theta}_n^* = 0} \quad (3.63)$$

$$\dot{\tilde{\theta}}_n|_{(\tilde{I}_n^*, \tilde{\theta}_n^*)} = 0 \quad \Rightarrow \quad \boxed{-\Delta_2 - \xi\tilde{I}_n^* + 2\xi\bar{I}_2 \cos 2\tilde{\theta}_n^* = 0} \quad (3.64)$$

1. Case 1: $\tilde{I}_n^* = 0$.

The condition for $\dot{\tilde{I}}_n = 0$ is satisfied by $\tilde{I}_n^* = 0$ and the condition on $\tilde{\theta}_n^*$ such that $\dot{\tilde{\theta}}_n = 0$ is

$$\cos 2\tilde{\theta}_n^* = \frac{\Delta_2}{2\xi\bar{I}_2} = \frac{\Delta_{20}}{4\xi\bar{I}_2} - \frac{1}{2}.$$

Note that if $I_n = 0$, the phase of the mode n is not well-defined. In this case, the motion of the action variable is always stationary. Thus a second-order resonant Hamiltonian can never populate an initially unoccupied mode. However, once a small seed is present, the mode can grow and enter the dynamics.

2. Case 2: $\sin 2\tilde{\theta}_n^* = 0$ ($\cos 2\tilde{\theta}_n^* = \pm 1$)

The condition for $\dot{\tilde{I}}_n = 0$ is satisfied by $\sin 2\tilde{\theta}_n^* = 0$ and the condition on \tilde{I}_n^* such that $\dot{\tilde{\theta}}_n = 0$ is

$$\tilde{I}_n^* = -\frac{\Delta_2}{\xi} \pm 2\bar{I}_2 = -\frac{\Delta_{02}}{2\xi} + \bar{I}_2 \pm 2\bar{I}_2 \quad (\text{for } \cos 2\tilde{\theta}_n^* = \pm 1).$$

Classification of Stationary Points

Following Tabor (1989) we outline a method for determining the stability of the stationary points by linearizing about the fixed points. Consider a general second order differential equation, written as a pair of first-order differential equations,

$$\dot{x} = f(x, y) \quad (3.65)$$

$$\dot{y} = g(x, y) \quad (3.66)$$

that has stationary points $\{(x^*, y^*) | f(x^*, y^*) = 0, g(x^*, y^*) = 0\}$. The stability of these points can be determined by linearizing about the stationary points.

$$\begin{pmatrix} \Delta \dot{x} \\ \Delta \dot{y} \end{pmatrix} = \begin{pmatrix} \frac{\partial f}{\partial x} |_{x^*, y^*} & \frac{\partial f}{\partial y} |_{x^*, y^*} \\ \frac{\partial g}{\partial x} |_{x^*, y^*} & \frac{\partial g}{\partial y} |_{x^*, y^*} \end{pmatrix} \begin{pmatrix} \Delta x \\ \Delta y \end{pmatrix}. \quad (3.67)$$

The solution to these equations of motion, $\dot{\mathbf{x}} = \mathbf{A}\mathbf{x}$, is $\mathbf{x} = c_1 e^{\lambda_1 t} \mathbf{v}_1 + c_2 e^{\lambda_2 t} \mathbf{v}_2$ where λ_j is an eigenvalue of \mathbf{A} with corresponding eigenvector \mathbf{v}_j . The stability of the fixed points is determined from the eigenvalues, $\lambda_j = a_j + ib_j$, $a_j, b_j \in \mathbf{R}$. The fixed points are classified as follows,

1. center: $a_{1,2} = 0$
2. spiral: $b_{1,2} \neq 0$. Stable for $a_{1,2} < 0$. Unstable for $a_{1,2} > 0$.
3. node: $b_{1,2} = 0$. Stable for $a_{1,2} < 0$. Unstable for $a_{1,2} > 0$
4. saddle point: $b_{1,2} = 0$, $a_1 < 0$, $a_2 > 0$

The linearized equations of motion for the second order Hamiltonian (3.58) are

$$\mathbf{A} = \begin{pmatrix} -\frac{\partial^2 \tilde{h}_n}{\partial \tilde{\theta}_n \partial \tilde{I}_n} |_{\tilde{I}_n^*, \tilde{\theta}_n^*} & -\frac{\partial^2 \tilde{h}_n}{\partial \tilde{\theta}_n^2} |_{\tilde{I}_n^*, \tilde{\theta}_n^*} \\ \frac{\partial^2 \tilde{h}_n}{\partial \tilde{I}_n^2} |_{\tilde{I}_n^*, \tilde{\theta}_n^*} & \frac{\partial^2 \tilde{h}_n}{\partial \tilde{I}_n \partial \tilde{\theta}_n} |_{\tilde{I}_n^*, \tilde{\theta}_n^*} \end{pmatrix} = \begin{pmatrix} 4\xi \bar{I}_2 \sin 2\tilde{\theta}_n^* & 8\xi \tilde{I}_n \bar{I}_2 \cos 2\tilde{\theta}_n^* \\ -\xi & -4\xi \bar{I}_2 \sin 2\tilde{\theta}_n^* \end{pmatrix}. \quad (3.68)$$

For each set of fixed points, we calculate the eigenvalues of the matrix, given by $\det|\mathbf{A} - \lambda\mathbf{I}| = 0$ to determine the type of fixed point.

1. **Fixed Point 1:** $(\tilde{I}_n^*, \tilde{\theta}_n^*) = (0, \frac{1}{2} \cos^{-1}(\Delta_2/(2\xi\bar{I}_2)))$

The eigenvalues are given by

$$\lambda = \pm 4\xi\bar{I}_2 \left[1 - \left(\frac{\Delta_2}{2\xi\bar{I}_2} \right)^2 \right]^{1/2} = \pm 2\xi \left[(2\bar{I}_2)^2 - \left(\frac{\Delta_2}{\xi} \right)^2 \right]^{1/2}. \quad (3.69)$$

These eigenvalues are real for $|\Delta_2| < 2\xi\bar{I}_2$. Given that the bare detuning, Δ_{02} , is always positive for the second-order Hamiltonian (see Table 3.2) and the typical population of the fixed modes, \bar{I}_2 is also positive, this condition leads to a critical value of the nonlinearity parameter, ξ ,

$$\boxed{\xi_c = \frac{\Delta_{02}}{6\bar{I}_2}} \quad (3.70)$$

For $\xi \geq \xi_c$ this fixed point is a saddle point and the separatrix passes through this point.

2. **Fixed Point 2:** $(\tilde{I}_n^*, \tilde{\theta}_n^*) = (-\Delta_2/\xi + 2\bar{I}_2, m\pi)$, $m = \text{integer}$

$$\lambda = \pm 2\sqrt{2}\xi\bar{I}_2^{1/2} \left[\frac{\Delta_2}{\xi} - 2\bar{I}_2 \right]^{1/2}. \quad (3.71)$$

For $\tilde{I}_n^* = -\Delta_2/\xi + 2\bar{I}_2 > 0$ the fixed point is a center, and for $\tilde{I}_n^* < 0$ it is a saddle point. We exclude the unphysical values $\tilde{I}_n^* < 0$. The stationary points for $\tilde{I}_n^* > 0$ is at $\cos(2\tilde{\theta}_n) = +1$, are the physical resonances for the second order driving terms, with resonant value given by

$$\boxed{I_{\text{res}} = -\frac{\Delta_{02}}{2\xi} + 3\bar{I}_2.} \quad (3.72)$$

Furthermore the condition for the existence of this type of resonance is $\xi > \xi_c$.

3. **Fixed Point 3:** $(\tilde{I}_n^*, \tilde{\theta}_n^*) = (-\Delta_2/\xi + 2\bar{I}, (2m+1)\pi/2)$, $m = \text{integer}$

For $\cos(2\tilde{\theta}_n^*) = -1$, the value of \tilde{I}_n is always negative and thus not relevant to the current analysis.

Separatrix Height

The separatrix passes through the fixed point at $\tilde{I}_n^* = 0$, $\tilde{\theta}_n^* = \frac{1}{2} \cos^{-1}(\Delta_2/(2\xi\bar{I}_2))$ when $\tilde{\theta}_n^*$ is real. The contour plots of \tilde{h}_n confirm that the separatrix passes through this fixed point. The maximum value of \tilde{I}_n along the separatrix can be found by solving for \tilde{I}_n when $\tilde{h}_n = 0$. Given

$$\begin{aligned}\tilde{h}_n &= -\Delta_2\tilde{I}_n - \frac{\xi}{2}\tilde{I}_n^2 + 2\xi\tilde{I}_n\bar{I}_2 \cos 2\tilde{\theta}_n = 0, \\ \tilde{I}_n &= -\frac{2\Delta_2}{\xi} + 4\bar{I}_2 \cos 2\tilde{\theta}_n = -\frac{\Delta_{02}}{\xi} + 2\bar{I}_2(1 + 2 \cos 2\tilde{\theta}_n).\end{aligned}$$

The maximum height of the separatrix occurs at $\tilde{\theta}_n = 0$ and is given by

$$\boxed{\tilde{I}_{\text{sep}} = -\frac{\Delta_{02}}{\xi} + 6\bar{I}_2.} \quad (3.73)$$

In Fig. 3.5(a)-(b) the phase plots for the second order Hamiltonian is plotted for nonlinearities above and below the critical value. For $\xi \leq \xi_c$, there is no resonance in the phase-space that corresponds to physical values of \tilde{I}_n . In Fig. 3.5(b), where $\xi > \xi_c$, there is a resonance and the separatrix is defined by the contour $\tilde{h}_n = 0$ which is plotted in black. The resonance values and separatrix height are labeled by the values given by (3.72) and (3.73), respectively.

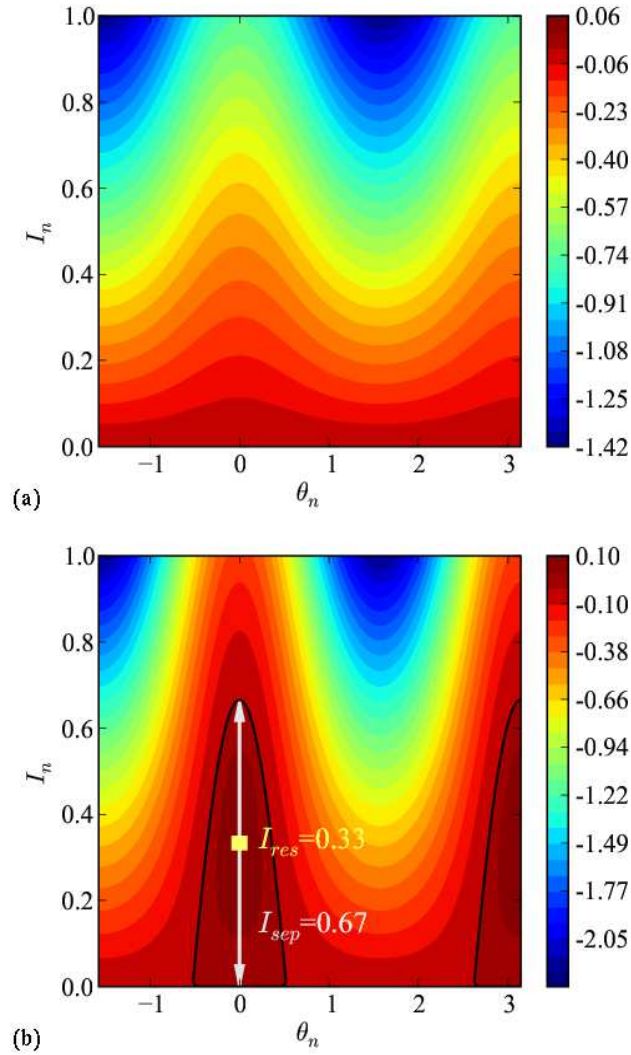


Figure 3.5: Phase-space plots for the second order Hamiltonian. (a) $\xi = 0.5$ ($\kappa = 0.16$ for $N_s = 11$). There is no resonance in the range $0 \leq \tilde{I}_n \leq 1$ for $\xi < \xi_c = 1$. (b) $\xi = 1.5$ ($\kappa = 0.49$ for $N_s = 11$). $\bar{I}_2 = 1/3$, $\Delta_{02} = 2$. For $\xi > \xi_c$ the resonant value is given by (3.72) and the separatrix with is given by (3.73).

The values of the action variable at resonance and the separatrix height are plotted in Fig. 3.6 for the two second-order Hamiltonians as a function of the nonlinearity, ξ for the two lowest bare detunings. The two detunings are $\Delta_{02} = 2$, corresponding to $(n+1, n-1) \rightarrow (n, n)$ and $\xi_c = 2\bar{I}_2/3$, and $\Delta_{02} = 8$ for $(n+2, n-2) \rightarrow (n, n)$ and

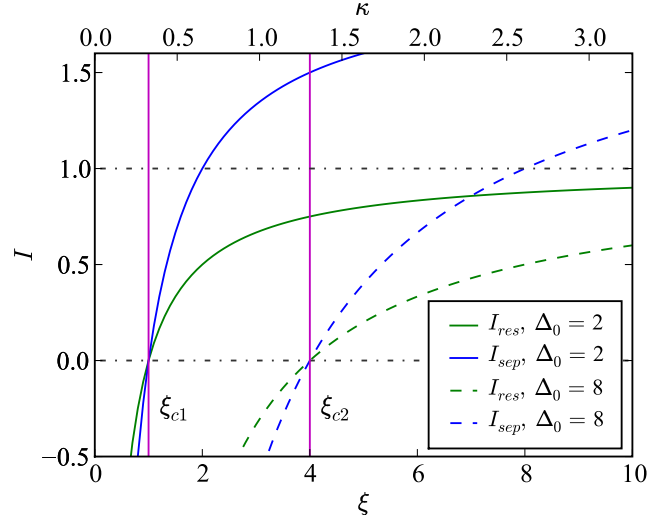


Figure 3.6: Resonant values and separatrix width for second-order resonance for $\Delta_{02} = 2$ $[(n+1, n-1) \rightarrow (n, n)]$ and for $\Delta_{02} = 8$ $[(n+2, n-2) \rightarrow (n, n)]$. $\bar{I} = 0.33$. Vertical lines: $\Delta_{20} = 2$: $\xi_{c1} = 1/3\bar{I}_2 = 1$, $\Delta_{02} = 8$: $\xi_{c2} = 4/3\bar{I}_2 = 4$. The upper x-axis gives the corresponding values of κ for $N_s = 11$.

$\xi_c = 4\bar{I}_2/3$. It is clear from the plot that for the second order resonant Hamiltonian there is a critical value of the nonlinearity such that below that value there are no physical resonances present.

3.3 Failure of Chirikov's Criterion

The Chirikov criterion for the onset of global chaos is governed by the ratio of the width of the separatrix and the distance between the resonances for individual resonances. When the width of the separatrices becomes comparable to the distance between the resonances, the Chirikov parameter \mathcal{K} satisfies the inequality,

$$\mathcal{K} \equiv \frac{\text{separatrix width}}{\text{distance between resonances}} = \frac{\Delta I}{I_{\text{res1}} - \bar{I}_{\text{res2}}} \gtrsim 1, \quad (3.74)$$

and the system is predicted to be chaotic.

We should note that the study of resonances in the BHM is quite different from the case of the kicked rotor. In particular, it is not possible to independently vary the frequency of the drive and the strength of the drive in the BHM. In addition, in the canonical transformation to the rotating reference frame the action variable is unchanged, $\tilde{I}_n = I_n$, so that the resonant values of \tilde{I}_n are not well-spaced in the original action coordinates. Furthermore in the BHM, for the first order resonances, a single driving term has resonances at multiple action values.

Note that for a generic driving term, $(n + p, n + m - p) \rightarrow (n, n + m)$, the bare detuning is given by

$$\begin{aligned}
\Delta_0 &= (n + p)^2 + (n + m - p)^2 - n^2 - (n + m)^2 = \\
&= n^2 + 2np + p^2 + n^2 + m^2 + p^2 - 2np - 2mp + 2nm \\
&\quad - [n^2 + n^2 + 2nm + m^2] \\
&= 2p^2 - 2mp,
\end{aligned} \tag{3.75}$$

which is always constant.

We present several ways to deduce the criterion governing the threshold for the mean-field Bose-Hubbard model and see that the various methods are in agreement.

Onset of Second-Order Resonances First we consider the case of the second-order resonance, where the analytic expression is simple.

From the previous analysis for the second order resonance, the separatrix width is given by,

$$I_{\text{sep}} = \frac{-\Delta_0}{\xi} + 6\bar{I}. \tag{3.76}$$

The distance between resonances is proportional to ξ^{-1} ,

$$\Delta I_{\text{res}} = I_{\text{res}}(\Delta_b) - I_{\text{res}}(\Delta_a) = \frac{\Delta_{0a} - \Delta_{0b}}{\xi}. \quad (3.77)$$

For the lowest two resonances, a naive comparison of the separatrix height and distance between the resonances gives,

$$\mathcal{K} \equiv \frac{I_{\text{sep}}}{\Delta I_{\text{res}}} = \frac{-2/\xi + 6\bar{I}}{6/\xi} \quad (3.78)$$

and chaos exists for

$$\mathcal{K} \gtrsim 1 \Rightarrow \boxed{\bar{I}\xi \gtrsim \frac{5}{3}} \quad (3.79)$$

However, but looking at Fig. 3.6 , we see that once the second resonance appears, the two resonances overlap. Thus we take the appearance of the second resonance as the criterion for the second-order case, which gives

$$\xi > \xi_{c2} = \frac{4}{3\bar{I}} \text{ or } \boxed{\bar{I}\xi \gtrsim \frac{4}{3}}. \quad (3.80)$$

Overlap of resonances within first-order resonant Hamiltonian For the first-order resonance, the resonances of \tilde{I}_{n2}^* grow from zero and exist for any $\xi > 0$. However, the separatrix of the resonance is small and thus even though the resonances may overlap, the population is still expected to be confined in a narrow region of phase-space. However, there are additional resonances at larger values of \tilde{I}_n , which are initially inaccessible and move down from above. For the first-order resonance we use the criterion that the two separatrices of the same first-order Hamiltonian overlap - i.e. all of phase

space is accessible to a single mode. The condition for being able to explore the entire phase-space for a given I_n is thus

$$\xi \geq \xi_{c1} \equiv -\frac{\Delta_{01}}{(1 + 3\sqrt[3]{2})\bar{I}_1} \quad (3.81)$$

which is equivalent to

$$\bar{I}\xi \geq -\frac{\Delta_{01}}{(1 + 3\sqrt[3]{2})}. \quad (3.82)$$

For the lowest bare detuning, $\Delta_{01} = -4$, the criterion is

$$\boxed{\bar{I}\xi \geq \frac{4}{(1 + 3\sqrt[3]{2})} \approx 0.84} \quad (3.83)$$

which is the comparable to the results for the second order resonance.

Dimensional Analysis An alternate way of coming to this conclusion is to consider dimensional grounds. The starting point is to assume:

1. Typical mode occupation: $\bar{I} \sim \frac{1}{\Delta n}$
2. Resonant approximation: only include resonant terms in equations of motion.
3. Quadratic dispersion instead of cosine: $\omega_n = \tilde{\omega}_1 n^2$

These are the same ingredients for the previous analytic analysis. A quadratic dispersion leads to translational invariance. The momentum distribution can be shifted with no effect. The resonant equations are invariant under a shift in 'n', thus the frequency scale is set by $\tilde{\omega}_1$. As a consequence of the resonant approximation, the equations of motion only couple neighboring modes. Thus, μ_0 and Δn can only enter as $\frac{\mu_0}{\Delta n}$. Thus the only parameters are $\mu_0/\Delta n$ and $\tilde{\omega}_1$. The only dimensionless combination of these quantities is $\mu_0/(\hbar\tilde{\omega}_1\Delta n) = \xi/\Delta n$, so this parameter must be what governs the Chirikov threshold.

Significantly, all of these methods give the same functional form of the criterion and are identical up to numerical factors.

3.3.1 Thermodynamic Limit

Next we consider how \mathcal{K} scales in the thermodynamic limit, ($N_s \rightarrow \infty$ while $U = \text{const}$, $J = \text{const}$, $N_a/N_s = \text{const}$). Additionally, the width of the momentum distribution remains fixed, $\Delta n/N_s = \text{const}$. In this limit, the nonlinearity parameter κ is constant while $\xi \sim N_s^2$. The typical occupation of the fixed modes is given by $\bar{I} \sim (\Delta n)^{-1} \sim (N_s)^{-1}$. We find that the Chirikov parameter,

$$\mathcal{K} \approx \xi \bar{I} \sim \frac{N_s^2}{N_s} \sim N_s \quad (3.84)$$

diverges in the thermodynamic limit, predicting that there is no threshold in that limit and \mathcal{K} is always greater than one indicating that the system is always chaotic. However, this is not what we have observed numerically. At a minimum Chirikov predicts the threshold to scales linearly with the size of the system and our numerics indicate that the threshold depends on parameters that are independent of the system size.

3.3.2 Continuous Limit

To check this threshold, we also consider the continuum limit, in which the length of the system, normalization and interaction parameter are fixed, while the distance between lattice sites goes to zero: $L, N_a, \mu_0 = \text{const}$, $a \rightarrow 0, N_s \rightarrow \infty$.

$$\mathcal{K} \sim \frac{U}{J} \left(\frac{N_a}{\Delta n} \right) N_s = \frac{\mu_0 N_s}{N_a} \frac{2mL^2}{\hbar^2 N_s^2} \left(\frac{N_a}{\Delta n} \right) N_s = \frac{2\mu_0 m L^2}{\hbar^2} \left(\frac{1}{\Delta n} \right) \sim \frac{1}{N_s} \rightarrow 0 \quad (3.85)$$

In the continuum limit, the number of modes in the initial momentum distribution, Δn , must diverge, so that $N_a = \Delta n |\bar{\psi}_n|^2$ remains constant. Alternatively we can say that $\Delta n/N_s$ is fixed. From either perspective, it is clear that \mathcal{K} vanishes in the continuum limit, predicting regular motion, as expected due to the known integrability of the continuous NLS equation.

This leads to the question: Why does the Chirikov analysis fail in this case? Several possible explanations are:

1. non-quadraticity of the spectrum
2. break down of the resonant approximation
3. interferences between resonances.

First there are possible corrections due to the lattice and that we have assumed a quadratic dispersion instead of a cosine dispersion. We conjecture that the Chirikov analysis is incorrect because the resonant approximation is wrong and off-resonant terms are significant. That is the motion is not dominated by single driving terms. It is also possible that the single resonance approximation is incorrect and a multi-resonance model is necessary for recovering the correct scaling.

Chapter 4

Conserved Quantities of the Ablowitz-Ladik Lattice

From the numerical work on the Bose-Hubbard Model, we have seen regions where although individual trajectories are chaotic the system does not relax to the expected thermal state. Additionally there are regions in the parameter space of nonlinearity, κ , and energy-per-particle, ε_T , where the system relaxes even though chaos is not present. Additionally it has been found that the slow relaxation times for individual states with the same nonlinearity and energy-per-particle vary widely. What is the origin of these phenomena?

There are at least three nearby integrable systems of the BHM. These are the noninteracting case ($\kappa = 0$), the continuum limit, which is the continuous nonlinear Schrödinger equation and the integrable discrete nonlinear Schrödinger equation (IDNLS) also known as the Ablowitz-Ladik (AL) lattice, which we discuss in this section. Looking at the relaxation of individual realizations, it appears that initial states which have a higher quasi-momentum also have a higher final spectral entropy. The total quasi-momentum is not a conserved quantity of the BHM. It is however, a conserved quantity of all three nearby integrable systems. In some cases the normalized spectral entropy may not vanish because the system has a very slow relaxation time. In other cases it may be that it will never fully relax because of the nearby conserved quantities. Are the slow relaxation times governed by the conserved quantities of the nearby integrable systems? In the regions where it is clear that the steady-state is not the

thermal state, what governs the steady-state? This evidence suggests that the integrals of motion of the nearby conserved quantities play a role in the relaxation dynamics of the BHM. In this section, we derive the conserved quantities of the AL.

4.1 Integrable Discrete Nonlinear Schrödinger (IDNLS) Equation

The continuous Nonlinear Schrödinger (NLS) Equation is given by,

$$i\dot{q} + q_{xx} + \sigma|q|^2q = 0 \quad (4.1)$$

where $\dot{q} = dq/dt$ and $q_x = dq/dx$, is known to be completely integrable. The corresponding Hamiltonian is

$$H(q, q^*) = - \int_0^L \left[q_x q_x^* + \frac{1}{2} \sigma (qq^*)^2 \right] dx, \quad (4.2)$$

with canonical pairs q, q^* . Periodic boundary conditions are assumed. The mean-field Bose-Hubbard model is a discretization of the NLS equation. In real space, the Hamiltonian can be written as:

$$H = - \sum_n (q_n q_{n+1}^* + q_n^* q_{n+1} - 2|q_n|^2) + \frac{\sigma}{2} \sum_n |q_n|^4 \quad (4.3)$$

with the Poisson brackets

$$\{q_m, q_n^*\} = i\delta_{m,n}, \quad \{q_m, q_n\} = \{q_m^*, q_n^*\} = 0. \quad (4.4)$$

The equations of motion, which are given by $\dot{q}_n = \{H, q_n\}$, are

$$i\dot{q}_n = -(q_{n+1} + q_{n-1} - 2q_n) + \sigma|q_n|^2 q_n. \quad (4.5)$$

This equation, also known as the Diagonal Discrete Nonlinear Schrödinger (DDNLS) Equation, does not preserve the integrability of the continuous case. An alternate discretization, which is integrable (Ablowitz and Ladik, 1976), has equations of motion:

$$i\dot{q}_n = -(q_{n+1} + q_{n-1} - 2q_n) + \sigma|q_n|^2(q_{n+1} + q_{n-1})/2 \quad (4.6)$$

and is suitably called the Integrable Discrete Nonlinear Schrödinger (IDNLS) Equation, also known as the Ablowitz-Ladik lattice (AL). This equation can be derived from the Hamiltonian (Scharf and Bishop, 1991; Herbst *et al.*, 1994)

$$H = -\sum_n (q_n q_{n+1}^* + q_n^* q_{n+1}) - \frac{4}{\sigma} \sum_n \ln \left(1 - \frac{\sigma}{2} |q_n|^2 \right) \quad (4.7)$$

with the nonstandard Poisson brackets

$$\{q_m, q_n^*\} = i \left(1 - \frac{\sigma}{2} |q_n|^2 \right) \delta_{m,n}, \quad \{q_m, q_n\} = \{q_m^*, q_n^*\} = 0. \quad (4.8)$$

The equations of motion are derived in the usual way, $\dot{q}_m = \{H, q_m\}$. Using the following properties of Poisson brackets,

$$\{a, bc\} = b\{a, c\} + \{a, b\}c \quad (4.9)$$

$$\{f(a), b\} = \frac{\partial f}{\partial a} \{a, b\}, \quad (4.10)$$

the AL equation can be derived from the equations of motion of Hamiltonian (4.7),

$$\begin{aligned}
\dot{q}_m &= \{H, q_m\} \\
&= - \sum_n (\{q_n q_{n+1}^*, q_m\} + \{q_n^* q_{n+1}, q_m\}) - \frac{4}{\sigma} \sum_n \{\ln(1 - \frac{\sigma}{2}|q_n|^2), q_m\} \\
&= - \sum_n (q_n \{q_{n+1}^*, q_m\} + \{q_n^*, q_m\} q_{n+1}) - \frac{4}{\sigma} \sum_n \left[\frac{\partial}{\partial q_n^*} \ln(1 - \frac{\sigma}{2}|q_n|^2) \right] \{q_n^*, q_m\} \\
&= - \sum_n \left[q_n \cdot (-i)(1 - \frac{\sigma}{2}|q_{n+1}|^2) \delta_{m,n+1} + q_{n+1} \cdot (-i)(1 - \frac{\sigma}{2}|q_n|^2) \delta_{m,n} \right] \\
&\quad + \frac{4}{\sigma} \sum_n \frac{(\sigma/2)q_n}{1 - \frac{\sigma}{2}|q_n|^2} \cdot (-i)(1 - \frac{\sigma}{2}|q_n|^2) \delta_{m,n} \\
&= i \left[q_{m-1}(1 - \frac{\sigma}{2}|q_m|^2) + q_{m+1}(1 - \frac{\sigma}{2}|q_m|^2) \right] - 2iq_m \\
&= i(q_{m-1} + q_{m+1} - 2q_m) - i\frac{\sigma}{2}|q_m|^2(q_{m-1} + q_{m+1}).
\end{aligned}$$

This equation is completely integrable and has an infinite number of conserved quantities (for the infinite lattice) and can be solved by the method of Inverse Scattering Transform (IST) developed by Gardner, Greene, Kruskal and Mira (Gardner *et al.*, 1967).

4.2 Conserved Quantities of the AL equation

In this section, we outline the approach of inverse scattering and the work of Ablowitz and Ladik for calculating the conserved quantities of the AL equation (Ablowitz and Ladik, 1976; Ablowitz and Segur, 1981).

The method of inverse scattering is analogous to the Discrete Fourier Transform. In the direct scattering problem, scattering data is derived from initial data, the potential. The time evolutions of the scattering data is simple. From the scattering data at some time 't', the potential can be calculated via the (non-trivial) inverse scattering transform.

In order to calculate the conserved quantities is it only necessary to calculate the scattering data. From the scattering data it is clear which quantities are time independent.

The following is an outline of Ablowitz and Ladik (1976) with details filled in using (Ablowitz and Segur, 1981). For the AL equation, we taking $S_n(t) = T_n(t) = 0$ in (Ablowitz and Ladik, 1976). The canonical pairs are R_n and Q_n . In the end we set $R_n = \pm\alpha Q_n^*$.

To begin, consider the generalized eigenvalue problem,

$$\begin{aligned} V_{1,n+1} &= zV_{1,n} + Q_n(t)V_{2,n} \\ V_{2,n+1} &= \frac{1}{z}V_{2,n} + R_n(t)V_{1,n}, \end{aligned} \tag{4.11}$$

which can be equivalently expressed as

$$\begin{pmatrix} \hat{E} & -Q_n(t) \\ -R_n(t) & \hat{E} \end{pmatrix} \begin{pmatrix} V_1 \\ V_2 \end{pmatrix} = \begin{pmatrix} z & 0 \\ 0 & 1/z \end{pmatrix} \begin{pmatrix} V_1 \\ V_2 \end{pmatrix} \tag{4.12}$$

where \hat{E} is the shift operator: $\hat{E}X_n = X_{n+1}$. In this form, one can see the analogy with the Schrödinger equation in quantum mechanics with Q_n and R_n playing the role of the potential. The potentials correspond to the real-space classical fields ψ_n, ψ_n^* in the AL. The time-dependence is postulated to have the form

$$\begin{aligned} \dot{V}_{1,n} &= A_n(t)V_{1,n} + B_n(t)V_{2,n} \\ \dot{V}_{2,n} &= C_n(t)V_{1,n} + D_n(t)V_{2,n}. \end{aligned} \tag{4.13}$$

The associated equations of motion for A_n, B_n, C_n, D_n are generated by cross-differentiating (4.11) and (4.13)

$$\begin{aligned}
\frac{\partial}{\partial t}(V_{1,n+1}) &= z\dot{V}_{1,n} + \dot{Q}_n V_{2,n} + Q_n \dot{V}_{2,n} \\
&= z(A_n V_{1,n} + B_n V_{2,n}) + \dot{Q}_n V_{2,n} + Q_n (C_n V_{1,n} + D_n V_{2,n}) \\
\frac{\partial}{\partial t}(V_{2,n+1}) &= \frac{1}{z}\dot{V}_{2,n} + \dot{R}_n V_{1,n} + R_n \dot{V}_{1,n} \\
&= \frac{1}{z}(C_n V_{1,n} + D_n V_{2,n}) + \dot{R}_n V_{1,n} + R_n (A_n V_{1,n} + B_n V_{2,n}) \\
\left(\frac{\partial V_{1,n'}}{\partial t}\right)_{n'=n+1} &= A_{n+1} V_{1,n+1} + B_{n+1} V_{2,n+1} \\
&= A_{n+1} (zV_{1,n} + Q_n V_{2,n}) + B_{n+1} \left(\frac{1}{z}V_{2,n} + R_n V_{1,n}\right) \\
\left(\frac{\partial V_{2,n'}}{\partial t}\right)_{n'=n+1} &= C_{n+1} V_{1,n+1} + D_{n+1} V_{2,n+1} \\
&= C_{n+1} (zV_{1,n} + Q_n V_{2,n}) + D_{n+1} \left(\frac{1}{z}V_{2,n} + R_n V_{1,n}\right)
\end{aligned} \tag{4.14}$$

where the eigenvalue, z is time-invariant and the explicit time-dependence has been dropped. Requiring $\frac{\partial}{\partial t}V_{i,n+1} = \left(\frac{\partial}{\partial t}V_{i,n'}\right)_{n'=n+1}$,

$$\begin{aligned}
&z(A_n V_{1,n} + B_n V_{2,n}) + \dot{Q}_n V_{2,n} + Q_n (C_n V_{1,n} + D_n V_{2,n}) \\
&= A_{n+1} (zV_{1,n} + Q_n V_{2,n}) + B_{n+1} \left(\frac{1}{z}V_{2,n} + R_n V_{1,n}\right) \\
&\frac{1}{z}(C_n V_{1,n} + D_n V_{2,n}) + \dot{R}_n V_{1,n} + R_n (A_n V_{1,n} + B_n V_{2,n}) \\
&= C_{n+1} (zV_{1,n} + Q_n V_{2,n}) + D_{n+1} \left(\frac{1}{z}V_{2,n} + R_n V_{1,n}\right)
\end{aligned} \tag{4.15}$$

and equating the coefficients of $V_{i,n}$ for each equation results in the following time-evolution equations,

$$\begin{aligned}
z\Delta_n A_n + R_n B_{n+1} - Q_n C_n &= 0 \\
(1/z)B_{n+1} - zB_n + Q_n(A_{n+1} - D_n) &= \dot{Q}_n \\
zC_{n+1} - (1/z)C_n - R_n(A_n - D_{n+1}) &= \dot{R}_n \\
(1/z)\Delta_n D_n + Q_n C_{n+1} - R_n B_n &= 0,
\end{aligned} \tag{4.16}$$

where $\Delta_n X_n \equiv X_{n+1} - X_n$.

The linear dispersion relation and the above equations suggest the following expansions for the functions of (4.13):

$$\begin{aligned}
A_n &= z^2 A_n^{(2)} + A_n^{(0)} \\
B_n &= z B_n^{(1)} + \frac{1}{z} B_n^{(-1)} \\
C_n &= z C_n^{(1)} + \frac{1}{z} C_n^{(-1)} \\
D_n &= D_n^{(0)} + \frac{1}{z^2} D_n^{(-2)}
\end{aligned} \tag{4.17}$$

The coefficients of these expansions are determined by substituting back into (4.16),

$$\begin{aligned}
& z^3 \Delta_n A_n^{(2)} + z \Delta_n A_n^{(0)} + z R_n B_{n+1}^{(1)} + (1/z) R_n B_{n+1}^{(-1)} \\
& \quad - z Q_n C_n^{(1)} - (1/z) Q_n C_n^{(-1)} = 0 \\
& B_{n+1}^{(1)} + (1/z^2) B_{n+1}^{(-1)} - z^2 B_n^{(1)} - B_n^{(-1)} + Q_n (z^2 A_{n+1}^{(2)} + A_{n+1}^{(0)}) \\
& \quad - D_n^{(0)} - (1/z^2) D_n^{(-2)} = \dot{Q}_n \\
& z^2 C_{n+1}^{(1)} + C_{n+1}^{(-1)} - C_n^{(1)} - (1/z^2) C_n^{(-1)} - R_n (z^2 A_n^{(2)} + A_n^{(0)}) \\
& \quad - D_{n+1}^{(0)} - (1/z^2) D_{n+1}^{(-2)} = \dot{R}_n \\
& (1/z) \Delta_n D_n^{(0)} + (1/z^3) \Delta_n D_n^{(-2)} + z Q_n C_{n+1}^{(1)} - (1/z) Q_n C_{n+1}^{(-1)} \\
& \quad - z R_n B_n^{(1)} - (1/z) R_n B_n^{(-1)} = 0,
\end{aligned} \tag{4.18}$$

and solving in powers of 'z':

$$\begin{aligned}
O(z^3) : \quad \Delta_n A_n^{(2)} = 0 & \quad \Rightarrow A_{n+1}^{(2)} = A_n^{(2)} \equiv A_-^{(2)} \\
O\left(\frac{1}{z^3}\right) : \quad \Delta_n D_n^{(-2)} = 0 & \quad \Rightarrow D_{n+1}^{(-2)} = D_n^{(-2)} \equiv D_-^{(-2)} \\
O(z^2) : \quad B_n^{(1)} - Q_n A_n^{(2)} = 0 & \quad \Rightarrow B_n^{(1)} = Q_n A_-^{(2)} \\
& C_{n+1}^{(1)} - R_n A_n^{(2)} = 0 & \quad \Rightarrow C_n^{(1)} = R_{n-1} A_-^{(2)} \\
O\left(\frac{1}{z^2}\right) : \quad B_{n+1}^{(-1)} - Q_n D_n^{(-2)} = 0 & \quad \Rightarrow B_n^{(-1)} = Q_{n-1} D_-^{(-2)} \\
& C_n^{(-1)} - R_n D_n^{(-2)} = 0 & \quad \Rightarrow C_n^{(-1)} = R_n D_-^{(-2)} \\
O(z) : \quad \Delta_n A_n^{(0)} = Q_n C_n^{(1)} - R_n B_{n+1}^{(1)} & \\
& \quad = -A_-^{(2)} (Q_{n+1} R_n - Q_n R_{n-1}) \\
& \Rightarrow A_n^{(0)} = -A_-^{(2)} Q_n R_{n-1} + A_-^{(0)} \\
O\left(\frac{1}{z}\right) : \quad \Delta_n D_n^{(0)} = R_n B_n^{(-1)} - Q_n C_{n+1}^{(-1)} & \\
& \quad = -D_-^{(-2)} (Q_n R_{n+1} - Q_{n-1} R_n) \\
& \Rightarrow D_n^{(0)} = -D_-^{(-2)} Q_{n-1} R_n + D_-^{(0)}.
\end{aligned} \tag{4.19}$$

The zeroeth order yields the time-dependence of the potentials,

$O(z^0)$:

$$\begin{aligned}
\dot{Q}_n &= B_{n+1}^{(1)} - B_1^{(-1)} + Q_n \left(A_{n+1}^{(0)} - D_n^{(0)} \right) \\
\dot{Q}_n &= \left(A_-^{(2)} Q_{n+1} - D_-^{(-2)} Q_{n-1} \right) (1 - Q_n R_n) + Q_n \left(A_-^{(0)} - D_-^{(0)} \right) \\
\dot{R}_n &= C_{n+1}^{(-1)} - C_n^{(1)} - R_n \left(A_n^{(0)} - D_{n+1}^{(0)} \right) \\
\dot{R}_n &= \left(D_-^{(2)} R_{n+1} - A_-^{(-2)} R_{n-1} \right) (1 - Q_n R_n) - R_n \left(A_-^{(0)} - D_-^{(0)} \right).
\end{aligned} \tag{4.20}$$

In summary, the coefficients of the time-evolution equations are given by

$$\begin{aligned}
A_n &= A_-^{(2)} (z^2 - Q_n R_{n-1}) + A_-^{(0)} \\
B_n &= A_-^{(2)} Q_n z - D_-^{(-2)} Q_{n-1} (1/z) \\
C_n &= A_-^{(2)} R_{n-1} z - D_-^{(-2)} R_n (1/z) \\
D_n &= D_-^{(-2)} ((1/z^2) - Q_{n-1} R_n) + D_-^{(0)},
\end{aligned} \tag{4.21}$$

while the time evolutions of Q_n and R_n are governed by

$$\dot{Q}_n = \left(A_-^{(2)} Q_{n+1} - D_-^{(-2)} Q_{n-1} \right) (1 - Q_n R_n) + Q_n \left(A_-^{(0)} - D_-^{(0)} \right) \tag{4.22a}$$

$$\dot{R}_n = \left(D_-^{(2)} R_{n+1} - A_-^{(-2)} R_{n-1} \right) (1 - Q_n R_n) - R_n \left(A_-^{(0)} - D_-^{(0)} \right) \tag{4.22b}$$

4.2.1 AL equation

To obtain the AL equation, we let $R_n = \pm \alpha Q_n^*$, $A_-^{(2)} = -D_-^{(-2)} = i$, and $A_-^{(0)} = -D_-^{(0)} = -i$. In this case equation (4.22a) becomes

$$\dot{Q}_n = i \left[Q_{n+1} + Q_{n-1} - 2Q_n \mp \alpha |Q_n|^2 (Q_{n+1} + Q_{n-1}) \right], \tag{4.23}$$

which is the AL equation. With these substitutions, the time-dependent function A_n, \dots, D_n obey

$$\begin{aligned}
A_n &= i(z^2 \mp \alpha Q_n Q_{n-1}^* - 1) \\
B_n &= i(zQ_n - (1/z)Q_{n-1}) \\
C_n &= \pm i\alpha(zQ_{n-1}^* - (1/z)Q_n^*) \\
D_n &= i(1 - (1/z^2) \pm \alpha Q_{n-1} Q_n^*).
\end{aligned} \tag{4.24}$$

4.2.2 Direct Scattering Problem

Asymptotic Solution of Generalized Eigenvalue Problem First of all we assume that Q_n and R_n are on compact support, that is that as $|n| \rightarrow \infty$, $Q_n, R_n \rightarrow 0$. In the limit $|n| \rightarrow \infty$, the generalized eigenvalue problem becomes,

$$|n| \rightarrow \infty : \quad \begin{cases} V_{1,n+1} = zV_{1,n} \\ V_{2,n+1} = \frac{1}{z}V_{2,n}. \end{cases} \tag{4.25}$$

To solve this direct scattering problem, define the time-independent eigenfunctions, $\phi_n, \bar{\phi}_n, \psi_n, \bar{\psi}_n$ which have the asymptotic forms:

$$\begin{aligned}
n \rightarrow -\infty : \quad \phi_n &\sim \begin{pmatrix} 1 \\ 0 \end{pmatrix} z^n, & \bar{\phi}_n &\sim \begin{pmatrix} 0 \\ -1 \end{pmatrix} z^{-n} \\
n \rightarrow +\infty : \quad \psi_n &\sim \begin{pmatrix} 0 \\ 1 \end{pmatrix} z^{-n}, & \bar{\psi}_n &\sim \begin{pmatrix} 1 \\ 0 \end{pmatrix} z^n.
\end{aligned} \tag{4.26}$$

These eigenfunctions satisfy the generalized eigenvalue problem at a fixed time, which will be taken to be $t=0$. They do not solve the time-evolution equations, which we will return to later. One can establish by induction, that

$$\begin{aligned}
 z^{-n}\phi_n, z^n\psi_n &\text{ are polynomial in powers of } \frac{1}{z} \text{ and are analytic for } |z| > 1 \\
 z^n\bar{\phi}_n, z^{-n}\bar{\psi}_n &\text{ are polynomial in powers of } z \text{ and are analytic for } |z| < 1 \text{ } (|z| < \infty)
 \end{aligned}
 \tag{4.27}$$

given that Q_n and R_n are on compact support.

Wronskian and Linear Independence The Wronskian of a set of functions $\{\phi_1, \dots, \phi_n\}$ is defined by:

$$W(\phi_1, \dots, \phi_n) \equiv \begin{vmatrix} \phi_1 & \phi_2 & \cdots & \phi_n \\ \phi_1' & \phi_2' & \cdots & \phi_n' \\ \vdots & \vdots & \ddots & \vdots \\ \phi_1^{(n-1)} & \phi_2^{(n-1)} & \cdots & \phi_n^{(n-1)} \end{vmatrix} \tag{4.28}$$

If the Wronskian is non-zero in some interval, then the functions are linearly independent in that interval.

For this problem, the Wronskian is defined as $W_n(u, v) = u_{1,n}v_{2,n} - u_{2,n}v_{1,n}$. The Wronskian of the functions that obey (4.11) can be found by

$$\begin{aligned}
W_{n+1}(u, v) &= u_{1,n+1}v_{2,n+1} - u_{2,n+1}v_{1,n+1} \\
&= (zu_{1,n} + Q_n u_{2,n})((1/z)v_{2,n} + R_n v_{1,n}) \\
&\quad - ((1/z)u_{2,n} + R_n u_{1,n})(zv_{1,n} + Q_n v_{2,n}) \\
&= u_{1,n}v_{2,n} + zR_n u_{1,n}v_{1,n} + (1/z)Q_n u_{2,n}v_{2,n} + Q_n R_n u_{2,n}v_{1,n} \\
&\quad - (u_{2,n}v_{2,n} + (1/z)Q_n u_{2,n}v_{2,n} + zR_n u_{1,n}v_{1,n} + Q_n R_n u_{2,n}v_{1,n}) \\
&= (1 - R_n Q_n)(u_{1,n}v_{2,n} - u_{2,n}v_{1,n}) \\
&= (1 - R_n Q_n)W_n(u, v)
\end{aligned} \tag{4.29}$$

Using the asymptotic forms of $\phi_n, \bar{\phi}_n, \psi_n, \bar{\psi}_n$, one gets

$$\begin{aligned}
\lim_{n \rightarrow -\infty} W_n(\bar{\phi}, \phi) &= -\bar{\phi}_{2,n}\phi_{1,n} = -(-z^{-n})(z^n) = 1 \\
\lim_{n \rightarrow +\infty} W_n(\bar{\psi}, \psi) &= -\bar{\psi}_{1,n}\psi_{2,n} = (z^n)(z^{-n}) = 1.
\end{aligned} \tag{4.30}$$

By induction, one can show that the Wronskian of the eigenfunctions obey

$$W_n(\bar{\phi}, \phi) = \prod_{i=-\infty}^n (1 - R_i Q_i), \quad W_n(\bar{\psi}, \psi) = \prod_{i=n+1}^{\infty} (1 - R_i Q_i)^{-1} \tag{4.31}$$

for z on the unit circle. For $R_n = -Q_n^*$, W_n is positive-definite so that $\bar{\phi}_n, \phi_n$ are linearly independent. Otherwise assume that initially R_n and Q_n are less than one. Likewise one can show that $\bar{\psi}_n, \psi_n$ are linearly independent. Thus one can define the scattering data by

$$\begin{aligned}
\phi_n &= a(z, t)\bar{\psi}_n + b(z, t)\psi_n \\
\bar{\phi}_n &= -\bar{a}(z, t)\psi_n + \bar{b}(z, t)\bar{\psi}_n
\end{aligned} \tag{4.32}$$

where t is a parameter.

Time Dependence The eigenfunctions $\phi, \bar{\phi}, \psi, \bar{\psi}$ satisfy the generalized eigenvalue problem, but not the time evolution equations (4.13). In the asymptotic limit (4.13) becomes

$$\begin{aligned}\dot{V}_{1,n} &= A_{\pm} V_{1,n} \\ \dot{V}_{2,n} &= D_{\pm} V_{2,n}\end{aligned}\tag{4.33}$$

where

$$\begin{aligned}A_{\pm} &= \lim_{n \rightarrow \pm\infty} (A_n) = z^2 A_-^{(2)} + A_-^{(0)} \\ D_{\pm} &= \lim_{n \rightarrow \pm\infty} (D_n) = (1/z^2) D_-^{(2)} + D_-^{(0)}.\end{aligned}\tag{4.34}$$

Define a new set of eigenfunctions which will satisfy both the generalized eigenvalue problem and the time-dependence

$$\begin{aligned}\phi_n^{(t)} &= \phi_n \exp(A_{\pm} t) & \psi_n^{(t)} &= \psi_n \exp(D_{\pm} t) \\ \bar{\phi}_n^{(t)} &= \bar{\phi}_n \exp(D_{\pm} t) & \bar{\psi}_n^{(t)} &= \bar{\psi}_n \exp(A_{\pm} t)\end{aligned}\tag{4.35}$$

Both $\{\bar{\phi}_n^{(t)}, \phi_n^{(t)}\}$ and $\{\bar{\psi}_n^{(t)}, \psi_n^{(t)}\}$ are linearly independent, so we may write

$$\begin{aligned}\phi_n^{(t)} &= a_0 \bar{\psi}_n^{(t)} + b_0 \psi_n^{(t)} \\ \bar{\phi}_n^{(t)} &= -\bar{a}_0 \psi_n^{(t)} + \bar{b}_0 \bar{\psi}_n^{(t)}\end{aligned}\tag{4.36}$$

where $a_0, \bar{a}_0, b_0, \bar{b}_0$ equal the scattering coefficients, a, \bar{a}, b, \bar{b} at $t=0$. Substituting (4.35) into (4.36) gives

$$\begin{aligned}\phi_n &= a_0 e^{[(A_+ - A_-)t]} \bar{\psi}_n + b_0 e^{[(D_+ - A_-)t]} \psi_n \\ \bar{\phi}_n &= -\bar{a}_0 e^{[(D_+ - D_-)t]} \psi_n + \bar{b}_0 e^{[(A_+ - D_-)t]} \bar{\psi}_n\end{aligned}\tag{4.37}$$

Comparing with (4.32) and noting that $A_+ = A_-$ and $D_+ = D_-$, the scattering coefficients are

$$\begin{aligned} a &= a_0, & b &= b_0 e^{[(D_+ - A_-)t]} \\ \bar{a} &= \bar{a}_0, & \bar{b} &= \bar{b}_0 e^{[(D_+ - A_-)t]}. \end{aligned} \quad (4.38)$$

The most significant result here, for our purposes, is that the coefficients a, \bar{a} are constant. In the next section, we use this to derive the conserved quantities of the AL equation.

4.2.3 Conservation Laws

The conservation laws can be derived by considering the asymptotic form of $\bar{a}(z)$.

$$\bar{\phi}_n \sim -\bar{a}(z) \begin{pmatrix} 0 \\ 1 \end{pmatrix} z^{-n} + \bar{b}(z) \begin{pmatrix} 1 \\ 0 \end{pmatrix} z^n \quad \Rightarrow \quad \bar{a}(z) \sim -z^n \bar{\phi}_{2,n} \quad (4.39)$$

Next substitute $\bar{\phi}_n$ into the eigenvalue problem (4.11),

$$z^{n-1} \bar{\phi}_{1,n+1} = z^n \bar{\phi}_{1,n} + z^{n-1} Q_n \bar{\phi}_{2,n} \quad (4.40a)$$

$$z^n \bar{\phi}_{2,n+1} = z^{n-1} \bar{\phi}_{2,n} + z^n R_n \bar{\phi}_{1,n}. \quad (4.40b)$$

Solve (4.40b) for $z^n \bar{\phi}_{1,n}$ and substitute into (4.40a), to eliminate $\bar{\phi}_{1,n}$

$$\begin{aligned} z^n \bar{\phi}_{1,n} &= \frac{1}{R_n} (z^n \bar{\phi}_{2,n+1} - z^{n-1} \bar{\phi}_{2,n}) = \frac{1}{z R_n} \Delta_n (z^n \bar{\phi}_{2,n}) \\ z^{n-2} \frac{1}{R_{n+1}} \Delta_n (z^{n+1} \bar{\phi}_{2,n+1}) &= \frac{1}{z R_n} \Delta_n (z^n \bar{\phi}_{2,n}) + z^{n-1} Q_n \bar{\phi}_{2,n} \\ \frac{1}{z^{2n+3} R_{n+1}} \Delta_n (z^{n+1} \bar{\phi}_{2,n+1}) &- \frac{1}{z^{2n+1} R_n} \Delta_n (z^n \bar{\phi}_{2,n}) = Q_n z^{-2n-1} (z^n \bar{\phi}_{2,n}), \end{aligned} \quad (4.41)$$

which can be written as,

$$\Delta_n \left(\frac{\Delta_n(z^n \bar{\Phi}_{2,n})}{z^{2n+1} R_n} \right) = Q_n z^{-2n-1} (z^n \bar{\Phi}_{2,n}). \quad (4.42)$$

Define

$$-z^n \bar{\Phi}_{2,n} = \prod_{k=-\infty}^n g_k \quad (4.43)$$

such that $\Delta_n(-z^n \bar{\Phi}_{2,n}) = \Delta_n(\prod_{k=-\infty}^n g_k) = (g_{n+1} - 1) \prod_{k=-\infty}^n g_k$ and substitute into (4.42) to get the recursion relation

$$g_{n+1}(g_{n+2} - 1) - z^2 \frac{R_{n+1}}{R_n} (g_{n+1} - 1) = z^2 R_{n+1} Q_n, \quad (4.44)$$

which can be re-written as

$$R_{n-1} g_n (g_{n+1} - 1) - z^2 R_n (g_n - 1) = z^2 R_n R_{n-1} Q_{n-1}. \quad (4.45)$$

Expand g_n and g_{n+1} in powers of z^2 ,

$$\begin{aligned} g_n &= g_n^{(0)} + z^2 g_n^{(1)} + z^4 g_n^{(2)} + \dots = \sum_{m=0} g_n^{(m)} z^{2m} \\ g_{n+1} &= g_{n+1}^{(0)} + z^2 g_{n+1}^{(1)} + z^4 g_{n+1}^{(2)} + \dots = \sum_{m=0} g_{n+1}^{(m)} z^{2m}. \end{aligned} \quad (4.46)$$

Substitute into the recursion relation for g_n, g_{n+1} ,

$$\begin{aligned} R_{n-1} \sum_{m=0} g_n^{(m)} z^{2m} \left(\sum_{l=0} g_{n+1}^{(l)} z^{2l} - 1 \right) - z^2 R_n \left(\sum_{m=0} g_n^{(m)} z^{2m} - 1 \right) \\ = z^2 R_n R_{n-1} Q_{n-1} \\ R_{n-1} \left[\sum_{m,l=0} z^{2(m+l)} g_n^{(m)} g_{n+1}^{(l)} - \sum_{m=0} z^{2m} g_n^{(m)} \right] - R_n \sum_{m=0} z^{2(m+1)} g_n^{(m)} \\ = z^2 R_n (R_{n-1} Q_{n-1} - 1). \end{aligned} \quad (4.47)$$

Solving recursively for $g_n^{(m)}$ in orders of z^2 , gives

$$\begin{aligned}
O(z^0) : \quad & g_n^{(0)} = 1 \\
O(z^2) : \quad & g_n^{(1)} = R_{n-1}Q_{n-2} \\
O(z^4) : \quad & g_n^{(2)} = R_{n-1}Q_{n-3}(1 - R_{n-2}Q_{n-2})
\end{aligned} \tag{4.48}$$

For orders of z^{2p} , $p \geq 2$, this recursion relation reduces to

$$R_{n-1} \left[\sum_{m=0}^p g_n^{(m)} g_{n+1}^{(p-m)} - g_n^{(p)} \right] = R_{n-1} \left[\sum_{m=1}^{p-1} g_n^{(m)} g_{n+1}^{(p-m)} + g_{n+1}^{(p)} \right] = R_n g_n^{(p-1)} \tag{4.49}$$

or

$$g_{n+1}^{(p)} = \frac{R_n}{R_{n-1}} g_n^{(p-1)} - \sum_{m=1}^{p-1} g_n^{(m)} g_{n+1}^{(p-m)}. \tag{4.50}$$

which gives expressions for higher orders of the coefficients,

$$\begin{aligned}
O(z^6) : \quad & g_n^{(3)} = \frac{R_{n-1}}{R_{n-2}} g_{n-1}^{(2)} - g_{n-1}^{(1)} g_n^{(2)} - g_{n-1}^{(2)} g_n^{(1)} \\
& = R_{n-1} Q_{n-4} (1 - R_{n-3} Q_{n-3} - R_{n-2} Q_{n-2} \\
& \quad + R_{n-3} Q_{n-3} R_{n-2} Q_{n-2}) \\
& \quad - R_{n-1} R_{n-2} Q_{n-3}^2 (1 - R_{n-2} Q_{n-2})
\end{aligned} \tag{4.51}$$

$$\begin{aligned}
O(z^8) : \quad & g_n^{(4)} = \frac{R_{n-1}}{R_{n-2}} g_{n-1}^{(3)} - g_{n-1}^{(1)} g_n^{(3)} - g_{n-1}^{(2)} g_n^{(2)} - g_{n-1}^{(3)} g_n^{(1)} \\
O(z^{10}) : \quad & g_n^{(5)} = \frac{R_{n-1}}{R_{n-2}} g_{n-1}^{(4)} - g_{n-1}^{(1)} g_n^{(4)} - g_{n-1}^{(2)} g_n^{(3)} - g_{n-1}^{(3)} g_n^{(2)} - g_{n-1}^{(4)} g_n^{(1)}
\end{aligned}$$

Next use the expansion

$$\log(1+x) = \sum_{n=1}^{\infty} \frac{x^n}{n} (-1)^{n+1} \tag{4.52}$$

to write out the series expansions,

$$\begin{aligned}
\log[\bar{a}(z)] &= \lim_{n \rightarrow \infty} \log \left(\prod_{k=-\infty}^n g_k \right) = \sum_{n=-\infty}^{\infty} \log(g_n) = \sum_{n=-\infty}^{\infty} \log \left[\sum_{m=0}^{\infty} g_n^{(m)} z^{2m} \right] \\
&= \sum_{n=-\infty}^{\infty} \log \left[1 + \sum_{m=1}^{\infty} g_n^{(m)} z^{2m} \right] = \sum_{n=-\infty}^{\infty} \sum_{p=1}^{\infty} \frac{(-1)^{p+1}}{p} \left[\sum_{m=1}^{\infty} g_n^{(m)} z^{2m} \right]^p.
\end{aligned} \tag{4.53}$$

Since $\bar{a}(z)$ is a constant of motion, each coefficients of $z^{2\alpha}$ in the above expansion of the must also be time-independent. These coefficients are the conserved quantities. Expanding the first few terms gives,

$$\begin{aligned}
\log[\bar{a}(z)] &= \sum_{n=-\infty}^{\infty} \sum_{p=1}^{\infty} \frac{(-1)^{p+1}}{p} [g_n^{(1)} z^2 + g_n^{(2)} z^4 + g_n^{(3)} z^6 + g_n^{(4)} z^8 \\
&\quad + g_n^{(5)} z^{10} + O(z^{12})]^p \\
&= \sum_{n=-\infty}^{\infty} g_n^{(1)} z^2 + \left(g_n^{(2)} - \frac{1}{2} [g_n^{(1)}]^2 \right) z^4 \\
&\quad + \left(g_n^{(3)} - g_n^{(1)} g_n^{(2)} + \frac{1}{3} [g_n^{(1)}]^3 \right) z^6 \\
&\quad + \left(g_n^{(4)} - \frac{1}{2} [g_n^{(2)}]^2 - g_n^{(1)} g_n^{(3)} + [g_n^{(1)}]^2 g_n^{(2)} - \frac{1}{4} [g_n^{(1)}]^4 \right) z^8 \\
&\quad + \left(g_n^{(5)} - g_n^{(4)} g_n^{(1)} - g_n^{(3)} g_n^{(2)} + [g_n^{(2)}]^2 g_n^{(1)} \right. \\
&\quad \quad \left. - g_n^{(3)} [g_n^{(1)}]^2 + g_n^{(2)} [g_n^{(1)}]^3 - \frac{1}{5} g_n^{(5)} \right) z^{10} \\
&\quad + O(z^{12}).
\end{aligned} \tag{4.54}$$

4.2.4 Conserved Quantities

The first few conserved quantities are:

$$\begin{aligned}
C_1 &= \sum_n g_n^{(1)} = \sum_n R_n Q_{n-1} \\
C_2 &= \sum_n g_n^{(2)} + \frac{1}{2} [g_n^{(1)}]^2 = \sum_n R_n Q_{n-2} (1 - R_{n-1} Q_{n-1}) + \frac{1}{2} R_n^2 Q_{n-1}^2 \\
C_3 &= \sum_n g_n^{(3)} + g_n^{(1)} g_n^{(2)} + \frac{1}{3} [g_n^{(1)}]^3 \\
&= \sum_n R_n Q_{n-3} (1 - R_{n-2} Q_{n-2} - R_{n-1} Q_{n-1} + R_{n-2} Q_{n-2} R_{n-1} Q_{n-1}) \\
&\quad - R_n R_{n-1} Q_{n-2}^2 (1 - R_{n-1} Q_{n-1}) + R_n^2 Q_{n-1} Q_{n-2} (1 - R_{n-1} Q_{n-1}) \\
&\quad + \frac{1}{3} (R_n Q_{n-1})^3 \\
C_4 &= \sum_n g_n^{(4)} + \frac{1}{2} [g_n^{(2)}]^2 + g_n^{(1)} g_n^{(3)} + [g_n^{(1)}]^2 g_n^{(2)} + \frac{1}{4} [g_n^{(1)}]^4 \\
C_5 &= \sum_n g_n^{(5)} + g_n^{(4)} g_n^{(1)} + g_n^{(3)} g_n^{(2)} + [g_n^{(2)}]^2 g_n^{(1)} + g_n^{(3)} [g_n^{(1)}]^2 + g_n^{(2)} [g_n^{(1)}]^3 + \frac{1}{5} g_n^{(5)}
\end{aligned} \tag{4.55}$$

Further conserved quantities can be determined by using the recursion relations and expansions given. From looking at these equations, we notice a few patterns. First of all, the leading order in α of C_m is $\sum_n \psi_n^* \psi_{n-m}$, and the largest order of α is α^m .

4.3 AL and BHM

To obtain the AL, 4.23 we let $R_n = \alpha Q_n^*$. Furthermore, to put it in a more familiar form, we write it in terms of the real-space fields, $\tilde{\Psi}_n = Q_n$, and $\tilde{\Psi}_n^* = Q_n^*$.

$$\frac{\partial}{\partial t} \tilde{\Psi}_n = i [(\tilde{\Psi}_{n+1} + \tilde{\Psi}_{n-1} - 2\tilde{\Psi}_n) - \alpha |\tilde{\Psi}_n|^2 (\tilde{\Psi}_{n+1} + \tilde{\Psi}_{n-1})] \tag{4.56}$$

Recall that in real-space the BHM has the form

$$\frac{\partial}{\partial t} \tilde{\Psi}_n = -i \left[-J (\tilde{\Psi}_{n+1} + \tilde{\Psi}_{n-1} - 2\tilde{\Psi}_n) + \mu_0 N_s |\tilde{\Psi}_n|^2 \tilde{\Psi} \right] \quad (4.57)$$

By defining a new time scale, $\tau = Jt$,

$$\frac{\partial}{\partial \tau} \tilde{\Psi}_n = i \left[(\tilde{\Psi}_{n+1} + \tilde{\Psi}_{n-1} - 2\tilde{\Psi}_n) - \frac{\mu_0 N_s}{J} |\tilde{\Psi}_n|^2 \tilde{\Psi}_n \right] \quad (4.58)$$

Note that here n is an index of real-space fields, following the notation of Ablowitz and Ladik (1976), while in earlier chapters it was used as a momentum index. From these two forms, it can be seen that these two equations are mathematically close for $\alpha = 2\mu_0 N_s / J \equiv 2\kappa N_s$ and identical in the limit $\psi_{n+1} + \psi_{n-1} \rightarrow 2\psi_n$.

The first few coefficients of g_n are

$$\begin{aligned} g_n^{(1)} &= \alpha \tilde{\Psi}_{n-1}^* \tilde{\Psi}_{n-2} \\ g_n^{(2)} &= \alpha \tilde{\Psi}_{n-1}^* \tilde{\Psi}_{n-3} (1 - \alpha |\tilde{\Psi}_{n-2}|^2) \\ g_n^{(3)} &= \frac{\alpha \tilde{\Psi}_{n-1}^*}{\alpha \tilde{\Psi}_{n-2}^*} g_{n-1}^{(2)} - g_{n-1}^{(1)} g_n^{(2)} - g_{n-1}^{(2)} g_n^{(1)} \\ &= \alpha \tilde{\Psi}_{n-1}^* \tilde{\Psi}_{n-4} (1 - \alpha |\tilde{\Psi}_{n-3}|^2 - \alpha |\tilde{\Psi}_{n-2}|^2 + \alpha^2 |\tilde{\Psi}_{n-3}|^2 |\tilde{\Psi}_{n-2}|^2) \\ &\quad - \alpha^2 \tilde{\Psi}_{n-1}^* \tilde{\Psi}_{n-2}^* \tilde{\Psi}_{n-3}^2 (1 - \alpha |\tilde{\Psi}_{n-2}|^2). \end{aligned} \quad (4.59)$$

In terms of the real-space fields $\{\tilde{\Psi}_n, \tilde{\Psi}_n^*\}$, the first few conserved quantities are

$$\begin{aligned}
C_1 &= \sum_n \alpha \tilde{\Psi}_n^* \tilde{\Psi}_{n-1} \\
C_2 &= \sum_n g_n^{(2)} + \frac{1}{2} [g_n^{(1)}]^2 = \sum_n \alpha \tilde{\Psi}_n^* \tilde{\Psi}_{n-2} (1 - \alpha |\tilde{\Psi}_{n-1}|^2) + \frac{1}{2} \alpha^2 (\tilde{\Psi}_n^*)^2 \tilde{\Psi}_{n-1}^2 \\
C_3 &= \sum_n g_n^{(3)} + g_n^{(1)} g_n^{(2)} + \frac{1}{3} [g_n^{(1)}]^3 \\
&= \sum_n \alpha \tilde{\Psi}_n^* \tilde{\Psi}_{n-3} (1 - \alpha |\tilde{\Psi}_{n-2}|^2 - \alpha |\tilde{\Psi}_{n-1}|^2 + \alpha^2 |\tilde{\Psi}_{n-2}|^2 |\tilde{\Psi}_{n-1}|^2) \\
&\quad - \alpha^2 \tilde{\Psi}_n^* \tilde{\Psi}_{n-1}^* \tilde{\Psi}_{n-2}^2 (1 - \alpha |\tilde{\Psi}_{n-1}|^2) \\
&\quad + \alpha [\tilde{\Psi}_n^*]^2 \tilde{\Psi}_{n-1} \tilde{\Psi}_{n-2} (1 - \alpha |\tilde{\Psi}_{n-1}|^2) \\
&\quad + \frac{1}{3} (\alpha \tilde{\Psi}_n^* \tilde{\Psi}_{n-1})^3.
\end{aligned} \tag{4.60}$$

In terms of the momentum-space fields $\{\Psi_p, \Psi_p^*\}$, C_1 and C_2 are

$$\begin{aligned}
C_1 &= \alpha \sum_p |\Psi_p|^2 e^{-2\pi i p / N_s} \\
&= \alpha \sum_p |\Psi_p|^2 \cos\left(\frac{2\pi p}{N_s}\right) - i\alpha \sum_p |\Psi_p|^2 \sin\left(\frac{2\pi p}{N_s}\right) \\
C_2 &= \alpha \sum_p |\Psi_p|^2 e^{-4\pi i p / N_s} - \frac{\alpha^2}{N_s} \sum_{p,q,r} \Psi_p^* \Psi_q^* \Psi_r \Psi_{p+q-r} e^{-2\pi i (p+r) / N_s} \\
&\quad + \frac{\alpha^2}{2N_s} \sum_{p,q,r} \Psi_p^* \Psi_q^* \Psi_r \Psi_{p+q-r} e^{-2\pi i (p+q) / N_s}.
\end{aligned} \tag{4.61}$$

As seen in earlier chapters, there is a threshold for chaos in the BHM. Below this threshold there are initial states that do not thermalize, but nevertheless relax to a steady-state. For fully integrable systems it is known that this steady-state can be described by a constrained thermodynamic ensemble that accounts for all of the integrals of motion. Anecdotal evidence suggests that the initial total quasi-momentum plays a role in the dynamics of the BHM for small nonlinearities, κ . Is it possible that the other integrals of

motion of the AL affect the dynamics? Is the nonthermal steady-state governed by a constrained ensemble that takes into account the conserved quantities of nearby integrable models? There are other nearby integrable models, which include the noninteracting case and the continuum limit. The imaginary part of the first conserved quantity of AL, $\text{Im } C_1$, is analogous to the total quasi-momentum and $\text{Re } C_1$ to the total kinetic energy. In the noninteracting limit the momentum distribution is conserved, so any higher moments of the momentum distribution is also conserved. If the mapping between the BHM and AL fields corresponded to simply equating the fields ($\psi_{n,\text{BHM}} = \psi_{n,\text{AL}}$), then conservation of C_1 in BHM would not distinguish between being close to the noninteracting case and close to AL. In contrast, the second and third terms of C_2 are not conserved in the noninteracting model. However, the mapping between the BHM fields and the AL is nontrivial and the nonlinear corrections to the mapping are expected to allow one to distinguish between effects of quasi-conserved quantities of AL and of the noninteracting case. A derivation of the mapping between the BHM and AL fields and a study of the role of the conserved quantities of AL in the dynamics of BHM is the subject of proposed future work.

Chapter 5

Outlook and Conclusion

5.1 Summary of Results

One of the fundamental assertions of statistical mechanics is that the time average of a physical observable is equivalent to the average over phase-space, with microcanonical measure. A system for which this is true is said to be ergodic and one can calculate dynamical properties of the system from static phase-space averages. Dynamics of a system which is fully integrable, that is has as many conserved quantities as degrees of freedom, is constrained to a reduced phase space and thus not ergodic, although it may relax to a modified equilibrium. What happens as one moves away from the fully integrable case?

In this work we have studied the relationship between chaos and thermalization in the one-dimensional Bose-Hubbard model in the classical-field approximation. We have compared two quantitative measures of chaos and thermalization: (1) the finite-time maximal Lyapunov exponent, averaged over a microcanonical ensemble and (2) the normalized spectral entropy, which is a measure of equipartition of a modified energy in the independent mode approximation. There is a strong correspondence between the Lyapunov exponents and normalized spectral entropy.

We find a threshold for chaos and a corresponding broad transition from incomplete to complete thermalization. The stochasticity threshold is governed by two parameters: the strength of the nonlinearity κ and the average energy-per-particle, ϵ_T . Both of these parameters are finite in the thermodynamic limit and suggest that the threshold will

survive in that limit. Far above the threshold, in the strongly chaotic regime, relaxation to the thermal state is complete. In this region, the fluctuations in kinetic energy scale as $\sqrt{N_s}$ confirming their thermal nature. We study the size scaling of the Lyapunov exponent and find that it is universal with respect to the size of the lattice. For small nonlinearities, the stochasticity and thermalization thresholds are finite for the range of energies studied and don't show tendencies to vanish at high energies.

In the vicinity of the threshold the relationship between chaos and thermalization is complex. There is a transient regime supporting both chaotic and regular trajectories, so that the Lyapunov exponent is non-zero, but full thermalization does not occur. Remarkably, in this region individual initial states with larger Lyapunov exponent tend to relax closer to the thermal state. There is also a region where although the Lyapunov exponent is zero, there is significant relaxation towards the thermal state. We conjecture that this redistribution in the phase-space is due to the quasi-regular dynamics governed by the nearby Ablowitz-Ladik lattice, which is integrable. Above $\varepsilon_T \simeq 0.6J$, both the stochasticity threshold and thermalization threshold overlap very closely and appear to depend only on the nonlinearity strength. This suggests that there is a critical nonlinearity, $\kappa_c \simeq 0.2$, such that the system is regular for $\kappa < \kappa_c$ independent of the energy of the system. In the opposite limit of small energy and large nonlinearity, there is a separation of thresholds, where almost complete relaxation to the thermal distribution is observed in the absence of chaos.

An analysis of resonances of the BHM gives a Chirikov's criterion for the chaos threshold that depends on parameters which vanish in the thermodynamic limit. This conclusion is confirmed on dimensional grounds. The criterion predicted by the Chirikov criterion is different from the one inferred from numerical calculations, signifying the failure of the standard Chirikov's approach.

Anecdotal evidence suggests that the total quasi-momentum may play a role in the relaxation dynamics. The quasi-momentum is strictly conserved in the nearby fully integrable Ablowitz-Ladik model, as well as in the non-interacting and continuum limits.

There are at least three known near-by integrable models: the Ablowitz-Ladik lattice, the continuous nonlinear Schrödinger equation and the noninteracting model. We outline the method of Inverse Scattering Transform and generate all of the integrals of motion of the closely related, fully integrable model of Ablowitz-Ladik. We conjecture that the presence of quasi-conserved quantities may alter the scaling of the chaos criterion.

5.2 Open Questions

These observations lead to many questions that deserve further investigation.

- What is the reason for the failure of the Chirikov criterion to accurately predict the chaos threshold? Is it related to interference between resonances due to near-by integrable systems? Could the proper scaling be recovered in a multiple-resonance model?
- What is the underlying theory that governs the threshold?
- For $\kappa \gtrsim 1$, how does the chaos threshold scale in the thermodynamic limit? Is the number of modes involved relevant?
- What governs the slow relaxation times where they appear? Is it related to the conserved quantities of the near-by integrable systems? If this is the case, which near-by integrable system?

- For those states that show no signs of thermalization, what governs the steady-state? Can these states be described by a constrained ensemble? Which “quasi-conserved quantities” are the relevant for the constrained ensemble?

Bibliography

- Ablowitz, M., and H. Segur, 1981, *Solitons and the Inverse Scattering Transform* (Philadelphia, PA: SIAM).
- Ablowitz, M. J., and J. F. Ladik, 1976, *Journal of Mathematical Physics* **17**(6), 1011.
- Ablowitz, M. J., C. Schober, and B. M. Herbst, 1993, *Physical Review Letters* **71**(17), 2683.
- Anderson, M. H., J. R. Ensher, M. R. Matthews, C. E. Wieman, and E. A. Cornell, 1995, *Science* **269**(5221), 198.
- Andrews, M. R., C. G. Townsend, H.-J. Miesner, D. S. Durfee, D. M. Kurn, and W. Ketterle, 1997, *Science* **275**(5300), 637.
- Arnold, V., 1963, *Russian Math. Survey* **18**, 85.
- Arnold, V., and A. Avez, 1968, *Ergodic Problems of Classical Mechanics* (Benjamin).
- Aspect, A., E. Arimondo, R. Kaiser, N. Vansteenkiste, and C. Cohen-Tannoudji, 1988, *Physical Review Letters* **61**(7), 826.
- Bose, S., 1924, *Z. Phys.* **26**, 178.
- Bouchoule, I., K. V. Kheruntsyan, and G. V. Shlyapnikov, 2007, *Physical Review A* **75**(3), 031606.
- Boyanovsky, D., C. Destri, and H. J. de Vega, 2004, *Physical Review D* **69**(4), 045003.
- Bradley, C. C., C. A. Sackett, J. J. Tollett, and R. G. Hulet, 1995, *Physical Review Letters* **75**(9), 1687.
- Castin, Y., 2001, in *Coherent Atomic Matter Waves*, edited by R. Kaiser, C. Westbrook, and F. David (Springer-Verlag).
- Castin, Y., 2004, cond-mat/0407118 .
- Chirikov, B. V., 1979, *Physics Reports* **52**(5), 263.

- Chu, S., L. Hollberg, J. E. Bjorkholm, A. Cable, and A. Ashkin, 1985, *Physical Review Letters* **55**(1), 48.
- Contopoulos, G., L. Galgani, and A. Giorgilli, 1978, *Physical Review A* **18**(3), 1183.
- Contopoulos, G., and N. Voglis, 1997, *Astronomy and Astrophysics* **317**(1), 73.
- Davis, K. B., M. O. Mewes, M. R. Andrews, N. J. van Druten, D. S. Durfee, D. M. Kurn, and W. Ketterle, 1995, *Physical Review Letters* **75**(22), 3969.
- Durfee, D. S., Y. K. Shaham, and M. A. Kasevich, 2006, *Physical Review Letters* **97**(24), 240801.
- Eckhardt, B., and D. Yao, 1993, *Physica D: Nonlinear Phenomena* **65**(1-2), 100.
- Einstein, A., 1925, *Sitzber. Kgl. Preuss. Akad. Wiss.* **3**.
- Esteve, J., J.-B. Trebbia, T. Schumm, A. Aspect, C. I. Westbrook, and I. Bouchoule, 2006, *Physical Review Letters* **96**(13), 130403.
- Fermi, E., J. Pasta, and S. Ulam, 1974, *Appl. Math* **15**, 143.
- Folman, R., P. Kröger, J. Schmiedmayer, J. Denschlag, and C. Henkel, 2002, *Advances In Atomic, Molecular, and Optical Physics* **48**, 263.
- Ford, J., 1992, *Physics Reports* **213**(5), 271.
- Fortagh, J., and C. Zimmermann, 2007, *Reviews of Modern Physics* **79**(1), 235.
- Gardner, C. S., J. M. Greene, M. D. Kruskal, and R. M. Miura, 1967, *Physical Review Letters* **19**(19), 1095.
- Gerhardt, G. J. L., M. Frichembruder, F. B. Rizzato, and S. R. Lopes, 2002, *Chaos, Solitons & Fractals* **13**(6), 1269.
- Girardeau, M., 1960, *Journal of Mathematical Physics* **1**(6), 516.
- Greiner, M., O. Mandel, T. Esslinger, T. W. Hansch, and I. Bloch, 2002, *Nature* **415**(6867), 39.
- Gross, E., 1961, *Il Nuovo Cimento (1955-1965)* **20**(3), 454.
- Gustavson, T. L., A. Landragin, and M. A. Kasevich, 2000, *Classical and Quantum Gravity* **17**(12), 2385.
- Hamer, C. J., and J. B. Kogut, 1979, *Physical Review B* **20**(9), 3859.
- Hansel, W., P. Hommelhoff, T. W. Hansch, and J. Reichel, 2001, *Nature* **413**(6855), 498.

- Herbst, B. M., and M. J. Ablowitz, 1989, *Physical Review Letters* **62**(18), 2065.
- Herbst, B. M., F. Varadi, and M. J. Ablowitz, 1994, *Math. Comput. Simul.* **37**(4-5), 353.
- Izrailev, F., and B. Chirikov, 1966, in *Dokl. Akad. Nauk SSSR*, volume 166, p. 57.
- Jaksch, D., C. Bruder, J. I. Cirac, C. W. Gardiner, and P. Zoller, 1998, *Physical Review Letters* **81**(15), 3108.
- Jaynes, E. T., 1957a, *Physical Review* **106**(4), 620.
- Jaynes, E. T., 1957b, *Physical Review* **108**(2), 171.
- Kagan, Y., and B. V. Svistunov, 1997, *Physical Review Letters* **79**(18), 3331.
- Kinoshita, T., T. Wenger, and D. S. Weiss, 2006, *Nature* **440**(7086), 900.
- Kolmogorov, A., 1954, *Dokl. Akad. Nauk SSSR* Vol **48**, 527.
- Lebowitz, J. L., 1999, *Physica A* **263**(1-4), 516.
- Lieb, E. H., 1963, *Physical Review* **130**(4), 1616.
- Lieb, E. H., and W. Liniger, 1963, *Physical Review* **130**(4), 1605.
- Livi, R., M. Pettini, S. Ruffo, M. Sparpaglione, and A. Vulpiani, 1985, *Physical Review A* **31**(2), 1039.
- Livi, R., M. Pettini, S. Ruffo, and A. Vulpiani, 1987, *Journal of Statistical Physics* **48**(3), 539.
- Mishmash, R. V., and L. D. Carr, 2008, 0810.2593 .
- Moser, J., 1962, *Nachr. Akad. Wiss. Goett. II, Math.-Phys. Kl* **2**, 1.
- Ohberg, P., and S. Stenholm, 1997, *Journal of Physics B: Atomic, Molecular and Optical Physics* **30**(12), 2749.
- Ott, H., J. Fortagh, G. Schlotterbeck, A. Grossmann, and C. Zimmermann, 2001, *Physical Review Letters* **87**(23), 230401.
- Paredes, B., A. Widera, V. Murg, O. Mandel, S. Fölling, I. Cirac, G. V. Shlyapnikov, T. W. Hänsch, and I. Bloch, 2004, *Nature* **429**(6989), 277.
- Penrose, O., and L. Onsager, 1956, *Physical Review* **104**(3), 576.
- Phillips, W. D., and H. Metcalf, 1982, *Physical Review Letters* **48**(9), 596.
- Pitaevskii, L., 1961, *Soviet Physics JETP-USSR* **13**(2), 451.

- Proukakis, N. P., J. Schmiedmayer, and H. T. C. Stoof, 2006, *Physical Review A* **73**(5), 053603.
- Rigol, M., V. Dunjko, V. Yurovsky, and M. Olshanii, 2007, *Physical Review Letters* **98**(5), 050405.
- Scharf, R., and A. R. Bishop, 1991, *Physical Review A* **43**(12), 6535.
- Schumm, T., S. Hofferberth, L. M. Andersson, S. Wildermuth, S. Groth, I. Bar-Joseph, J. Schmiedmayer, and P. Kruger, 2005, *Nat. Phys.* **1**(1), 57.
- Tabor, M., 1989, *Chaos and integrability in nonlinear dynamics: an introduction* (Wiley).
- Tuck, J., and M. Menzel, 1972, *Adv. Math* **9**, 399.
- Vidal, G., 2004, *Physical Review Letters* **93**(4), 040502.
- Villain, P., and M. Lewenstein, 2000, *Physical Review A* **62**(4), 043601.
- Voglis, N., and G. J. Contopoulos, 1994, *Journal of Physics A: Mathematical and General* **27**(14), 4899.
- Wang, Y.-J., D. Z. Anderson, V. M. Bright, E. A. Cornell, Q. Diot, T. Kishimoto, M. Prentiss, R. A. Saravanan, S. R. Segal, and S. Wu, 2005, *Physical Review Letters* **94**(9), 090405.
- Weiss, D. S., B. C. Young, and S. Chu, 1994, *Applied Physics B: Lasers and Optics* **59**(3), 217.
- Wicht, A., J. M. Hensley, E. Sarajlic, and S. Chu, 2002, *Physica Scripta* **T102**, 82.
- Yukalov, V., 2009, *Laser Physics* **19**(1), 1.
- Zabusky, N. J., and M. D. Kuskal, 1965, *Physical Review Letters* **15**(6), 240.
- Zaslavsky, G. M., 1999, *Physics Today* **52**(8), 39.

Appendix A

Thermodynamic Distribution within Hartree-Fock

A.1 Hartree Fock

In this section, the following integrals are used:

$$\begin{aligned}\int_0^\infty dx e^{-\alpha x} &= \frac{1}{\alpha} \\ \int_0^\infty dx x e^{-\alpha x} &= \frac{1}{\alpha^2} \\ \int_0^\infty dx x^2 e^{-\alpha x} &= \frac{2}{\alpha^3}\end{aligned}\tag{A.1}$$

Note that N is the number of degrees of freedom and $a = L/N$ is the lattice spacing.

Within Hartree-Fock the form of the density distribution function is taken to be Gaussian and the thermal expectation value of the Grand Potential,

$$\langle F \rangle = \langle H \rangle - T \langle S \rangle - \mu \langle N_a \rangle,\tag{A.2}$$

is minimized, where N_a is the norm. The density distribution function with two-body interactions has the form,

$$\sigma_{HF} = \frac{1}{Z} \exp \left(\sum_{n,n'} -\alpha_{n,n'} \psi_n \psi_{n'}^* \right) = \frac{1}{Z} \exp \left(- \sum_n \alpha_n I_n \right).\tag{A.3}$$

In the second step, we assume that off-diagonal terms are zero. The α_n coefficients are unknown and are determined by the condition of minimizing the grand potential. The partition function Z , normalizes σ_{HF} so that the integration of σ_{HF} over all of phase space is 1. Throughout the sums run from 1 to N , where N is the number of lattice sites.

$$\begin{aligned}
Z &= \frac{1}{(2\pi\hbar)^N} \int d^N\theta \int d^N I e^{-\sum_n \alpha_n I_n} \\
&= \frac{1}{(2\pi\hbar)^N} \int_0^{2\pi} d\theta_1 \int_0^{2\pi} d\theta_2 \cdots \int_0^{2\pi} d\theta_N \int_0^\infty dI_1 \int_0^\infty dI_2 \cdots \int_0^\infty dI_N e^{-\sum_n \alpha_n I_n} \\
&= \frac{1}{\hbar^N} \int_0^\infty dI_1 e^{-\alpha_1 I_1} \int_0^\infty dI_2 e^{-\alpha_2 I_2} \cdots \int_0^\infty dI_N e^{-\alpha_N I_N} \\
&= \prod_{i=1}^N \frac{1}{\hbar \alpha_i}
\end{aligned} \tag{A.4}$$

The expectation values of each term in the Grand Potential is calculated, using the Hartree-Fock density distribution function, σ_{HF} . The expectation value of a generic observable is given by

$$\begin{aligned}
\langle O \rangle &= \frac{1}{(2\pi\hbar)^N} \int d^N\theta \int d^N I O(\{I_n, \theta_n\}) \sigma_{HF} \\
&= \frac{1}{(2\pi)^N} \prod_{i=1}^N \alpha_i \int d^N\theta \int d^N I O e^{-\sum_n \alpha_n I_n}
\end{aligned} \tag{A.5}$$

The expectation values of the relevant observable are calculated below.

Norm

$$\begin{aligned}
\langle Norm \rangle &= \frac{1}{(2\pi\hbar)^N} \prod_{i=1}^N \hbar\alpha_i \int d^N\theta \int d^N I \left[\frac{1}{\hbar} \sum_n I_n \right] e^{-\sum_m \alpha_m I_m} \\
&= \prod_{i=1}^N \alpha_i \sum_n \frac{1}{\hbar} \int_0^\infty dI_1 e^{-\alpha_1 I_1} \dots \int_0^\infty dI_n I_n e^{-\alpha_n I_n} \dots \int_0^\infty dI_N e^{-\alpha_N I_N} \\
&= \sum_{n=1}^N \frac{1}{\hbar\alpha_n}
\end{aligned}$$

Hamiltonian - Kinetic Term

$$\begin{aligned}
\langle H_0 \rangle &= \frac{1}{(2\pi\hbar)^N} \prod_{i=1}^N \hbar\alpha_i \int d^N\theta \int d^N I \left[\sum_n I_n \omega_n \right] e^{-\sum_m \alpha_m I_m} \\
&= \sum_{n=1}^N \frac{\omega_n}{\alpha_n}
\end{aligned}$$

Hamiltonian - Interaction Term

(A.6)

$$\begin{aligned}
\langle H_I \rangle &= \frac{1}{(2\pi\hbar)^N} \prod_{i=1}^N \hbar\alpha_i \int d^N\theta \int d^N I \\
&\quad \left[\frac{\mu_0}{2\hbar^2} \sum_{m,p,q,r} (I_m I_p I_q I_r)^{1/2} \delta_{m+p,q+r} e^{-i(\theta_m + \theta_p - \theta_q - \theta_r)} \right] e^{-\sum_n \alpha_n I_n} \\
&= \frac{1}{(2\pi)^N} \prod_{i=1}^N \alpha_i (2\pi)^N \int d^N I \frac{\mu_0}{2\hbar^2} \left(\sum_m I_m^2 + 2 \sum_{m \neq p} I_m I_p \right) e^{(-\sum_n \alpha_n I_n)} \\
&= \frac{\mu_0}{2\hbar^2} \prod_{i=1}^N \alpha_i \left(\prod_{j=1}^N \frac{1}{\alpha_j} \sum_m \frac{2}{\alpha_m^2} + 2 \sum_{m \neq p} \frac{1}{\alpha_m} \frac{1}{\alpha_p} \right) \\
&= \frac{\mu_0}{\hbar^2} \left(\sum_m \frac{1}{\alpha_m^2} + \sum_{m \neq p} \frac{1}{\alpha_m} \frac{1}{\alpha_p} \right) \\
&= \frac{\mu_0}{\hbar^2} \sum_{m,p} \frac{1}{\alpha_m} \frac{1}{\alpha_p}
\end{aligned}$$

Entropy

$$\begin{aligned}
S &= -\frac{1}{(2\pi\hbar)^N} \int d^N\theta \int d^N\sigma_{HF} \log \sigma_{HF} \\
&= \frac{1}{(2\pi\hbar)^N} \int d^N\theta \int d^N \frac{1}{Z} e^{-\sum_n \alpha_n I_n} \left(-\sum_n \alpha_n I_n + \log Z \right) \\
&= \frac{1}{\hbar^N} \prod_{i=1}^N (\hbar\alpha_i) \int d^N e^{-\sum_n \alpha_n I_n} \left(-\sum_n \alpha_n I_n + \log \prod_{j=1}^N \frac{1}{\hbar\alpha_j} \right) \\
&= \sum_n \alpha_n \frac{1}{\alpha_n} - \sum_j \log(\hbar\alpha_j) \\
&= N - \sum_j \log(\hbar\alpha_j)
\end{aligned} \tag{A.7}$$

A.2 Minimization of the Grand Potential

The thermal expectation value of the Grand Potential within Hartree-Fock is given by

$$\langle F \rangle = \sum_m \frac{\omega_m}{\alpha_m} + \frac{\mu_0}{\hbar^2} \sum_{m,p} \frac{1}{\alpha_m} \frac{1}{\alpha_p} - T \left(N - \sum_m \log(\hbar\alpha_m) \right) - \mu \sum_m \frac{1}{\hbar\alpha_m} \tag{A.8}$$

Taking the variation with respect to α_n , and setting it equal to zero gives

$$\frac{\delta \langle F \rangle}{\delta \alpha_n} = -\frac{\omega_n}{\alpha_n^2} - 2\frac{\mu_0}{\hbar^2} \frac{1}{\alpha_n^2} \sum_m \frac{1}{\alpha_m} + \frac{T}{\alpha_n} + \frac{\mu}{\hbar\alpha_n^2} = 0 \tag{A.9}$$

Using $\sum_m \alpha_m^{-1} = \hbar N_a$ and solving for α_n ,

$$\alpha_n = \frac{1}{\hbar T} [\hbar\omega_n + 2\mu_0 N_a - \mu] \tag{A.10}$$

The thermal expectation values of the occupation of momentum mode n become

$$\langle I_n \rangle = \frac{1}{\alpha_n} = \frac{\hbar T}{\hbar\omega_n + 2\mu_0 N_a - \mu}. \tag{A.11}$$

In general, the coefficients μ and T are unknown and are determined by imposing constraints on the norm and energy, which come from the dynamical code. The constraints are

$$\begin{aligned} N_a = \langle N_a \rangle &= \frac{1}{\hbar} \sum_n \langle I_n \rangle \\ E_T = \langle H \rangle &= \sum_n \omega_n \langle I_n \rangle + \frac{\mu_0}{\hbar^2} \sum_{m,n} \langle I_m \rangle \langle I_n \rangle = \sum_n \omega_n \langle I_n \rangle + \mu_0 N_a^2 \end{aligned} \quad (\text{A.12})$$

Beginning with the expression for $\langle I_n \rangle$, we can solve for T in terms of μ , N_a and energy.

$$T = \omega_n \langle I_n \rangle + 2 \frac{\mu_0}{\hbar} N_a \langle I_n \rangle - \frac{\mu}{\hbar} \langle I_n \rangle \quad (\text{A.13})$$

Summing over n

$$T = \frac{1}{N} [E_k + 2\mu_0 N_a^2 - \mu N_a] \quad (\text{A.14})$$

where $E_k \equiv \sum_n \omega_n \langle I_n \rangle$. This expression for T can be substituted back into the constraints to reduce the system to two equations with two unknowns. Using the expression for temperature and normalization condition, a single constraint remains to be solved,

$$\frac{1}{N} \sum_n \frac{[E_k + 2\mu_0 N_a^2 - \mu N_a]}{[\hbar \omega_n + 2\mu_0 N_a - \mu]} - N_a = 0 \quad (\text{A.15})$$